Theses and Dissertations

2019

Model Study of the Static and Cyclic Lateral Capacity of Finned Piles

Kepha Odhambo Abongo
Lehigh University, abongo1979@gmail.com

MODEL STUDY OF THE STATIC AND CYCLIC LATERAL

CAPACITY OF FINNED PILES

By

Kepha O. Abongo

Presented to the Graduate and Research Committee

Of Lehigh University

In Candidacy for the Degree of

Doctor of Philosophy

in

Civil Engineering

Lehigh University

January 2019

© 2018 Copyright

Kepha O. Abongo

Kepha O Abongo

Model Study of the Static and Cyclic Lateral Capacity of Finned Piles

Approved and recommended for acceptance as a dissertation in partial fulfillment of

the requirements for the degree of Doctor of Philosophy in Civil Engineering on this

date of _____.

_____

Sibel Pamukcu, PhD.

Dissertation Supervisor and Advisor

Department of Civil & Environmental

Engineering

Lehigh University

_____

Dan Frangopol, PhD.

Committee Member

Department of Civil &Environmental

Engineering

Lehigh University

_____

Spencer Quiel, PhD.

Committee Chairperson

Department of Civil & Environmental

Engineering

Lehigh University

_____

Jeffrey Evans, PhD.

External Committee Member

Department of Civil &Environmental

Engineering

Bucknell University

_____

Mesut Pervizpour, PhD.

Co-Dissertation Advisor

Department of Civil &Environmental

Engineering

Lehigh University

Date Accepted:

_____

iii

Acknowledgment

For the completion of this work I have enjoyed the assistance and support of many people, to all of whom I am greatly indebted. First, my deepest gratitude is due to my academic advisor, Professor Sibel Pamukcu, for her enthusiasm and constant encouragement. With her there was never a problem that could not be solved. For the past years, I have also had the great privilege of working with Professor Mesut Pervizpour who gave valuable advice in numerical work during the final stages of the doctoral endeavor. Finally, I am grateful to Professor Spencer Quiel for assuming the chairmanship of the doctoral committee and Professors Dan Frangopol and Jeffrey Evans for their valuable input during the doctoral committee meetings.

For the instrumental of pile and setting up the equipment, I was able to rely on the experience and wisdom of the following staff at Lehigh University, whom I'm greatly indebted to: Dan Zeroka, Carl Bowman, Edmond Tomlinson, Eugene Matlock, Peter Bryan and Darrick Fritchman. Many thanks to Jianbo Gu of Lehigh University providing valuable help with numerical modelling.

Special thanks to Victory Chapel Christian Fellowship, Allentown for their prayers and encouragement. Special thanks to my family, later Dad, Mum, my Sisters Dr. Deborah Abongo, Daisy Abongo and Tabitha Abongo and to my brothers John Abongo and Joshua Abongo for their constant encouraging words.

My special appreciation is due to my dear wife Sarah, my daughter Allison and son Ethan for enduring through hardship and choosing to support Daddy with the hope of a better tomorrow.

iv

Table of Contents

ix

List of Tables

List of Figures

List of Symbols

c	Cohesion of soil
C_u and C_c	Uniformity coefficient and coefficient of soil
D_p	Diameter of pile
D^*	Effective diameter of a finned pile considering the budge factor
E_p	Elasticity modulus of pile
e	Load eccentricity
e_0	Initial void ratio
e_{max} and e_{min}	Maximum and minimum void ratio
E	Effective young modulus of soil
$E_p I_p$	Bending (flexural) stiffness of pile
E_{inc}	Increase in soil modulus per unit depth
FP	Finned pile
f	Loading frequency in Hz
g	Acceleration due to gravity
$H_{(FP)}$ and $H_{(MP)}$	Lateral load on fin pile and monopile at same displacement
H_{max},	Maximum applied cyclic load
H_{min}	Minimum applied cyclic load
K_a	Rankine's active pressure coefficient
K_p	Rankine's passive pressure coefficient
K_q	Hansen's earth pressure coefficient
K_{rs}	Relative stiffness of pile
K_{br}	Meyerhof earth pressure coefficient
K_{br}	Coefficient of earth pressure at rest
L_f	Length of fin
L_p	Length of pile
l_a, l_c, l_2	Lengths of loading in the cyclic device
M	Bending moment of pile

m_1, m_2 and m_3	Mass of used in cyclic load test
MP	Monopile
N	Number of cycles
P_{sh}	Pressure on the shaft
P_w	Pressure on the wing can be defined as
R_p	Efficiency of fin in terms of pressure on shaft and fin
p	Horizontal Soil reaction
P_u, H_u	Ultimate lateral load pressure
s	Seconds
W_f	Width of pile
y	Pile lateral deflection
$y_{max, N}$	Maximum cyclic displacement
$y_{min, N}$	Minimum cyclic displacement
y_N	Accumulated pile head displacement
z	Depth of pile inside the soil
z_{ref}	Reference depth
ΔH	Cyclic loading amplitude
ϕ	Friction angle of soil
ϕ_p	Peak friction angle of soil
ϕ_r	Residual friction angle of soil
ψ	Dilatancy friction angle of soil
γ	Unit weight of soil
σ_v	Vertical earth pressure
η	Shape factor in Zhang's formula (for pressure in front of the pile)
ξ	Shape factor in Zhang's formula (for drag force at the side of the pile)
ζ_b,	Cyclic load magnitude

ζ_c	Cyclic load ratio
η_H	Lateral load efficiency of a finned pile
$\eta\theta$	Pile head rotation efficiency of a finned pile
$\eta\delta$	Pile head deflection efficiency of a finned pile
η_H	Lateral load efficiency of a finned pile
η_M	Bending moment efficiency of a finned pile
p_{max}	Maximum frontal passive earth pressure of soil ahead of pile shaft.
τ_{max}	Maximum side shear resistance of soil at pile shaft
δ	Interface friction angle between pile surface and soil
κ_w	Budge factor of a finned pile
K_h	Modulus subgrade reaction
n_h	Coefficient of subgrade reaction.
e_{max} and e_{min}	Maximum and minimum void ratio
θ	Pile head rotation
θ_N	Accumulated pile head rotation
$\mu\varepsilon$	Macrostrain
ω	Angular rotation

Abstract

The main objective of this thesis is to examine systematically the proposed improved performance of finned piles over monopiles when subjected to lateral static and cyclic loading. In order to achieve this objective, both physical and numerical simulations were conducted on finned and monopile and outcomes were analyzed for design recommendations. The physical tests were performed on scaled model piles at 1:100 reductions of typical wind turbine monopile foundations.

The cyclic lateral load tests were conducted on the scaled down foundation models at 1g condition. Cyclic tests were conducted to evaluate the long-term performance of the finned piles under cyclic wind loading conditions. Both the lateral and rotational responses of the foundation systems were evaluated at 1000 cycles of loading. The long-term performance at 10^7 cycles, defined as the fatigue limit state of the offshore wind turbine foundation, was derived from data fitting using power laws proposed by other researches. The results of both the static and cyclic lateral loading tests confirmed improved performance indicators of finned piles over monopiles. The major indicators were increased lateral capacity and decreased pile head rotation, both of which are important design and performance considerations of supported wind turbines, as the increase in lateral capacity translates into increase in factor of safety against excessive lateral pile head rotation.

The laboratory lateral static test results were verified numerically using PLAXIS modeler. The physical and numerical simulation results were found to corroborate well, allowing to determine the optimum fin dimensions from numerical analysis.

1

CHAPTER 1

1 GENERAL OVERVIEW

1.1 Background information

Various techniques have been used to increase lateral capacity of steel piles. Some of these techniques include improving the surrounding soil, increasing the size, number and length of piles and using expanded pile caps for piles in groups. For example, when an existing bridge foundation is found to have inadequate lateral resistance, additional piles or micro piles may be added. Subsequently, an expanded pile cap or connecting beams are often required to structurally integrate the new piles to the existing pile group. This approach, although proven to provide the required lateral resistance, can be relatively expensive and time consuming (NCHRP 697, 2011).

An alternative approach for increasing the lateral capacity of pile is employing soil improvement techniques to increase the strength and stiffness of the surrounding soil. Although soil improvement is cost effective and reduces construction time, few studies (NCHRP 697, 2011; Weaver and Chitoori, 2011) are available to fully evaluate and validate the effectiveness of this method.

Steel plates welded on to the perimeter of piles have been utilized to enhance the uplift and axial capacity of open ended steel piles for over four decades (Campbell et al., 1987; Lee and Gilbert, 1980; Lutenegger, 2012; Nottingham and Christopher, 1990; Reinert and Newarn, 2007). Fins welded orthogonally (i.e. straight) or at an angle

2

(i.e. slanted) onto the surface of a monopole, as shown in Figure 1-1, have been reported to increase the uplift and axial capacity of steel pipe piles. Tests conducted by Lee and Gilbert (1980) on straight finned piles in soft clay under static and repeated loading showed that presence of fins greatly improved the cyclic capacity of the monopile. Slanted finned piles have been reported to provide even higher bearing and uplift capacity. Nottingham and Christopher (1990) conducted field test and reported that slanted finned piles;

    (i)   Have high tensile capacity in a low embedded depth

    (ii) Can reduce the pile length by as much as 50% in soft soils under axial load

    (iii) Exhibit significant reserve strength with cyclic axial loading.

    (iv) Absorb large amount of energy though deflection without loss of strength.

Because of the above advantages, this type of pile has been used to increase pile tension capacity and provide enhanced positive anchorage near pile tip, negating the need to use larger or longer piles. In addition, short piles with straight fins have been used effectively to resists uplift forces on transmission towers (Reinert and Newark, 2007).

Model test on lateral capacity of finned piles have shown that fins can increase the lateral capacity of pile by as much as 80% (Duhrkorp and Grabe, 2008; Peng et al., 2005, Songlin, 2007). Cyclic load test on finned piles (Peng et al., 2011) showed that fins reduced the lateral displacement of the pile by 50%. PND Engineers in Anchorage Alaska have used spin piles (Figure 1-1) in marine environment to construct docks, dolphins, retaining wall tiebacks, wave barriers, seismic anchors and oil platform

3

foundations where uplift or impact load failures were anticipated. Because of their load deformation characteristics, these piles allowed substantial pile overload deformation without catastrophic failure after repeated loadings.

The use of fin piles in offshore wind turbine foundations has not been explored despite the numerous advantages they pose over monopiles. The support structure for offshore wind turbines (OWTs) plays a significant role in maintaining the structural reliability during their service lives. The cost of foundation contributes 15% to 40% of the total capital cost of an offshore wind project. The choice of a foundation in these structures has great potential in their overall cost reduction up to 6% by 2020 (The Oxford Institute for Energy Studies, 2015). The selection of foundation depends on the water depth, seabed soil condition, wave height, and turbine capacity. The monopile foundation has been widely used for the existing shallow water OWTs, which currently accounts for more than 78% of all the installed OWTs in Europe (Stiesdal, 2009).

This thesis aims studying the static lateral and cyclic lateral behavior of finned piles in comparison with monopiles, to propose an efficient and economic foundation system that satisfies the requirements of wind turbines under the specified loads.

1.2 Research Objectives

The main objective of this study is to evaluate the performance of finned pile foundation systems that can support offshore wind turbines considering both the capacity and serviceability requirements under lateral static and cyclic loading. In order to achieve this objective physical and numerical simulations were conducted on finned piles and monopiles.

The general objectives of the proposed study program are as following:

(a) To investigate the efficiency (i.e., ratio of the lateral load on the finned pile to that on the monopile at a specified pile head displacement or pile head rotation) of the fin in improving the lateral capacity of pile with respect to the number and the orientation of the fins, and the direction of loading. The effect of the fin in shortening the required pile length is investigated.

(b) To evaluate soil pile-interaction of finned and monopiles and estimate the ultimate lateral capacity of multi-finned (i.e., two, three and four fins) piles in non-cohesive soils.

(c) To investigate the effect of fins in reducing the accumulated pile heads rotation under long term one-way cyclic loading.

5

(d) To determine the fin dimensions (i.e., length and width), and their positioning along the pile (i.e., top, middle or bottom) that will result in maximum efficiency.

1.3 Methodology and novelty of the approach

This research investigates the performance finned pile foundations proposed for wind turbines under lateral static and cyclic loading using experimental and numerical approaches. The new processes and findings identified as original contributions are:

1) A detailed comparative study of the fin piles with monopiles has been performed to better understand and benchmark the behavior of finned piles. The efficiency of fin in reducing the required length of pile; and the effect of the number of fins and the orientation of fin with respect to lateral loading direction on the lateral capacity of the pile have been explored effectively and explained clearly in this study.

2) Soil-pile interaction of instrumented piles has been studied and the p-y curves for both the finned and the monopiles developed. Experimental p-y curves have been compared with the theoretical p-y curves suggested by other researchers.

3) Long-term lateral cyclic response of the finned piles has been investigated and the efficiency of the finned pile was compared to that of the monopile at fatigue limit state.

6

4) Numerical simulation of the finned and monopile behavior under static lateral loading verified the experimental data to elucidate the behavior of the fin piles. The benchmarked analysis helped determine the optimum dimensions and positioning of the fins as well as the effect of the fin area on the fin efficiency.

1.4 Outline of the thesis

This study is based on mostly experimental and partially on numerical methods. Because of the difficulties and constrains of performing field tests on actual piles under static and cyclic lateral loads, scaled model tests at 1g were proposed and conducted in the laboratory. The experimental results were validated through numerical analysis using PLAXIS™ software. The experimental results were also compared with relevant information available in literature.

This dissertation is organized in seven chapters with the framework presented in Figure 1-2. A brief outline of each chapter is provided as follows:

Chapter 1 outlines the background of this research and it identifies the need for better understanding of the behavior of finned piles proposed for wind turbine pile foundations subjected to lateral cyclic loading. The main and specific objectives of the dissertation and the research program required to accomplish these objectives are briefly outlined. The original contributions of this study are identified and presented.

Chapter 2 provides a literature review of various types of foundation systems currently constructed for offshore wind turbines, and the methods used to estimate the lateral capacity of the piles used in these systems. Also provided in this chapter is a

7

review of various laboratory scale equipment developed by other researchers that have been used to study lateral cyclic loading of model piles.

In Chapter 3, a comprehensive description of the experimental work carried out in the laboratory is provided. Detailed information about the materials, such as the properties of the sand used to construct the soil medium for testing; description of the test setup, instrumentations; determination of the appropriate scaling factors, boundary effects; description of the test box preparation, loading mechanism, and the pile models used in the research are presented. Analysis of the benchmarked (i.e., with respect to the monopile) results from static lateral load test of piles with different number of fins and the effect of varying load direction with respect to the fin orientation are provided. The resulting fin efficiency in various configurations of the fins is presented in this chapter, also. Finally, the effect of fin in reducing the required length of monopile is determined and presented.

Chapter 4 discusses the response of instrumented model piles to lateral static loading. The multi-finned piles (i.e., two, three and four fins) and monopile were instrumented with strain gauges and earth pressure gauges. The bending moment and earth pressure distribution were determined along the length of the piles. Pile *p-y* curves were derived from the earth pressure data for both the finned and monopiles.

Chapter 5 presents the analysis of the results from the one-way cyclic testing of the finned and monopiles. One-way cyclic loading was applied to the piles at different cyclic load ratios. The results were used to evaluate the effects of fins in reducing

accumulated pile rotation. Long-term cyclic efficiency of finned pile was estimated and benchmarked.

The results of the numerical modelling of the finned and monopiles are presented in Chapter 6. The laboratory test results from static tests were verified numerical simulation. The optimum dimensions and positioning of fins were determined and suggested for design of finned foundation systems.

Lastly, Chapter 7 summarizes the main findings of this research and provides recommendations for future studies and research.
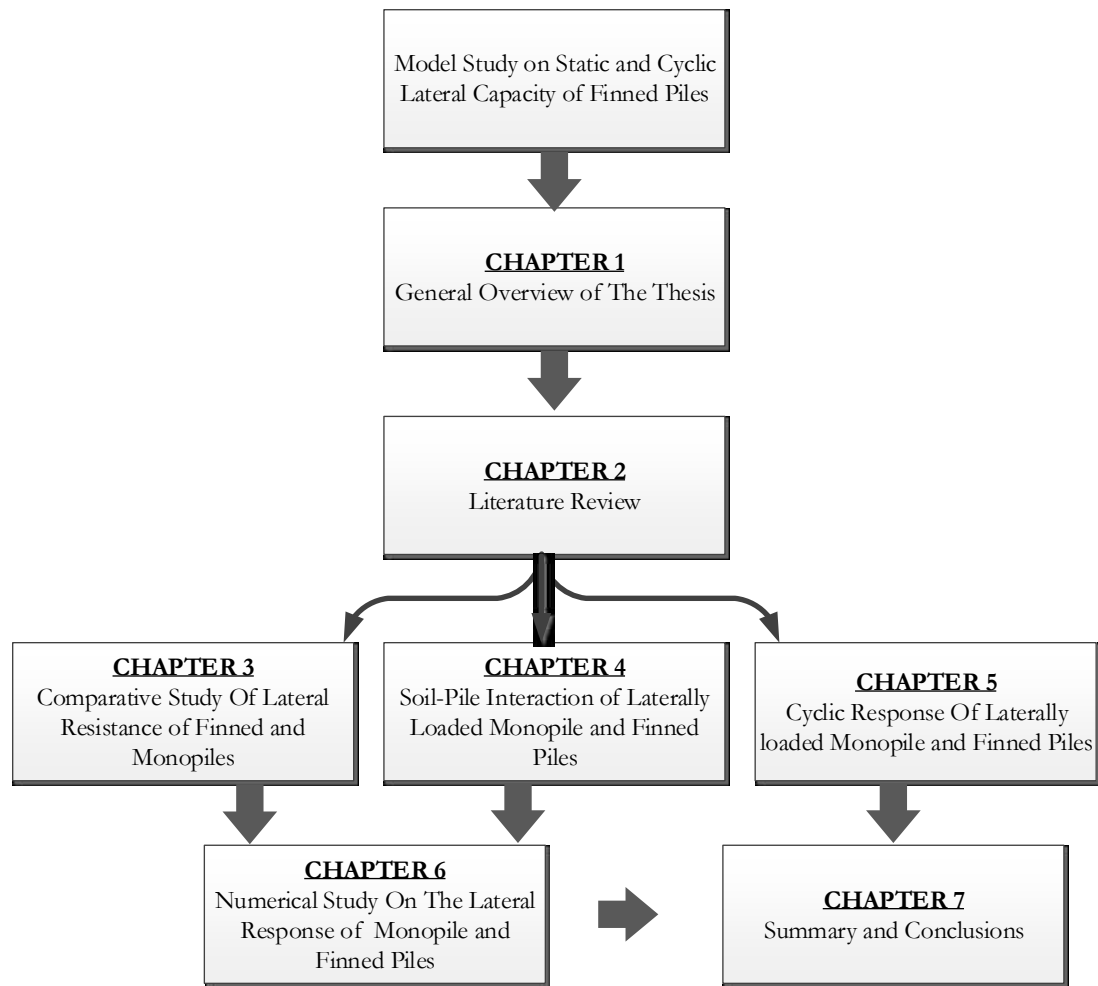
1.5 References

1. Campbell, R. Christopher, A. and Nottingham, D., (1987): Use of Fins on Piles for Increased Tension Capacity (Spin-Fin Piles). *Alaska Department of Transportation Final Report No. FHWA-AK-RD-87-16*, 50.

2. Duhrkop, J. and Grabe, J. (2008): Improving the lateral bearing capacity of monopiles by welded wings. *Proc. of the 2nd BGA International Conference on Foundations*, 1: 849-860.

3. Lutenegger, A. (2012): Tension Tests on Driven Fin Piles for Support of Solar Panel Arrays. *GeoCongress* 2012: 305-314.

4. Lee, P. Y. and Gilbert, L. W. (1980): The Behavior of Steel Rocket Shaped Pile," *Symposium on Deep Foundation, ASCE*: 244-266.

5. Nottingham, D. and Christopherson, A. (1990): Spin-Fin Pile Technology. *Proceedings of the 15th Annual Deep Foundations Members Conference*, 15

6. Peng, J. (2005): Behavior of finned piles in sand under lateral loading: PhD Thesis, University of New Castle Upon Tyne

7. The Oxford Institute of Energy (2015): Achieving a Cost-competitive Offshore Wind Power Industry: what is the most effective policy framework? https://www.oxfordenergy.org/wpcms/wp-content/uploads/2015/09/EL-15.pdf

8. TRB (2011): Design Guidelines for Increasing the Lateral Resistance of Highway-Bridge Pile Foundations by Improving Weak Soils. *NCHRP Report 697*.

9. Reinert, G.J and F. Barry Newman, F.B (2007): Steel Finned-Pipe foundation for single Pole Structure" *Proc of Electrical Transmission in a New Age*: 292-299.

10. Songlin, W. (2007). "Horizontal Resistance Behavior of Pile with Wings in Sand". *Proceedings of the 32nd Deep Foundations Annual Members Conference* (7): 253-259.

11. Stiesdal, H. (2009): Hywind. The world's first floating MW-scale wind turbine, *Wind Directions*, 31: 52-53.

12. Weaver, T.J and Chitoori, B (2007): Influence of Limited Soil Improvement on Lateral Pile" *Proc of Soil improvement, ASCE GSP,* 172: 1-10.

CHAPTER 2

2 LITERATURE REVIEW

2.1 Introduction

Today's focus on renewable energy sources as replacement for fossil fuels has caused the onshore and offshore wind industries to expand rapidly. World usage of renewable energy in the coming few decades has been estimated to represent about 10% of the generated energy by 2050 (ISEP, 2016: https://www.isep.or.jp/en/).

Pile foundations are widely used as foundations for wind farms or as anchors for floating facilities for oil and gas production (Bienen et al., 2012). Engineering experience with foundations for the offshore structures was derived mainly from the structural and operational requirements of the petroleum industry. However, there is a major difference between the foundations supporting the oil platforms and the wind turbines due to the difference in horizontal to vertical loads ratio. For wind turbine foundations, this ratio is much higher, which requires different foundation systems to support the large horizontal forces and the associated large moments. Considering the wind loads from the turbine and the water level at the installation site, different foundations options become more economically viable. For more than two decades of offshore wind turbines farms, the accumulation of experience and the advent of innovative powerful equipment now enable the installation of suitable foundations for these facilities. Generally, shallow foundations are considered as gravity structures in

small water depths (Fig. 2-1a). For larger water depths, deep foundation systems are used involving large diameter steel piles (Fig. 2-1b). For deep waters, suction caissons and tetrapod foundations or even floating foundation systems are used (Fig. 2-1c) (Abdelkader, 2016).

(a) Gravity Base   (b) Monopile   (c) Suction Caissons
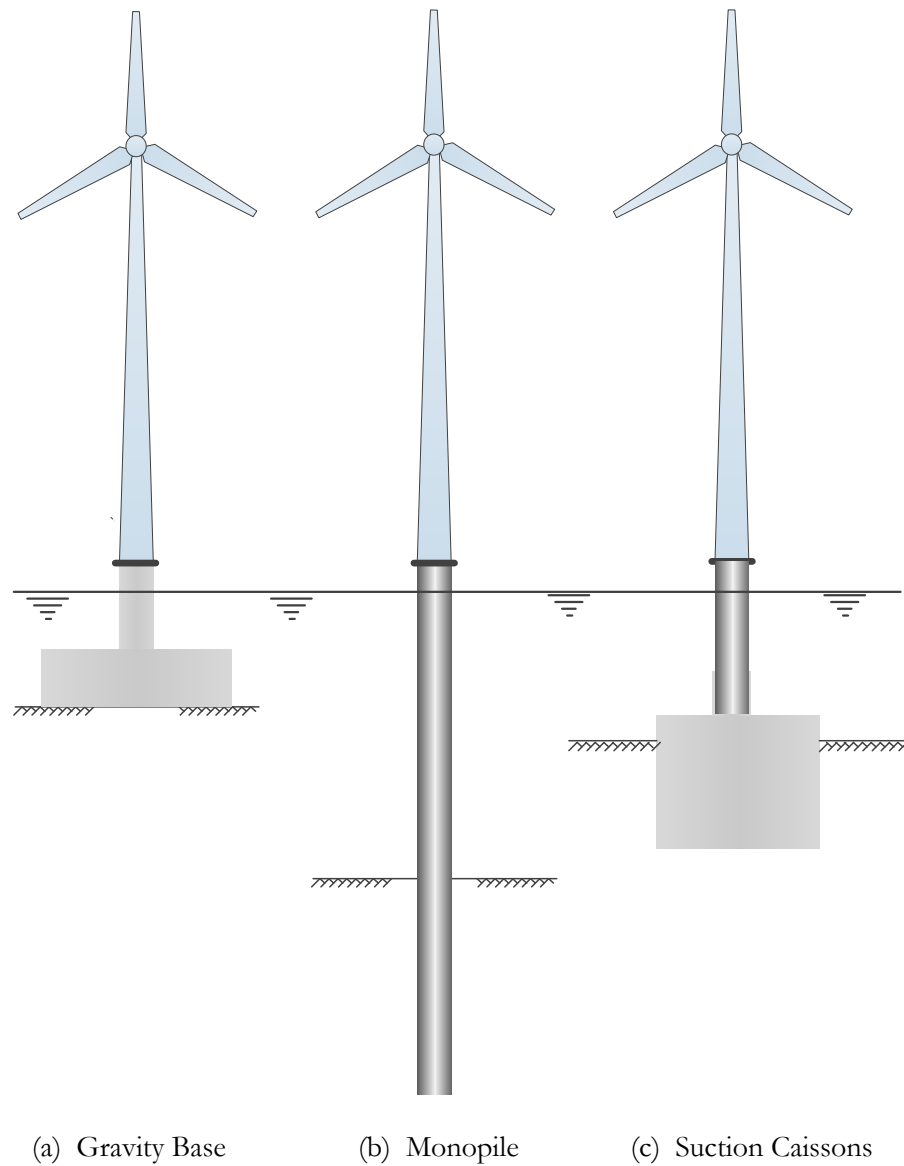
Wind turbine foundations for onshore or offshore structures have received much attention in an effort to develop new economical and reliable techniques, particularly with reduced construction cost (Houlsby and Byrne, 2001). Initial investigations were conducted on hybrid foundations by Carder and Brooks (1993). The hybrid foundation was an innovative system which comprised of a combination of shallow foundation and pile. Thus, the system performed similar to a retaining wall with a stabilizing base (Carder and Brooks, 1993). Another concept was to strengthen the pile by welding metal plates at its head to enhance its lateral and rotational resistance (Irvine et al., 2003; Lee and Gilbert, 1980).

By 2015, a total of 2920 support structures were fully installed in European offshore wind farms. The proportion for each type of the support structure is shown in Figure 2-2. The most commonly used were monopiles, where 2301 units were installed by the end of 2014 (78.8%). Gravity based foundations came second with 303 units installed (10.4%), followed by jacket foundations (137 units: 4.7%), tripods (120 units: 4.1%) and tri-piles (55 units: 1.9%). Two fully floating structures were already in the water in 2014 (EWEA, 2015).

2.2 Foundation Types for Offshore Wind Energy Converters

Offshore wind turbines need to be fixed to the seabed with a permanent or semi-permanent support structure. For deep waters a floating structure is used but the most common ones are the fixed foundations used at shallow depths (up to 50 meters).

14

Triples 55, 1.9%
Tripods 120, 4.1%
Jacket 137, 4.7%
Experimental 2, 0.1%
Floating 2, 0.1%
Gravity 303 10.4%
Monopiles 2,301 78.8%
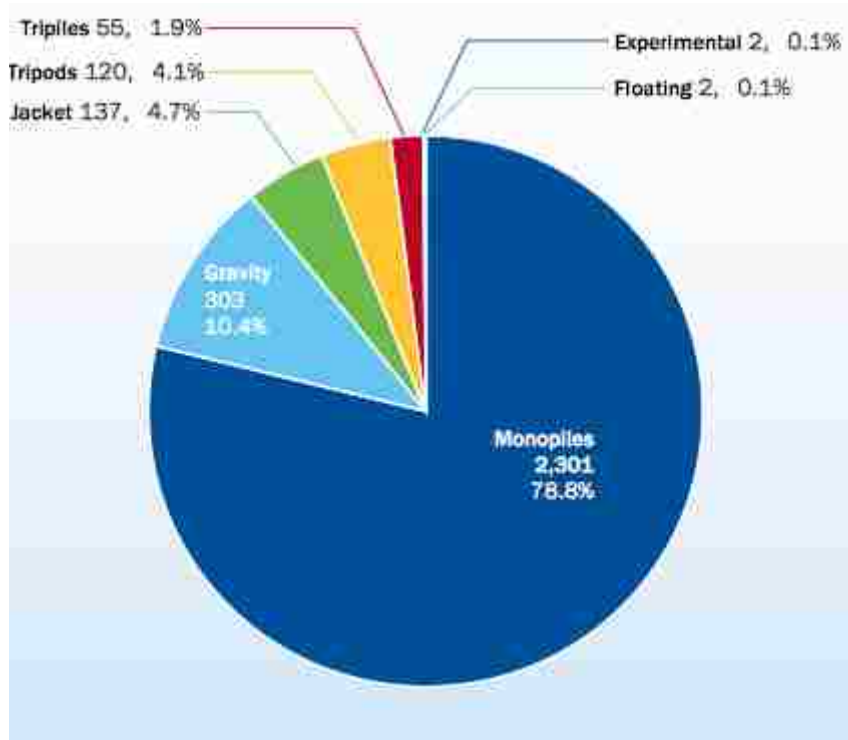
There are four types of foundations used for offshore wind turbines: gravity base foundations, suction buckets, floating foundations and monopiles. Each of these foundation systems is best suited for a particular water depth and as described below.

2.2.1 Gravity base foundation

Gravity base type foundation consists of an extremely heavy base, placed over the seabed as seen in Figure 2-3. It is a widely accepted traditional type of foundation for offshore structures. Gravity base foundation is mostly used for shallow depth water of 10m. It has been used mostly in Norwegian coast and in North Sea in UK for medium depth offshore structures. Gravity base foundation is designed against the failure modes of sliding, tilting, lifting and bearing capacity. In this type of foundation,

15

bearing capacity of the seabed and consolidation settlements should be considered. The wave and current forces in the water, along with high wind loading may lead to tilting or sliding of the foundation (Peng, 2003).

Bearing capacity limitation of the seabed brings about technical limitations to the design, hence performance expected from the structure for lateral loading that satisfy the tilting stability. Gravity base foundations often have large volumes and surface areas, resulting in increase of hydraulic forces due to waves and currents in the water. Increase in diameter of the structures results in increase of their mass. Gravity base foundation is not commercially preferred due to some of these physical limitations (Soker et al. 2000).
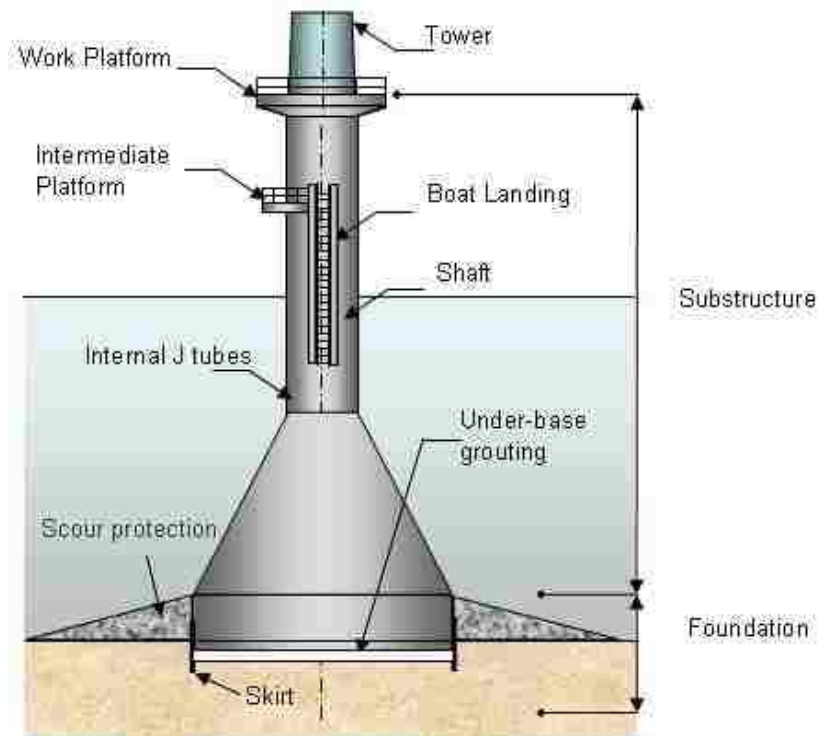
Calculations for the bearing capacity analysis of these structures are similar to those of shallow foundation capacity calculations. Bearing capacity equations by Meyerhof et al. (1978) are used. Site specific ground investigations such as SPT or CPT provide important information for design calculations (Peng, 2003). Sites where soft rock such as chalk is present can be suitable for the bearing capacity requirements for gravity base foundations, but site investigations should be done thoroughly (Zaaijer, 2001). In areas where high liquefaction risk is present in bottom sand, gravity base cannot be the preferred foundation type.

2.2.2   Suction Buckets

Suction buckets are tubular steel foundations that are installed by sealing the top and applying suction inside the bucket (Zaaijer et al. 2001). Water is evacuated from sealed bucket by a pump from the internal cavity and a net downward pressure is applied to the foundation forcing it to penetrate the seabed. This hydrostatic pressure difference between inside and outside the bucket, and the deadweight of the structure cause the bucket to be filled with the seabed material as it sinks into the ground and fixing it to the seabed slowly. These foundation systems have been constructed in the Norwegian oil and gas fields in North Sea, and in Angola coast (Birck and Gormesen, 1999). Figure 2-4 shows the illustration of suction bucket foundations.

The suction bucket foundation type is especially suitable when seabed material mainly consists of sands or soft clays. Suction bucket is not a favorable foundation type for water depths more than 15m. A diameter to length ratio of 10 is a practical maximum, which depends on water depth and soil properties (Birck and Gormesen, 1999).

The main shortcoming of this system is that, in the long term after construction, the soil inside the bucket will drain causing the suction force to reduce. In addition, lack of wide practical experience and unsuitability of suction bucket foundations for higher water depths makes other foundation choices more favorable.

(Source: https://psmag.com/news/could-giant-suction-cups-turn-lake-erie-into-a-regional-energy-hub)

2.2.3 Monopiles foundations

Monopile foundation (Figure 2-5) is one of the most popular and simplest offshore wind foundations, and it has been used widely in the last few decades. This foundation accounts for 78.8% of all existing ones in wind farms installed in Europe by the end of 2014 with total of 2301 of foundations (EWEA, 2015; Wang et al., 2018). The foundation is made of a hollow steel cylinder with a diameter of 3–6m and a length of 20–50m; and 40–50% of the length is inserted into seabed to provide the required resistances (DNV, 2013). The monopile foundation is constructed onshore and transported to designated location and installed by the pile driving. In this operation seabed preparations are not necessary.

(Source: https://www.scheuerle.com/communication/press/press-releases/detail/getarticle/News/detail/1300-tonnes-worlds-largest-monopile-1.html)

2.2.4 Floating foundations

Floating type foundations for offshore wind energy converters have developed since 1990s and they have the potential to provide usage of large sea surface area for wind turbines to be located. Floating foundations are suitable for steeper seabed conditions and very high water depths up to 500m (Tong, 1998). Figure 2-6 shows various types of floating foundations.

Floating wind power plants have different types of support structures. Some of them are anchored to seabed by one or several tension piles. The anchorage cables can be fixed to a tripod structure which holds the turbine and tower (Novem, 2002). Design of tension piles uses the same principles as in the calculation of the pull-out resistance of piles. Grouting can be required to lower their scour sensitivity at the anchorage location on seabed.
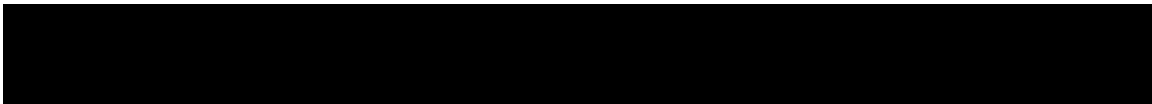
2.3 Tower and foundation load for wind turbine structures

DNV (2013) regulations state that a wind turbine structure must be analyzed for various loads that it will experience during its design life, including:

i. Aerodynamic loads that result from wind, drag and lift forces.

ii. Inertia loads that result from gravity, rotation, vibration, or gyroscopic motion.

iii. Functional loads from transient operation conditions of turbine such as braking torque, yawing and blade pitching moments, or transmitting power to generator.

iv. Other loads resulting from other environment sources such as waves and ice.

Figure 2-7 shows the loading acting on an offshore wind foundation.
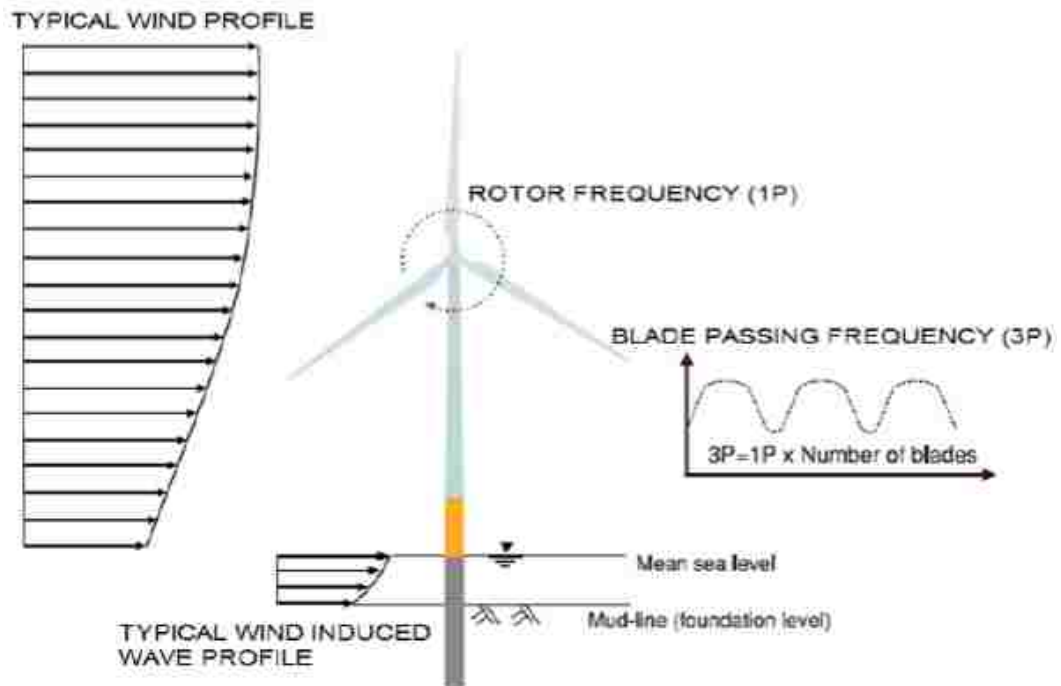
2.4 Frequency of loading of wind turbine foundation

Figure 2-8 presents the fundamental concept of the design frequency range for an offshore wind energy system. The response spectra in terms of power spectral density are plotted in the frequency domain for a Vestas V120 MW offshore wind turbine in the North Sea. The rotational speed of modern wind turbines typically ranges from 8.6-18.4 revolutions per minute, and the first excitation frequency (1P), which corresponds to a full revolution, typically ranges from 0.15-0.26 Hz. The 3P is defined as the blade passing frequency and is approximately 0.47-0.77 Hz for a three-bladed wind turbine. The 3P frequency results from shadowing effects of the blade on the tower caused by a drop in the upstream wind velocity in the vicinity of the tower as each of the three blades passes in front of the tower. An example of the dynamic wind loading is also shown in Figure 2-8. In this depiction Froya wind spectrum (Andersen and Lovseth, 2006) is used. The dynamic wave loads are modelled using the Pierson and Moskowitz (1964) spectrum at which predominant wave frequency is 0.1Hz, corresponding to10s wave period.

In order for turbines to remain unconditionally stable, and avoid unplanned resonance effects, they have to be designed to minimize the magnitude of the dynamic load applied to them. There are two challenges (Bhattacharya et al., 2011):

a) The foundation stiffness must be estimated accurately from the available soil data.

b) The potential for change in foundation stiffness with time as a result of the cyclic loading must be understood so that the risks of the system frequency coinciding with a loading frequency that can lead to resonance conditions can be avoided.
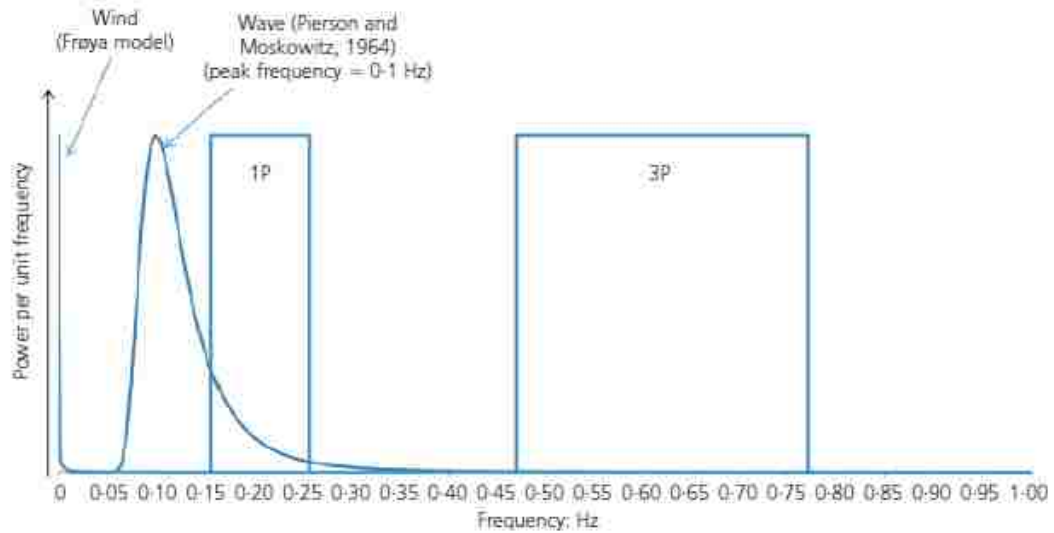
2.5 Lateral load transfer mechanism of single pile

The bearing capacity of a laterally loaded pile is mobilized due to the interaction between the pile displacement and the resistance of the soil also known as soil-pile interaction (Briaud and Smith 1983; and Smith, 1987). The applied load is carried by the single pile as a combination of soil pressures and friction acting on the pile. The soil response from these forces needs to be seen from a 3-dimensional perspective. A 2D sketch of the pressures acting on a pile cross section is shown in Figure 2-9. The pile is subjected to soil pressure and friction on the side of the pile. To simplify the 3-dimensional friction and pressure distributions, all these factors are merged into one single soil resistance, sometimes called the *modulus* approach. The ultimate lateral resustance (P_u) on a pile can then be calculated as the effective stress (σ_v) at a given

23

point multiplied by an earth pressure coefficient (*K*) and the pile diameter (*D* and integrated over the length of the pile (L). This can be written as:

$$P_u = \int_0^L KD\sigma_v \, dz \qquad (2\text{-}1)$$
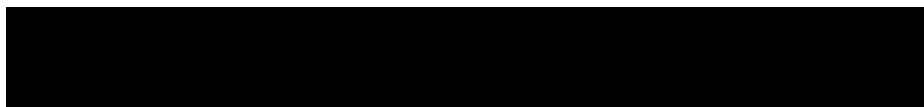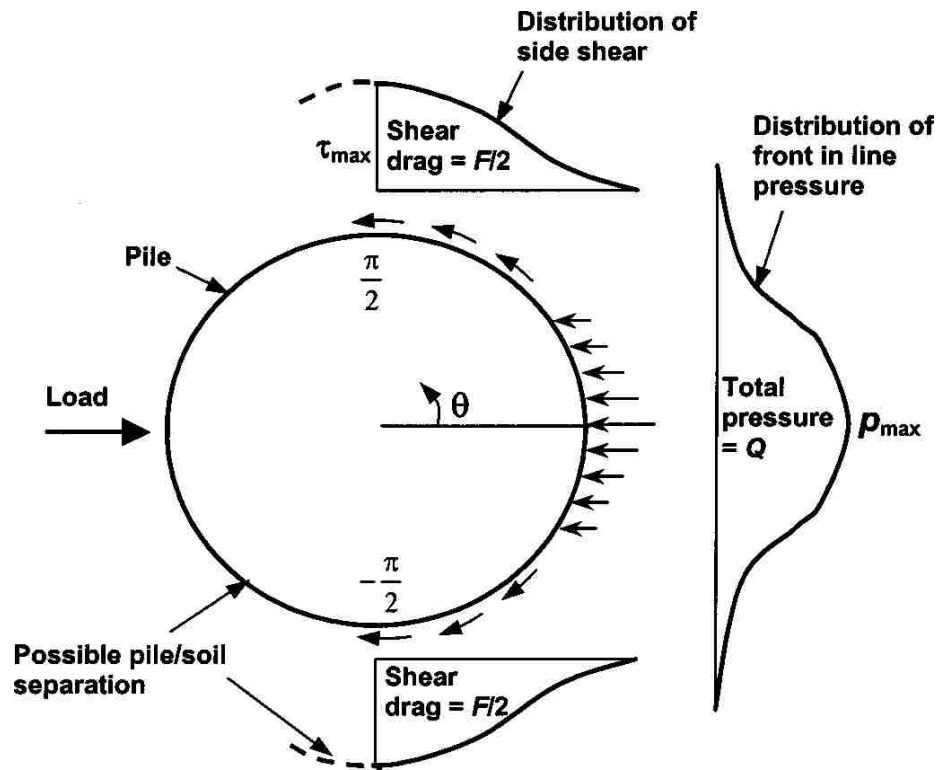
2.6 Methods of analysis of single pile under static lateral load

Various numerical and empirical approaches have been developed by many researchers for analyzing the static and cyclic lateral responses of single piles. Although these methods make slightly different assumptions, they can generally be classified as:

1) Ultimate resistance methods (Brinch Hansen, 1961; Broms, 1964; Meyerhof et al., 1981)

2) Subgrade reaction methods (Kishida et al., 1985; Matlock, 1970; O'Neill and Murchison, 1983; Reese et al., 1974). Some of the methods are briefly described below.

2.7 Ultimate lateral resistance methods

Numerous methods have been published in the literature for predicting the ultimate lateral resistance of piles in cohesionless soils (Brinch Hansen, 1961; Broms, 1964; Fleming, 1992; Meyerhof et al., 1981; Petrasovits and Award, 1972). The main difference between these methods is the assumed distribution pattern of the lateral earth pressure in front of pile during loading (Figure 2-10). Therefore, each method results in a different value for ultimate lateral load for the same soil conditions. After full mobilization of the lateral soil pressure due to lateral loading, some methods assume that pile rotates at the pile base, such as in the Broms method (1964). Other methods proposed by Petrasovits and Award (1972), Prasad and Chari (1999), Brinch Hansen (1961), and Meyerhof et al. (1981) consider that the point of pile rotation resides at a certain depth below the ground level.

25

2.7.1 Hansen method

Brinch Hansen (1961) recommended a method for the calculation of the ultimate lateral resistance of free-head rigid piles in uniform or layered soils. The ultimate lateral load acting on the pile can be calculated using Equation 2.2. The earth pressure coefficient K_q is based on earth pressure theory. A trial and error procedure is used to find the rotation point that satisfied the lateral force equilibrium. The ultimate lateral resistance of soil per unit length of the pile is obtained from equation 2-2.

$$p_u = K_q \sigma_v \qquad (2\text{-}2)$$

The parameter K_q is the Hansen's earth pressure coefficient which is a function of the internal friction angle of soil, ϕ, and the ratio of embedded depth to diameter of pile, z/D.

a) Brinch Hanson (1961) b) Broms (1964) c) Petrasovits & Award (1972) d) Meyerhof et al. (1981) e) Prasad & Chari (1999)

Deflection
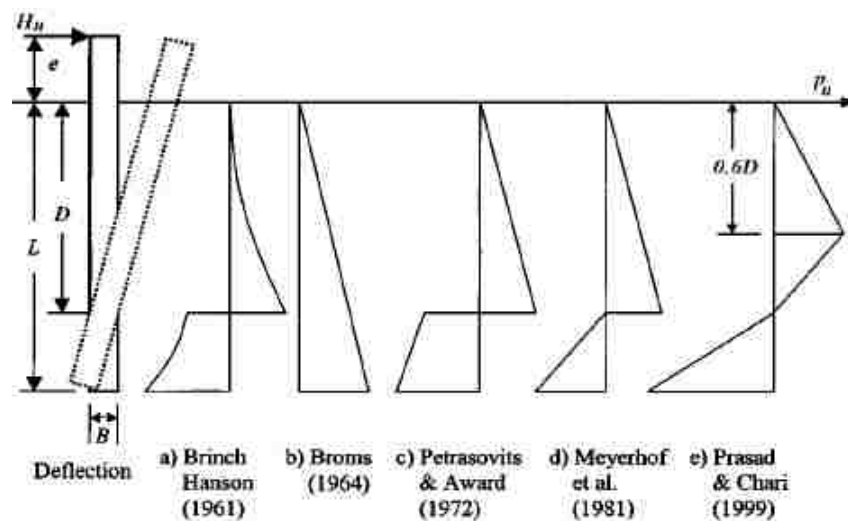
2.7.2 Broms method

Broms (1964) developed an empirical solution for predicting the behavior of laterally loaded rigid and flexible piles. For rigid piles failure occurs due to shear failure in soil whereas in flexible piles, ultimate failure load relates to the section properties of the pile. Broms method assumes that when displacement takes place due to lateral load, soil in front of the pile moves upwards and soil at the back of the pile moves downwards to the space generated by the movement of the pile. Based on this assumption, Broms method ignores the effect of pile rotation. The active soil pressure at the back of the pile is also ignored. On the other hand, soil pressure is multiplied by Rankine passive earth pressure coefficient and a factor 3 which is relatively conservative according to the field test results (Poulos and Davis, 1980). Equation (2-3) presented Broms approach for computation of the ultimate resistance of the soil per length of pile:

$$p_u = 3K_p \sigma_v \qquad (2\text{-}3)$$

2.7.3 Meyerhof method

Meyerhof et al. (1981) provided a solution for the analysis of laterally loaded rigid and flexible piles. According to their method, a flexible pile is defined when the relative stiffness of the pile, K_{rs} is less than 0.014, as described below:

$K_{rs} = E_p I / E_s L^4 < 0.014$

Where

E_s: Horizontal soil modulus at pile tip; E_p: Elasticity modulus of pile

27

L: Embedded length of the pile; *I:* Moment of inertia of the pile

Meyerhof et al. (1981) proposed that ultimate lateral load, *Qu*, can be expressed by net earth pressure computed using a lateral earth pressure coefficient K_{br}, function of the internal friction angle of soil as well as the shape of the pile (Equation 2-4). Shape of the pile is considered by the ratio of *D* to *L* in the coefficient.

For rigid piles in sand;

$$Q_u = 0.12 \gamma D L^2 K_{br} \qquad (2\text{-}4)$$

In Meyerhof method, the rotation point of pile is assumed at the tip of the pile and the soil reaction is assumed to be linear.

2.7.4 Petrasovits and Award method

Petrasovits and Award (1972) recommend that the ultimate lateral resistance per length of pile be calculated by Equation 2-5. Reactions of both passive and active pressures are considered in the equation and a shape factor of 3.7 is introduced.

$$p_u = (3.7 K_p - K_a) \gamma L \quad (2\text{-}5)$$

Where

p_u: Ultimate resistance of the soil per unit pile length; K_p: Rankine's passive pressure coefficient; K_a: Rankine's active pressure coefficient; γ: Unit weight of soil (kN/m^3); *L:* Embedded length of the pile

2.7.5 Fleming method

Fleming (1992) recommended the following form of Equation (2-5) for calculating the ultimate pile resistance.

28

$$p_u = 3K^2{}_p\sigma_v \qquad (2\text{-}6)$$

2.7.6 Prasad and Chari method

Prasad and Chari (1999) proposed Equation 2-7 for predicting ultimate soil resistance for laterally loaded pile in cohesionless soil.

$$p_u = 10^{(1.3tan\phi+0.3)}\sigma_v \qquad (2\text{-}7)$$

In Prasad and Chari method the depth of pile rotation is given as a function of embedment length and the load eccentricity.

2.7.7 Zhang method

More recently, Zhang et al. (2005) proposed a method for calculating the ultimate lateral soil resistance to piles in cohesionless soil considering both the frontal soil resistance and side shear resistance, as given by Equation (2-8) below:

$$p_u = (\eta p_{max} + \zeta \tau_{max}) \qquad (2\text{-}8)$$

Where,

η is the shape factor to account for the non-uniform distribution of earth pressure in front of the pile (Table 2-1); ζ is the shape factor to account for the non-uniform distribution of lateral shear drag (Table 2-1); p_{max} is maximum frontal passive earth pressure of soil ahead of pile shaft; and τ_{max} is maximum side shear resistance of soil at pile shaft.

Pile shape	η	ζ
Circular	0.8	1.0
Square	1.0	2.0

Values of (p_{max}) and (τ_{max}) are calculated using Equations 2-9 and 2-10, respectively.

$$p_{max} = K^2{}_p\sigma_v \qquad (2\text{-}9)$$

$$\tau_{max} = K_s\sigma_v tan\delta \qquad (2\text{-}10)$$

Where, *Ks* is lateral earth pressure coefficient (ratio of horizontal to vertical effective stress) and *δ* is interface friction angle between pile surface and soil, mostly a function of soil type and its density.

2.8 Subgrade reaction approach

A laterally loaded pile has often been treated as a beam on an elastic foundation as shown in Figure 2-11. For a true elastic medium, the soil reaction (*p*) and the deflection (*y*) at a given point are affected by reactions and deflections at all other points on the beam. Vesic (1961) has shown that the error inherent in Winkler's hypothesis is not significant. In the Winkler soil model, the soil reaction per unit length of pile (*p*) and lateral displacement (*y*) at a point are assumed to be related through a modulus of subgrade reaction (*K$_h$*) given bu equation 2-11 and 2-12 (Reese and Matlock, 1956).

$$K_h = \frac{P}{D} \qquad (2\text{-}11)$$

$$K_h = n_h z \qquad (2\text{-}12)$$

Where,

K_h = modulus subgrade reaction, (in units of F/L^3); D = diameter or width of pile (in units of L); n_h= coefficient of subgrade reaction.

Pile is usually assumed to act as a thin strip whose behavior is governed by standard beam-column Equation (2-13):

$$E_p I_p \frac{d^4 y}{dz^4} + p = 0 \qquad (2\text{-}13)$$

$E_p I_p$ and p are the bending (flexural) stiffness of pile and the lateral load per unit length of pile, respectively.

Prototype   Idealized using Winkler Spring Method
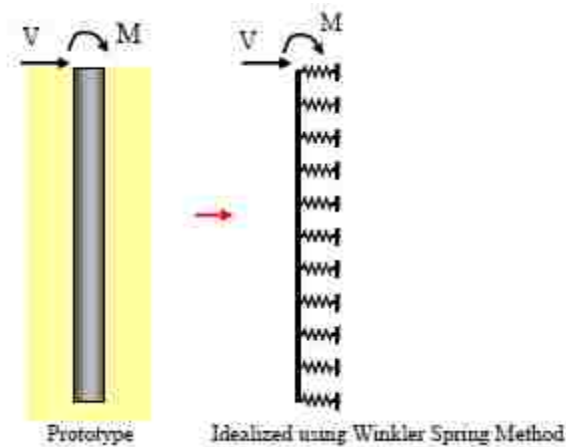
The above formula is known as the governing differential equation for elastic curve of a laterally loaded pile. Hence the subgrade reaction approach is based on the solution of the forth order differential equation (Equation 2-12), and it can be used for both free-and fixed head single piles. The nonlinear '*p-y*' curves for piles in sand described by Reese et al. (1974) and O'Neill and Murchison (1983), which were basically obtained from two full scale slender pile tests led to recommendations in the standards such as API, 1993. This method, which is adapted in the standards, uses a procedure to construct non-linear '*p-y*' curves for monopiles in sand subjected to cyclic loading as a function of the static ultimate lateral resistance (p_u), as given by equation (2-14).

$$p = Ap_u(\frac{K_h z}{Ap_u}y) + P = 0 \qquad (2\text{-}14)$$

The parameter *A* in Equation 2-14 is a reduction factor which was used to fit full-scale results on slender piles, and it was found to be *A*=0.9 for cyclic loading, and *A*=3-0.8*z*/*D* for monotonic loading.

Many methods for constructing "*p-y*" curves for various types of soil and loading conditions (static and cyclic) have been developed during the past few decades. Table 2.2 lists some of these methods found in the literature (Alladdwar, 2017).

Reference	'p-y' function	Remarks
Reese et al. (1974)	Relatively complex curves consist of four segments with the first and second straight lines connected by a parabola and the third straight line starting at 3B/80.	(1) Developed from results of full-scale field tests in clean fine sand; (2) The ultimate p_u is attained at y_u of $3B/80$ for any given set of 'p-y' curves.
O'Neill and Murchison (1983)	$$p = Ap_u \tanh\left(\frac{K_i z}{Ap_u} y\right)$$ $A = 0.9$ for cyclic loading $A = 3-0.8z/B$ for static loading	(1) Using a single analytical hyperbolic tangent function to describe 'p-y' curves; (2) Having defined p_u but y_u changing with depth; (3) The p_u is calculated from Reese et al. (1974).
Yan and Byrne (1992)	$$p = E_{max} y \quad (y < \rho^2 B)$$ $$p = \rho B E_{max}\left(\frac{y}{B}\right)^{0.5} \quad (y > \rho^2 B)$$ $\rho = 5(D_r)^{0.8}$ E_{max} = the maximum soil Young's modulus.	(1) Developed from results of small-scale model tests in fine silica sand; (2) the shape of 'p-y' curves is controlled by E_{max} which varies with depth, but 'p-y' curves have no defined p_u.
Wesselink et al. (1988)	$$p = RB\left(\frac{z}{z_0}\right)^d \left(\frac{y}{B}\right)^m$$ $z_0=1m$, R=650 kPa, d=0.7, and m= 0.65	(1) Empirical 'p-y' formula based on centrifuge model pile tests in calcareous sands; (2) the increase power curves never reach an ultimate resistance p_u.
Georgiadis et al. (1992) Castelli and Mougeri (2009)	$$p = \frac{y}{\frac{1}{K_i} + \frac{y}{p_u}}$$ K_i is the initial modulus of subgrade reaction	(1) Using a hyperbolic function to describe the 'p-y' curves; (2) The ultimate resistance p_u can be evaluated using Reese et al. (1974).

33

2.9 Laboratory cyclic loading

Peng et al., 2006 identified number of mechanical, electro mechanical and hydraulic loading devices used to impart cyclic loads on model piles. The most common devices are shown in Figure 2-12. Among these, the gravity, the gear drive and the hydraulic drive systems are commonly used for static loading (Figure 2-12 a-c). They have also been used in limited cyclical loading tests by manually controlling the loading systems (Peng et al. 2004; El Naggar and Wei 1999). The statnamic device in Figure 2-12 d has been successfully used in a field test with low loading frequency ranging from 0 to 10 Hz (Janes et al. 1991). There is no evidence of this equipment being tried in a laboratory test yet. The vibration system shown in Figure 2-12e has been used to provide cyclic loading with higher frequencies up to 50 Hz. These frequencies of loading are not suitable to model wind farm loading (Blaney and O'Neill 1989). The pneumatic loading device in Figure 2-12 f has been successfully used in one-way cyclic loading with up to 500 cycles in each test (Ramakrishna and Rao 1999). The mechanical loading system shown in Figure 2-12 g uses a gear box to control one-way or two-way cyclic loading at different frequencies (Purkayastha and Basack 1999). A three degree-of-freedom loading ring was used to provide combined loading in the system depicted in Figure 2-12 h where cyclic vertical and horizontal loads as well as moments were possible at the same time (Byrne and Houlsby 2004). A mechanical load rig driven by motor, originally developed by Rovere (2004), was used successfully to apply cyclic loads to a model pile (Le Blanc et al., 2010) and a model caisson foundation (Zhu et al., 2013).

34
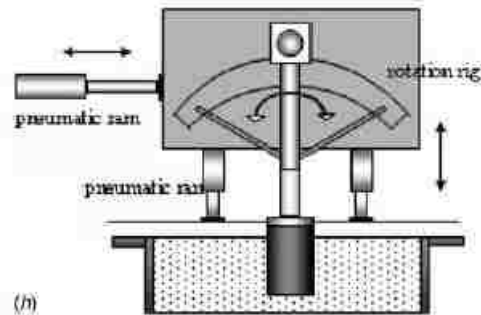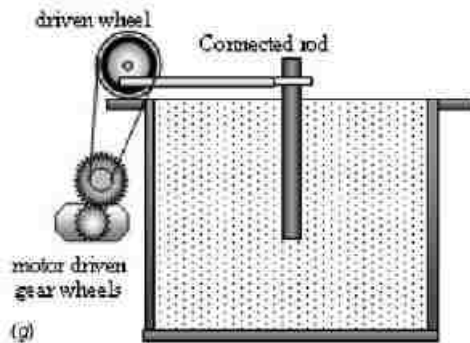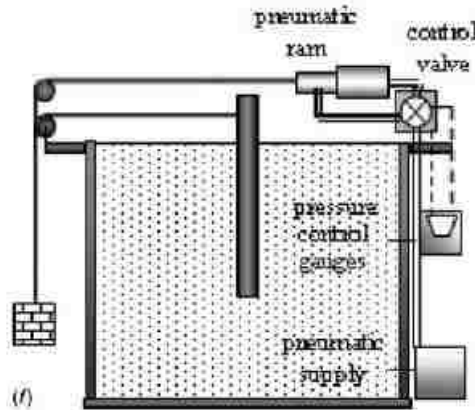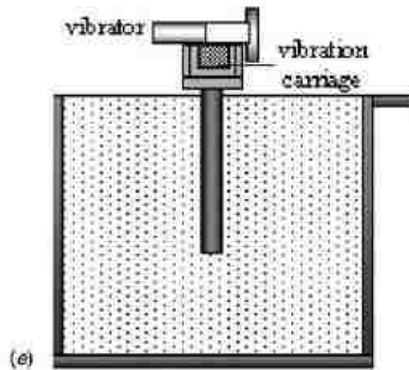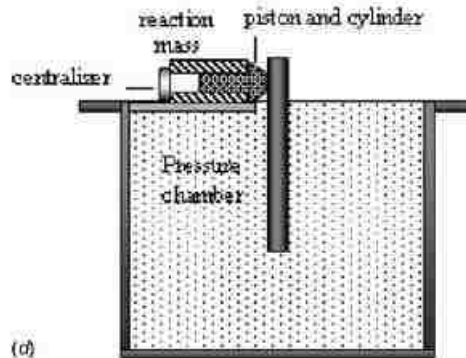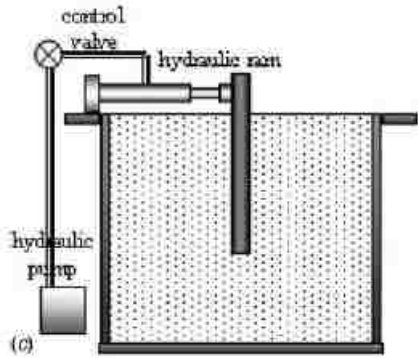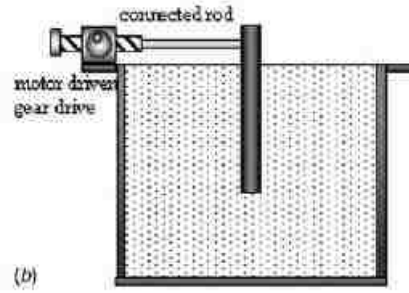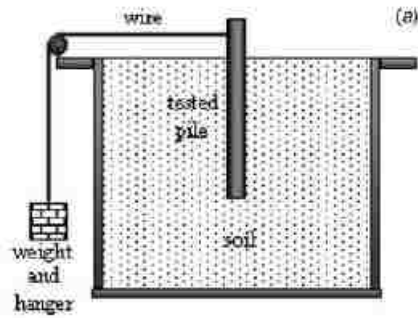
2.10 Summary and Issues to be addressed

This chapter reviewed the previous findings and developments in analysis of single monopile in sandy soils and subjected to lateral cyclic and static loading, with emphasis on those used for wind turbines. The literature review covered the following aspects: common types of wind turbine foundations used in the practice, loading patterns of wind turbines, traditional methods of analysis of lateral loading for single piles, assumptions of soil reaction around monopile due to lateral displacement, and the characteristics of the common static and cyclic loading devices used for conducting model pile load test.

The following academic and practice related issues remain unresolved, which will be attempted to address in this dissertation:

1. It has been emphasized by many that supporting foundation for offshore wind turbines (OWTs) plays a significant role in maintaining the structural reliability of these facilities during their service lives. During its life time, wind turbine will be subjected to long term sustained cyclic and/or repeated loading, magnitudes of which may also be cyclic in nature, such as ocean waves, wind, and sediment movement. Repeated loading and unloading of the supporting piles can lead to accumulated displacements and rotation of the pile head (Chang and Witman, 1988). Hence, large accumulation of displacement and rotation of pile head are likely to occur during the life time of wind turbine support piles (Leblance et al., 2010). Since finned piles have shown to improve lateral resistance of piles, they constitute good candidate foundation components to use to mitigate

36

accumulation of lateral displacement and potentially reduce rotation at pile head. There exists a need to better evaluate the effect of fins in improving the lateral displacement of piles under cyclic loading.

2. As fins are placed at select locations along the embedded depth of a pile and are not continuous, a finned pile can be considered a hybrid structure that exhibit different behaviors in the finned and the un-finned sections (i.e., moment of inertia). The soil resistance distribution resulting on the finned section of the pile should be investigated closely for clear understanding of the lateral behavior of the whole pile. Furthermore, influence of the orientation of the fins with respect to the loading direction and the changing geometry of the pile has not been studied adequately. A better understanding of the finned pile behavior for improved design and its recommendation for offshore wind turbine foundation structures hinges on these important analyses.

2.11 References

1. Abdelkader, M.R. (2016): *Investigation of hybrid foundation system for offshore wind turbine*. The University of West Ontario, Canada.

2. Andersen, O. J. and Lovesth, J. (2006): The Froya database and maritime boundary layer wind description. *Marine Structures* 19 (23): 173-192.

3. API. (1993): Recommended practice for planning, designing, and constructing fixed offshore platform: Working stress design, RP2A-WSD. 20th edition.

4. Bhattacharya, S., Lombardi, D. and Moor Wood, D. (2011): Similitude relationship for physical modelling of mono-pile supported wind turbines. International Journal of Physical Modelling in Geotechnics 11 (2):58-68.

5. Bienen, B., Duhrkop, J., Grabe, J., Randolph, M., and White, D. (2012): Response of piles with wings to monotonic and cyclic lateral loading in sand. Journal of Geotechnical and Environmental Engineering 138 (3): 364-375.

6. Birck, C. and Gormsen, C. (1999): Recent Developments in Offshore Foundation Design. *Proceedings of the European Wind Energy Conference*, France.

7. Blaney, G. W. and O'Neill, M. W. (1989) "Dynamic Lateral Response of Pile Group in Clay," *Geotechnical Testing Journal,* 12: 22–29.

8. Briaud, J.L. and Smith, T. D. (1983): Using the pressure meter curve to design laterally loaded piles. *Proceeding 15th Offshore Technology Conf.,* Houston, Paper 4501:495–502.

9. Brinch Hansen, J. (1961): The ultimate resistance of rigid piles against transversal forces. *Bulletin No. 12, Danish Geotechnical Institute*, Copenhagen, Denmark, pp. 5–9.

10. Broms, B.B.(1964): Lateral resistance of piles on cohesionless soils. *Journal of Soil Mechanics and Foundation Division, ASCE*, (SM3), Vol. 90, No. 3, pp. 123–156.

11. Byrne, B. W. and Houlsby, G. T. (2004): Experimental Investigation of the Response of Suction Caissons to Transient Combined Loading," *Journal of Geotechnical and Geoenvironmental Engineering,* 130 (3): 240–253.

12. Carder, D.R. and Brookes, N J. (1993). *Discussion in the Retaining structures (ed.C. R. I. Clsyton)*, pp.498-501. London: Thomas Telford.

13. Chang, C.S. and Whitman, R.V. (1988).: Drained permanent deformation of sand due to cyclic loading, *Journal of Geotechnical and Geoenvironmental Engineering, ASCE*, 96, (4):1605-1627

14. DNV (2013). Design of Offshore Wind Turbine Structures.

15. El Nagger, M. H. and Wei, J. Q., (1999): Response of Tapered Piles Subjected to Lateral Loading," *Canadian Geotechnical Journal,* 36: 52–71.

16. European Wind Energy Association. (2015). *The European offshore wind industry – key trends and statistics 2014* (1st edition). Retrieved from EWEA website:

17. Houlsby G.T. and Byrne B.W. (2001) "Novel Foundations for Offshore Wind Farms", Research Proposal to EPSRC (August 2001), Department of Engineering Science, Oxford University.

18. https://psmag.com/news/could-giant-suction-cups-turn-lake-erie-into-a-regional-energy-hub.

19. https://www.scheuerle.com/communication/press/pressreleases/detail/getarticle/News/detail/1300-tonnes-worlds-largest-monopile-1.html.

20. https://www.wind-energy-the-facts.org/offshore-support-structures.html

21. Institute for Sustainable Energy Policies, 2016: https://www.isep.or.jp/en/.

22. Irvine J.H., Allan P.G., Clarke B.G., Peng, J. (2003): Improving the lateral stability of monopile foundations. *International Conference on Foundations*, BGA, UK: 371-380.

23. Janes, M. C., Bermingham, P.D., and Horvath, R.C. (1991): An Innovative Dynamic Test Method for Piles," *Proceedings of 2nd International Conference on Recent Advances in Geotechnical Earthquake Engineering and Soil Dynamics*, St. Louis, pp. 252–256.

24. Kishida, H., Suzuki, Y., and Nakai, S. (1985): Behavior of a pile under horizontal cyclic loading. Proceeding of 11th ICSMFE, San Francisco, Vol. 3, pp. 1413-1416.

25. LeBlanc C., Houlsby G.T. and Byrne B.W. (2010): Response of stiff piles in sand to long-term cyclic lateral loading. *Géotechnique* 60 (2): 79-90.

26. Lee, P.Y. and Gilbert, L.W. (1980): The Behavior of Steel Rocket Shaped Pile *Symposium on Deep Foundation*, ASCE. 244-266.

27. Matlock, H. (1970): Correlations for design of laterally loaded piles in clay. Proceeding of 2nd Annual Offshore Technology Conference, Vol. 1, Houston, pp. 577-594.

28. Meyerhof, G. G. and Hanna, A. M., (1978): Ultimate Bearing Capacity of Foundations on Layered Soil under Inclined Load. *Canadian Geotechnical Journal* 15 (4):565-572.

29. Meyerhof, G. G., Mathur, S. K. and Valsangkar, A. J. (1981): Lateral resistance and deflection of rigid wall and piles in layered soils. *Canadian Geotechnical Journal*, 18: 159–170.

30. Novem (2002): Study to feasibility of and boundary conditions for floating offshore wind turbines

31. O'Neill, M., and Murchison, J. (1983): An evaluation of p-y relationships in sands. A report to the American Petroleum Institute, PRAC 82-41-1, University of Texas, Huston.

32. Peng, J., Clarke, B.G. and Mohamed Rouainia, M. (2006): A Device to Cyclic Lateral Loaded Model Piles. *Geotechnical Testing Journal*, 29 (4): 341-347.

33. Peng, J., Rouainia, M., Clarke, B., Allan, P., and Irvine, J. (2004): Lateral Resistance of Finned Piles Established from Model Tests. *Proceedings of the International Conference on Geotechnical Engineering–Beirut*, CFMS, Lebanon, pp. 565–571.

34. Peng, J., (2003): Offshore renewable energy foundations pp. 54-64.

35. Petrasovits, G., and Award, A. (1972): Ultimate lateral resistance of a rigid pile in cohesionless soil. Proceedings of 5th European Conference on Soil Mechanics and Foundation Engineering, Madrid, Vol.3, pp. 407-412.

36. Pierson, W.J., and Moskowitz, L. (1964): A proposed spectral form for fully developed wind seas based on the similarity theory of SA Kitaigordskii. *Journal of Geophysical Research* 60 (9): 715-721.

37. Poulos, H. G. and Davis E. H. (1980): *Pile Foundation Analysis and Design*, Wiley, New York.

38. Prasad, Y. V. S. N. and Chari, T. R. (1999): Lateral capacity of model rigid piles in cohesionless soils. *Soils and Foundations*, 39 (2):21–29.

39. Purkayastha, R. D. and Basack, S. (1999): Response of Model Piles Under Cyclic Loadings. *International Conference on Offshore and Nearshore Geotechnical Engineering*, pp. 227–232.

40. Ramakrishna, V. G. S. T. and Rao, S. N. (1999): Critical Cyclic Load Levels for Laterally Loaded Piles in Soft Clays. *International Conference on Offshore and Nearshore Geotechnical Engineering*, pp. 301–307.

41. Reese, L.C., Cox, W.R., and Koop, F.D. (1974): Analysis of laterally loaded piles in sand. Proceeding of 6th Annual Offshore Technology Conference, Vol. 2, Houston, pp. 473-484.

42. Reese, L.C. and Matlock, H. (1956): Non-dimensional solutions proportional to depth. Proceedings of 8th Texas conference on Soil Mechanics and Foundation Engineering, Special publication No.29, Austin, pp. 1-41.

43. Rovere, M. (2004): *Cyclic loading test machine for caisson suction foundations*. Politecnico di Milano, Milan, Italy.

44. Smith, T. D. (1987): Pile horizontal soil modulus values. *Journal of Geotechnical Engineering* 113 (9) :1040–1044.

45. Soker, H., Rehfeldt, K., Santjer, F., Strack, M. and Schreiber, M., (2000). *Offshore Wind Energy in the North Sea*. Deutsches Windenergie-Institut (DEWI), Wihelmshaven.

46. Tong, K. C. (1998): Technical and economic aspects of a floating offshore wind farm. *Journal of Wind Engineering and Industrial Aerodynamics,* 74-76 (98): 399-410.

47. Vesic, A. B. (1961): Beams on elastic subgrade and Winkler's hypothesis. *Proceeding of 5th International Conference on Soil Mechanic and Foundation Engineering*, Paris, : 845-850.

48. Wang, X., Zeng X., Yang, X. and Li, J (2018): Feasibility study of offshore wind turbines with hybrid monopile foundation based on centrifuge modeling. *Journal of Applied Energy* 209:127–39.

49. Zaaijer, M. B. (2001): Suction bucket foundation Feasibility and pre-design for the 6 MW DOWEC", *Delft University of Technology, Wind Energy Section,* Delft, The Netherlands

50. Zhang, L., Silva, F. and Grismala, R. (2005): Ultimate lateral resistance to piles in cohesionless soils. *Journal of Geotechnical and Geoenvironmental Engineering*, 131 (1): 78-83.

51. Zhu, B., Byrne, B.W. and Houlsby G.T. (2013): Long term lateral cyclic response of suction caisson foundations in sand. *Journal of Geotechnical and Geoenvironmental Engineering, ASCE* 139(1): 73-83.

CHAPTER 3

3 COMPARATIVE STUDY OF LATERAL RESISTANCE OF FINNED AND MONOPILES

3.1 Introduction and Background

Model tests on lateral capacity of finned piles have shown that fins can increase the lateral capacity of a pile by as much as 80% (Peng et al., 2005, Songlin, 2007; Duhrkorp and Grabe, 2008; Nasr, 2013). Fins have also been used to reduce the length of piles required to carry axial load in soft clay by as much as 50% (PND Engineers: http://www.pndengineers.com/research-and-development/applied-research-development/spin-fin-piles). It is anticipated that fins welded on the sides of the piles may also be used to reduce the required length of a pile needed for lateral load capacity. This may be particularly advantageous for offshore wind turbine foundations where the length of the pile drive into the sea bed can be up to 12 times the diameter of the pile (Byrne and Houlsby, 2003). The advantage of fins in reducing the required length of laterally loaded piles need to be investigated and its merits are weighed against those of monopile without fins.

In most cases lateral loads exerted on piles, particularly in the offshore environment, not only vary in magnitude but also in direction. Most of the previous studies on piles have considered uni-directional loading on circular monopiles where the lateral resistance do not change with the direction of loading. It is anticipated that

finned piles (with two, three or four fins) may exhibit difference in resistance with the direction of loading. Such variations in lateral resistance need to be understood adequately to select the best configuration of fins that minimize the anticipated variation of lateral resistance with direction of loading.

Finned piles have been used in groups to carry axial loads. Experience has shown that finned piles can reduce the required length and number of piles in a group to support the axial load% (PND Engineers:http://www.pndengineers.com/research-and-development/applied-research-development/spin-fin-piles).

When piles in a group are loaded laterally, the group behavior is generally different from that of a single pile due to the interaction of neighboring piles. There is often reduction in lateral load capacity of subsequent rows of piles the magnitude of which depends on the spacing between the piles. If the spacing between the piles is small, shadowing effect due to shear zone in front of the pile (illustrated in Figure 3-1) will greatly reduce the resistance of piles in the subsequent rows.

It's not clear how finned piles' spacing may affect their lateral load capacity if they were to be used in a group. It is important to recognize that as fins will modify significantly the behavior of a single pile, it will be difficult to determine the optimum pile-to-pile spacing to reduce the interference of finned piles in group. Determining the size and distribution of the respective shear zones created with finned piles of different configurations (i.e., different number of fins) may provide us with insight to predict optimum spacing of finned piles in groups.

A study on the behavior of finned piles under lateral loading may be achieved through suitable physical model tests with scaling adjustments. In this chapter, three main issues that motivated these experimental investigations, namely the effect of fins in reducing the required length of a pile to sustain lateral load; the effect of variation of the direction of loading with respect to the orientation of the fin on lateral resistance; and the size and distribution of the shear zone in front of the finned piles are investigated.
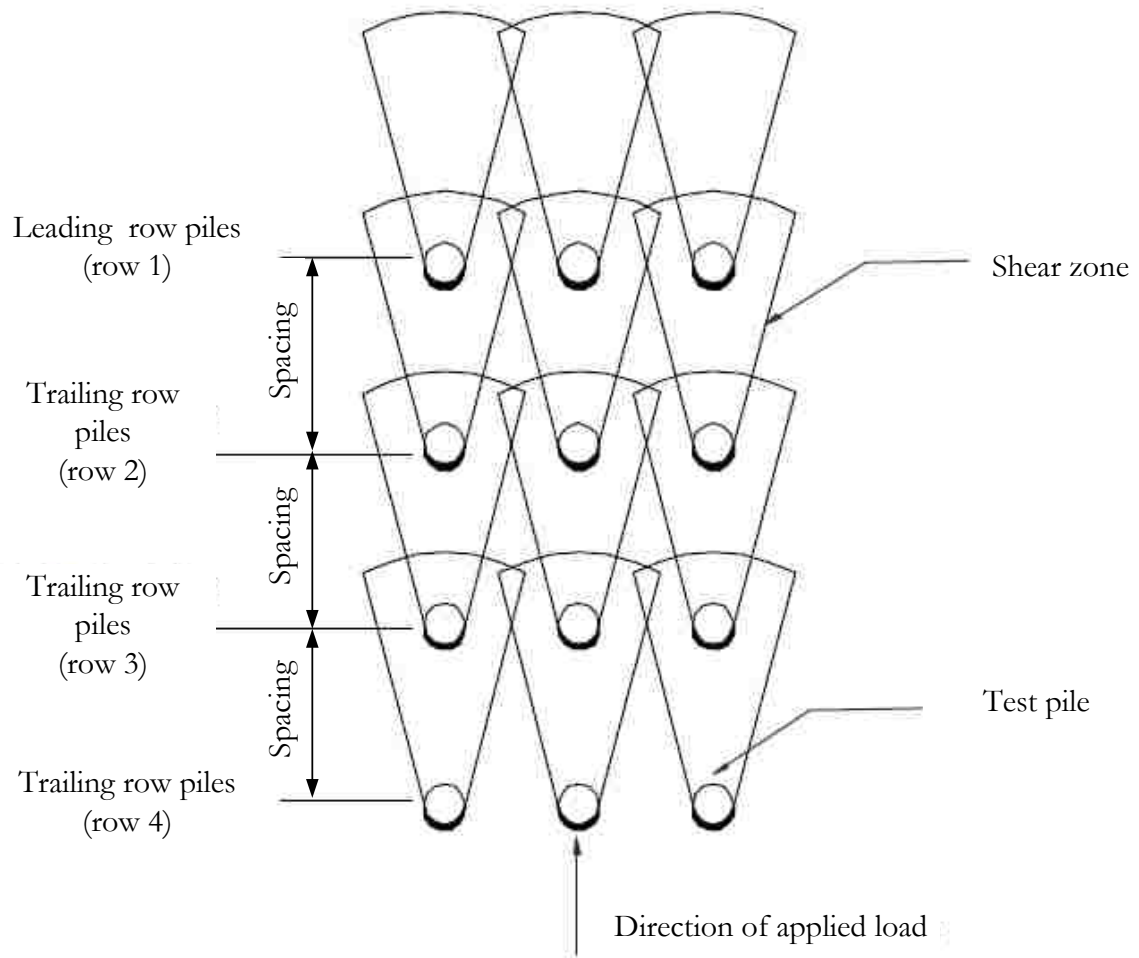
3.2 Aim of the study

In principle, the main purpose of the experimental investigations described in the chapter was to conduct a comparative study on the lateral resistance of finned pile (with two, three and four fins) and monopole taking into consideration length of pile, direction of loading and extend of shear zone in front of pile. The particular goals of this portion of the study were:

i.   To investigate the advantage of added fins in reduction of required monopile length for lateral loading.

ii.   To investigate the effect of loading direction with respect to the orientation of the fins and determine optimum lateral capacity.

iii. To investigate the size and distribution of the strain wedge for a laterally loaded fin pile.

3.3 Experimental Preparation

3.3.1 Experimental soil box

A steel soil box of dimension 0.9 m length, 0.7 m width and 0.7 m depth was constructed to conduct the lateral load tests for model piles in the laboratory. Figure 3-2 below shows a schematic representation of the test equipment. In this set up, similar to one used by Ramakrishna and Rao (1999) (see Figure 2-12 f) lateral load is applied though a cable attached to the pile. The cable runs over a frictionless pulley

47

and carries the weights required to apply a specified lateral load. Load cell and linear variable transducers (LVDTs) are mounted appropriately to measure the loads applied to the piles and the resulting horizontal displacement. The load cell and LVDTs records are collected by a data logger.
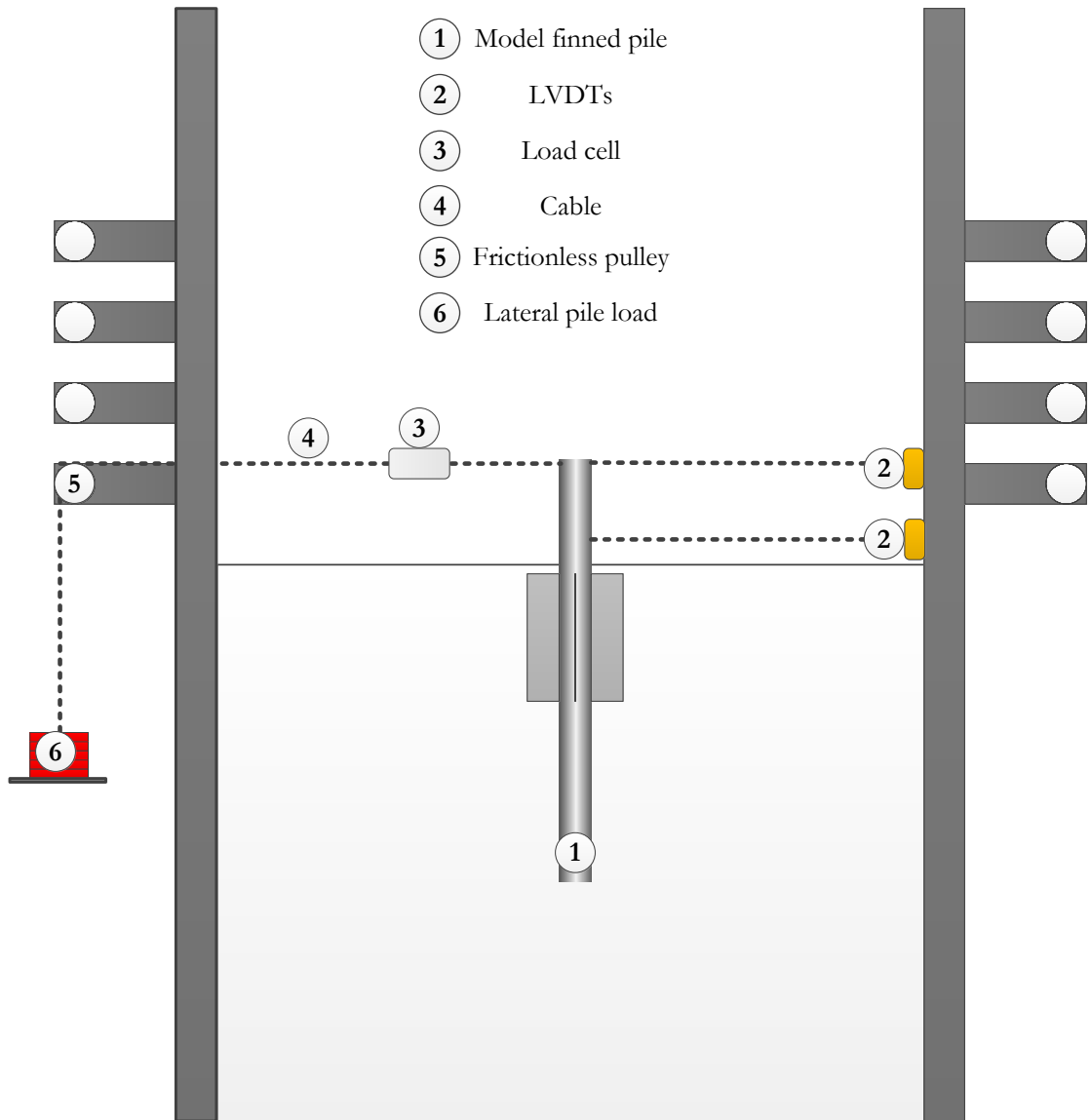
3.3.2 Materials

Dry silica sand is used as the soil substrate in all tests. Using the vibrating table test procedures (ASTM D 4253 and ASTM D 4254 (2006)), the characteristic maximum and minimum void ratios (i.e., e_{max} and e_{min}) of the sand were determined as 0.96 and 0.53, respectively. The specific gravity of the sand was determined as 2.65 (ASTM D 854 (2014)). The particle size distribution curve of the test sand is shown in Figure 3-3. The D_{10}, D_{30}, D_{50}, D_{60} indices were determined as 0.24mm, 0.42mm, 0.58mm and 0.63mm. The sand was classified as UNIFORM or POORLY GRADED with uniformity coefficient of C_u= 2.62, and coefficient of gradation of C_c= 1.16.

49
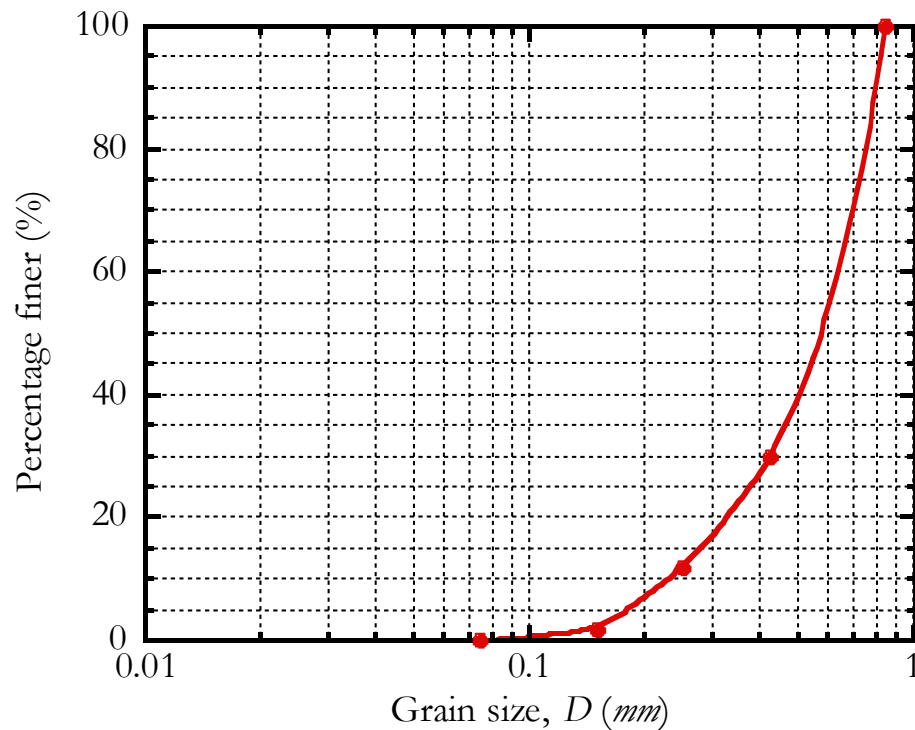
3.3.3 Characterization of soil

Direct shear test was conducted on a sample of the test sand at 32% relative density (γ =16.0 kN/m^3) according to ASTM D 3080 (2012). Five tests were conducted at vertical stresses of 31, 63, 94, 125 and 156 kPa. The shear stress versus displacement curves were developed as shown in Figure 3-4. The normal stress versus peak and residual stresses are presented in Figure 3-5 along with the fitted trend lines representing the failure and residual curves.

Using the results from the five tests the peak and residual soil the friction angles were obtained as ϕ_p =35.3° and ϕ_r =32.5°, respectively. The angle of dilatancy, ψ of 3.5° was obtained from the peak and the residual angle of friction (Bolton, 1986; Houlsby, 1991; Wood, 1984) using Equation 3-1.

$$\phi_p = \phi_r + 0.8\psi \qquad (3-1)$$

$$\tan \phi_p = 0.70926 \ \sigma_v$$

$$\tan \phi_r = 0.63794 \ \sigma_v$$
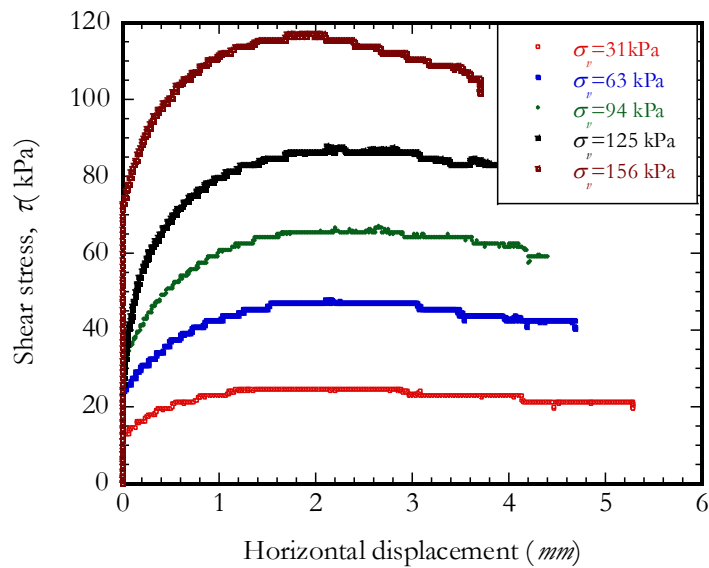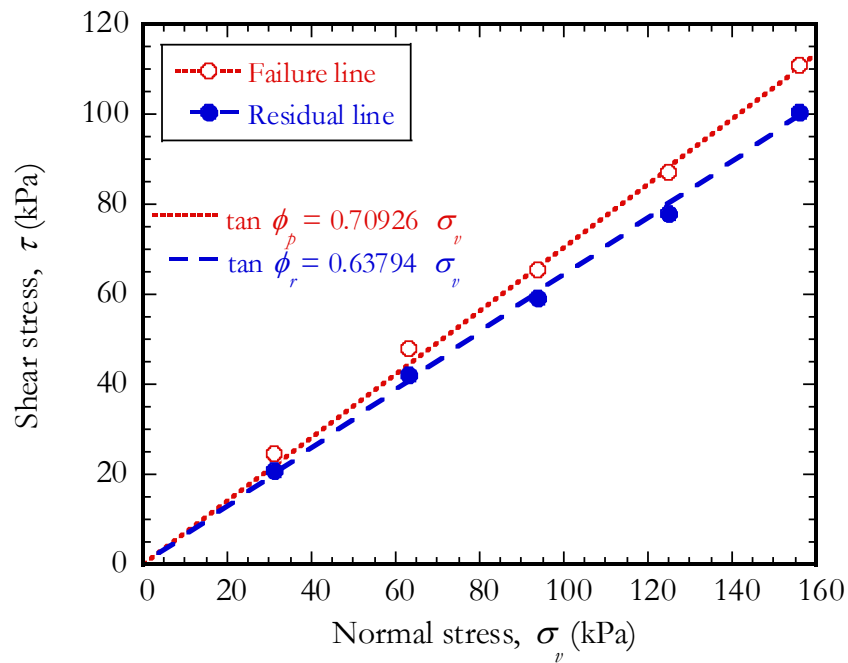
3.3.4 Model piles

Open ended steel pipe piles of 4cm outer and 3.8cm inner diameter were used in all the tests. These piles were designated as "short" type, as their length to diameter of pile ratio (L_p/D_p) was set at 9 (Byrne and Houlsby, 2003). The total length of the pile under test was 52cm, of which 36cm was embedded into the soil through driving. The lateral load was applied at the top of the pile providing an eccentricity of 16cm above the packed soil surface. The fins consisted of steel plates of 1mm thickness. Following the available findings for optimal fin dimensions in literature (Peng et al., 2011; Nasr, 2013), the length of fin to length of pile (L_f/L_p) ratio, and the width of fin to diameter of pile (W_f/D_p) ratio were selected as 0.45 and 1.0, respectively. A picture of the instrumented mono and finned piles tested under monotonic lateral load are given in Figure 3-6.

51
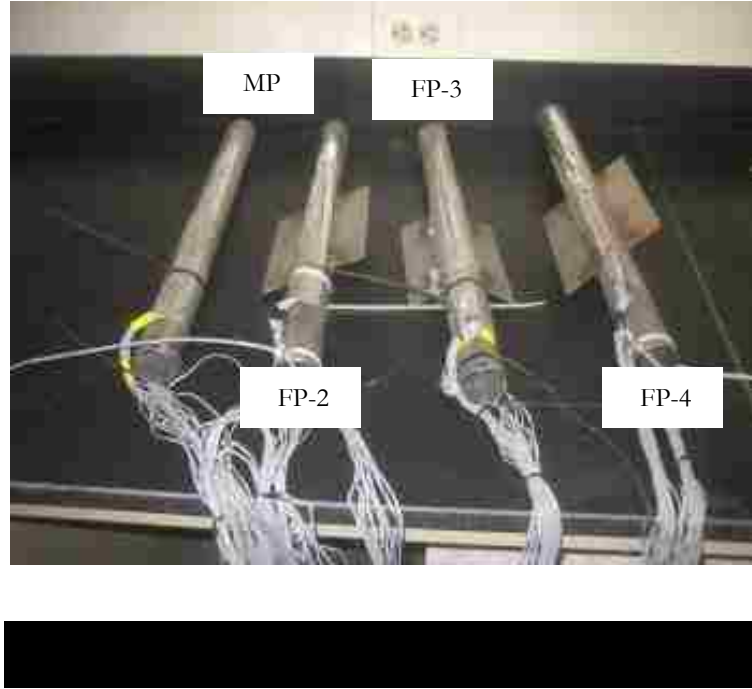
3.3.5 Preparation of the test soil

The experiments were conducted in packed dry silica sand prepared at 32% relative density. In order to prepare a uniform physical model, sand raining technique was adopted to achieve consistent density of the sand. This technique has been widely used in laboratory to prepare model soil substrate in load-displacement tests of model pile foundations (Turner and Kulhawy, 1994; Mezazigh and Levencher, 1998; Rosquoet et al, 2009).

The sand raining apparatus used in this study was fabricated from plywood. A box frame of 0.9m x 0.7m x 0.2m dimensions (same planar dimensions as the soil box), with No. 200 size mesh affixed at its base was used to discharge the sand into the soil box. Figure 3-7 shows the schematic representation of the raining device. The sand rainer was suspended over the soil box using four slings at the corner of the box connected to an overhead rail on top of the box. The vertical position of the sand

52

rainer was adjusted to achieve uniform raining height onto the filling sand layers to attain as uniform density of the final sand mass, as possible.

The total mass of dry sand required filling the box to a set level and mass density was determined from the known volume of the box to fill. Multiple pile tests were conducted at the same computed sand density to verify not only the repeatability of the test results but also the consistency of the sand preparation in the test box.

3.3.6 Scale and boundary effects

In laboratory testing small-scale pile models are widely preferred because a full scale loading test may not always be feasible due the high cost, long time demand and prohibiting requirements for construction, instrumentation, and loading. Alternatively, small-scale experiments can suffer from scaling effects which should be minimized to ensure that the observed behavior can be extrapolated to predict full scale behavior (Wood, 2004). For small-scale models the soil particle size, construction techniques and boundary effects are the most important factors to be considered. Particle size scale error can be neglected when the ratio of pile diameter, D_p to mean grain size, D_{50} is greater than 30 (Franke and Muth, 1985). In this study the D_p / D_{50} ratio was 67 therefore the particle size scaling error was negligible.

Upon extensive small scale model tests, Vesic (1977) showed that results from footings or foundations with diameters smaller than 30mm should not be considered as experimental evidence due to large scale effect. Following Vesic (1977) guideline, the pile diameter was selected as 40mm for all the experiments conducted in this work.

Ropes for adjusting heigh of sand raining device

sand raining device with screen at the bottom

Sand raining height
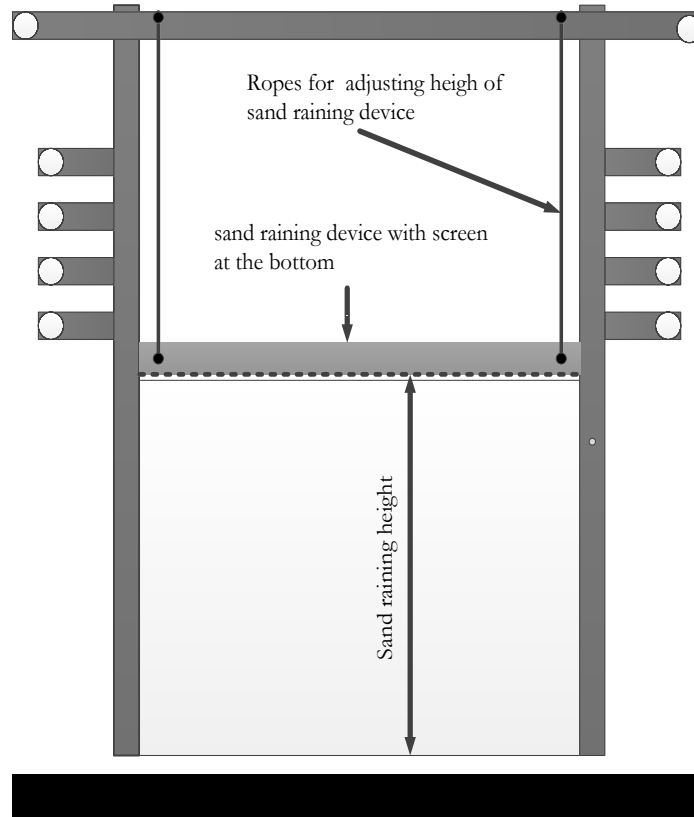
Bransby and Smith (1975) showed that using a relatively wide tank with smooth side walls minimize the side friction boundary effects on the results of the small-scale models. Furthermore, different authors reported that the zone of influence of laterally loaded piles ranged between $4D_p$ to $6D_p$. For example, NCHRP (2011) report identified that the zone of soil improvement around a laterally loaded pile should be around $4D_p$ to fully affect the lateral capacity of the pile. Similarly, Hajialilue-Bonab et al. (2013) measured the strain wedge of a laterally loaded rigid pile using particle image velocimetry and concluded that the zone of influence extended to a distance of about $5.5D_p$. In this study, the inside walls of the steel soil box was polished smoothly to reduce potential friction as much as possible. The distance from the center to the boundary of the soil box along the loading direction was set to be $12D_p$. This distance

54

is two times longer than the strain wedge measured by Hajialilue-Bonab et al. (2013). Hence the design of the box and the specific experimental procedures employed were assumed to minimize or render negligible any anticipated boundary effects.

3.3.7 Scaling of laboratory tests

LeBlanc et al., (2010) developed a scaling law for stiff pile in sand under monotonic lateral loading to predict the behavior of the full-scale structure from low stress laboratory tests using non-dimensional parameters, as shown in Table 3-1. The following were considered to address the scaling of the laboratory tests:

i. In a scaled test, the stress level controlling the test behavior is low resulting into higher soil friction angle and lower shear stiffness in comparison to full scale test. In order to ensure that the peak frictional angle in laboratory corresponded to that of the soil in a full-scale test, the test soil was prepared at low relative density up to 38%.

ii. Appropriate non-dimensional scaling parameters which accounted for low stress isotopic stress level were selected as shown in Table 3-1.

iii. Full scale behavior were estimated by plotting the non-dimensional moment $M/(L^3D\gamma)$ and non-dimensional lateral force $H/(L^2D\gamma)$ against rotation, θ and displacement, δ, respectively, while keeping constant void ratio, e and other parameters influencing stiffness of the soil.

The test results obtained in this study are presented and plotted in their non-dimensional forms following the scaling convention derived by Leblanc et al. (2010).

55

Moment loading	$\bar{M} = \dfrac{M}{L^3 D \gamma}$
Vertical load	$\bar{V} = \dfrac{V}{L^2 D \gamma}$
Horizontal load	$\bar{H} = \dfrac{H}{L^2 D \gamma}$
Rotation degreed	$\bar{\theta} = \theta \sqrt{\dfrac{p_a}{L \gamma}}$
Load eccetricity	$\bar{e} = \dfrac{M}{HL}$
Aspect ratio	$\lambda = \dfrac{L}{D}$
Displacement ratio	$\delta = \dfrac{y}{D}$

Where M= moment of the pile at the ground level, H=applied lateral load, θ= rotation of the pile, L=length of pile, D=diameter of the pile, γ=density of the soil and p_a=atmospheric pressure

3.3.8 Pile installation and lateral loading

A pictorial depiction of the sequence of lateral load testing followed in this study is presented in Figure 3-8. First the sand was rained and packed into the steel box Figure 3-8(a-b). Test pile was installed by driving into the sand to a depth corresponding to L_p/D_p ratio of 9 as shown Figure 3-8(c). Lateral load was applied through a cable-pulley system attached to the pile head. The load was applied incrementally, each increment lasting for the duration of 8 minutes. The strain measurements were taken at the end of each load-increment. The 8-minute duration was selected because initial calibration tests revealed that this time period was sufficiently long for cessation of any significant changes between two successive readings (i.e., less than $30\mu\varepsilon$) under the sustained load.

56

(a) Mesh for pouring soil

(b) Prepared testing ground

(c) Installed pile and testing
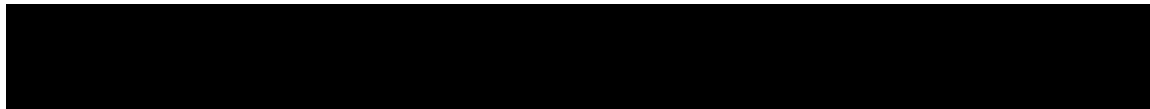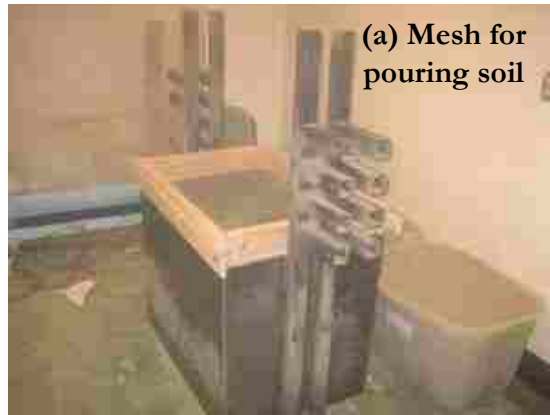
3.3.9 Test cases

The following convention was used for naming the test piles:

i. Acronyms: FP-finned pile; MP-Monopile (no fins).

ii. First set of numbers: 2, 3 and 4 refer to the number of fins welded on the pile.

iii. Second set of numbers: 90, 120, 180, 240 and 270 refer to the angle between the fins that can develop an effective pressure passive area.

For example, a model pile named as FP-2-180 is a finned pile with two fin wings at 180 degrees of separation between them.
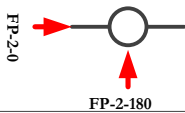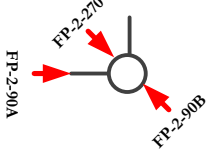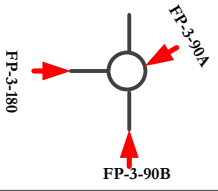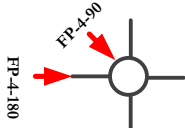
Three different series of tests were performed on the finned and the monopiles. The first series involved testing finned piles with different fin configurations to evaluate the effect of loading direction on their performance. The L_p/D_p ratio of 9 was kept constant in all of these tests. The test configurations of the first series are given in Table 3-2.

The arrow on each pile in Table 3-2 indicates the direction of loading on the pile. This is important because lateral loads, such as those imparted by wind or wave action can occur in any direction hence there is a need to evaluate the efficiency of the fin considering its orientation with respect to the loading direction.

Second series of tests involved testing monopiles of different L_p/D_p ratios designated as 16, 14, 12, 10 and 9, as shown in Figure 3-9. Results from the second series of tests were compared with those of the finned piles from first series in order to evaluate the effectiveness of fin in reducing the embedded length of the pile.

The third series of tests were conducted to determine the evolution of the shear zone (i.e., shear wedge) and its final length away from pile surface during lateral loading of a finned pile. In analysis of the soil-pile interaction under horizontal load, the behavior of the soil in front of the pile undergoing horizontal displacement is an important phenomenon which needs to be understood well for accurate pile capacity predictions.

Techniques such as particle image velocimetry (Ashour et al., 2013; Liu et al., 2011), X-ray CT scan (Otani et al., 2010) have been used to visualize the failure pattern and strain localization in the soil around a laterally loaded pile.

58

Pile type	Configuration	Lateral load bearing area		Increase in effective bearing area,a_f
		Loading direction	Effective bearing area	
MP		MP	$D_p \times L_p$	-
FP-2		FP-2-0	$D_p \times L_p$	0
		FP-2-180	$(D_p \times L_p)+(2W_f \times L_f)$	0.90
		FP-2-90A	$(D_p \times L_p)+(W_f \times L_f)$	0.45
		FP-2-90B	$(D_p \times L_p)+(1.414W_f \times L_f)$	0.64
		FP-2-270	$(D_p \times L_p)+(1.414W_f \times L_f)$	0.64
FP-3		FP-3-90A	$(D_p \times L_p)+(1.414W_f \times L_f)$	0.64
		FP-3-90B	$(D_p \times L_p)+(W_f \times L_f)$	0.45
		FP-3-180	$(D_p \times L_p)+(2W_f \times L_f)$	0.90
		FP-3-120	$(D_p \times L_p)+(1.732W_f \times L_f)$	0.78
		FP-3-240	$(D_p \times L_p)+(1.732W_f \times L_f)$	0.78
FP-4		FP-4-90	$(D_p \times L_p)+(1.414W_f \times L_f)$	0.64
		FP-4-180	$(D_p \times L_p)+(2W_f \times L_f)$	0.90

$D_p = W_f$ and $L_f = 0.45L_p$.
D_p and L_p are diameter and lengths of Pile
W_f and L_f are width and length of fin
Increase in effective bearing area is computed with respect to effective bearing are of MP
Two fins making 120° between then have an effective fin area of $A_f = 2W_f \times L_f \sin 60$
Two fins making 90° between then have an effective fin area of $A_f = 2W_f \times L_f \sin 45$

Despite such techniques being available, the evolution of the shape and length

of shear wedge in front of a laterally loaded pile, particularly of a finned pile is not

understood well. In addition, accurate determination of the extent of the lateral shear

www.manaraa.com

wedge is particularly important for the scaled tests conducted in order to determine the influence of any boundary effects, such as those discussed earlier. In the tests reported here, five miniature pressure sensors of type PDB-P, 6.5mm in diameter, with 200 kPa capacity and 350 Ω input/output resistances were positioned inside the sand on a linear path away from the pile surface at pre-determined distances of multiple pile diameters, D_p. These pressure sensors were used to monitor the evolution of lateral pressure in soil in the direction of pile deflection.

L_p/D_p varied fron 16 to 9

L_p/D_p fixed to 9

(a) MP

(b) FP
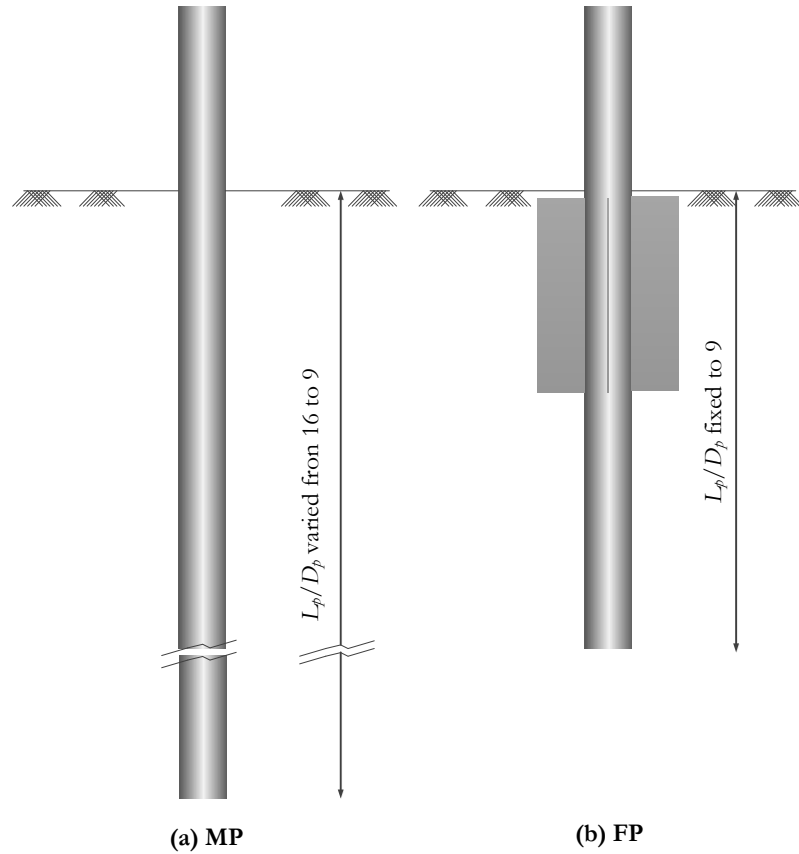
3.3.10 Placement of pressure sensors

The miniature pressure sensors were all buried at a depth of $2D_p$ below the ground surface. The layout of the sensors is shown in Figure 3-10. The sensors were positioned at distances of 2.5, 4.5, 6.5, 8.5 and $10D_p$ from the center of the pile as shown in Figure 3-10 (a) below. When the pluviated sand level reached just below $2D_p$ from top, the pressure sensors were held in their embedment position and pluviation of the sand was then resumed till the final height was achieved, as shown in Figure 10 (b).

(a) Earth pressure sensors placed at different distance

(b) Soil spread over the sensors before pluviation

3.4 Test results

3.4.1 Effect of loading direction with respect to orientation of fins

Figure 3-11 shows the measured lateral load verses displacement curves for the first series of tests. As expected the lateral resistance of the finned piles was higher than those of the monopole in all tests. The lateral load capacity of the finned piles showed marked improvement when compared to the monopole response at the same pile head displacement. All piles with fins displayed a considerable stiffer behavior than monopile. Also observed from Figure 3-11, the lateral resistance of a finned pile appears to depend upon the number of fins as well as the orientation of the fins to the direction of loading. Considering the lateral resistances of the piles at serviceability limit state, described as the lateral load at 10% of pile head displacement, the lateral resistance was shown to increase between 15% - 98 % depending on the number of fins and the orientation of the fins to loading direction. As the number of fins increases, the flexural rigidity $(E_p I_p)$ of the pile around the finned section increases resulting in the increase in lateral resistance.

The surface area and the length of a pile are the two important factors in determination of the lateral resistance of a pile. The effective area that bears against the soil is the area orthogonal to the lateral load. In the case of a monopile, the effective area is determined as the pile diameter multiplied by the pile length, while for a finned pile the section of the pile containing the fin has added effective bearing area equal to the width of the fin multiplied by the length of the fin (Peng, 2005). Orientation of fin with respect to the loading direction may effectively reduce or increase the bearing area.

62
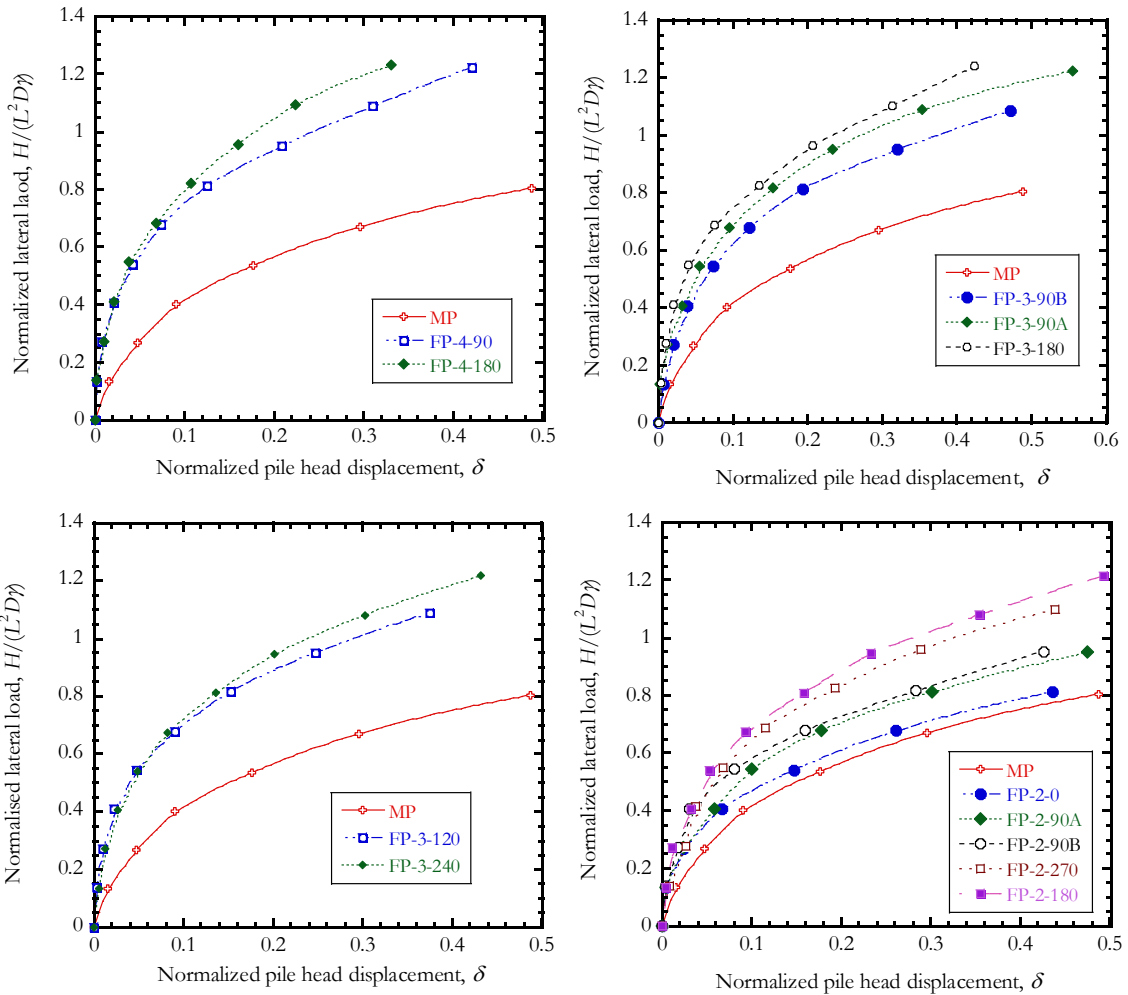
For example, fins oriented obliquely to the loading direction, such as those in FP-3-120 or FP-3-240 piles will have reduced effective bearing areas to sustain the passive pressure of soil when compared to FP-3-180 pile. As shown in Table 3-2, the FP-3-180 pile has an increased bearing area by a factor of 0.9 compared to that of FP-3-120 and FP-3-240 which have increased bearing areas by factor of 0.78. Similarly, FP-4-180 has increased bearing area by a factor of 0.9 compared to FP-4-90 which has an increased bearing area by a factor of 0.64. FP-4-180 showed higher resistance to

63

lateral load than FP-4-90 even though both configurations have similar flexural rigidity. Results from this test indicated that as the bearing area increases, the soil resistance in front of the fin will be increase leading to an overall increase in the expected lateral capacity of the finned pile.

3.4.2 Fin efficiency

Efficiency of a finned pile can be defined in terms of the increase in lateral load capacity compared to that of monopile at same pile head displacement; or in terms of the reduction in lateral pile head displacement at the same lateral load. In this work, the lateral load efficiency of a finned pile will be defined as the ratio of the difference in lateral load capacity of the finned and monopole ($H_{(FP)}$-$H_{(MP)}$) to that of the monopile ($H_{(MP)}$) taken at the same pile head displacement, as expressed by Equation 3-2.

$$\eta_H = \frac{H_{(FP)} - H_{(MP)}}{H_{(MP)}} \qquad (3\text{-}2)$$

Figure 3-12 shows the contribution of the effective bearing area to the finned pile efficiency. The two-finned piles showed broad variation in efficiency ranging between 15%-68% while those of the three-finned and four-finned piles varied between 50%-88 % and 92%-98%, respectively. The efficiency of the two-finned piles (FP-2-180, see Table 3-2) was similar to that reported by Nasr (2013). The three-finned piles with fins oriented at 120° from each other (see Table 3-2) showed a much smaller variation than the other cases, ranging from 80%-88%. As the directions of loading can vary over time, as in the case of wind loading for instance, use of three- or four-finned piles with less variability in their efficiency might meet the load demands best.

64

The deflection efficiency is defined as the ratio of the displacement difference in pile head between monopile and finned pile to displacement of the monopile pile at the same magnitude of lateral load, as expressed by Equation 3-3.

$$\eta_\delta = \frac{\delta_{(MP)} - \delta_{(FP)}}{\delta_{(MP)}} \qquad (3\text{-}3)$$

Figure 3-13 shows the variation of the deflection efficiency with normalized lateral load. In all cases, the finned piles reduced the lateral deflection of the pile by more than 65%. Duhrkop and Grabe (2008) reported also lateral deflection reduction of up to 65% from results of centrifuge tests in which they used fins of smaller aspect ratio than those reported in this dissertation. The results for pile FP-2-0 in Figure 3-13 indicated the least reduction in lateral deflection, which ranged ranging from 15%-45%.
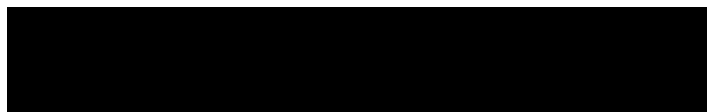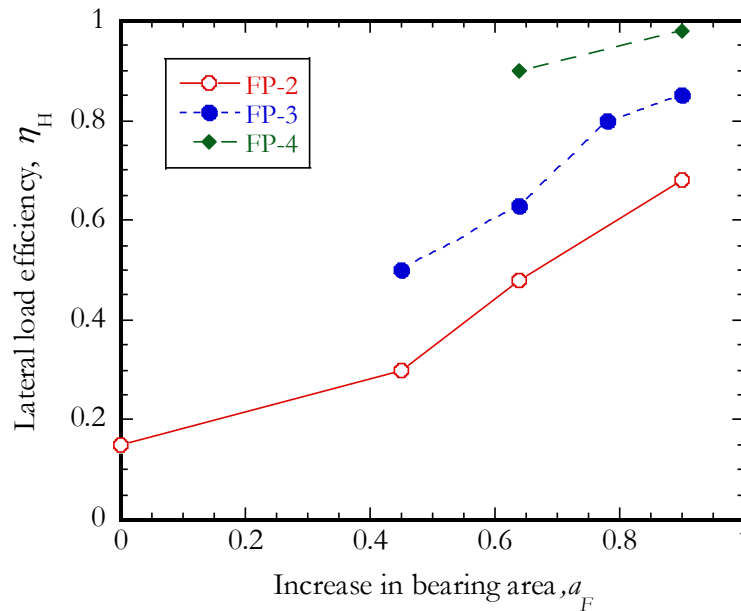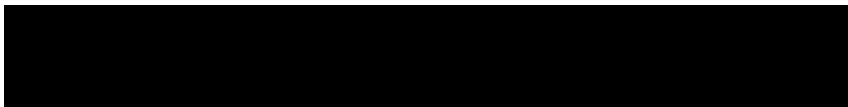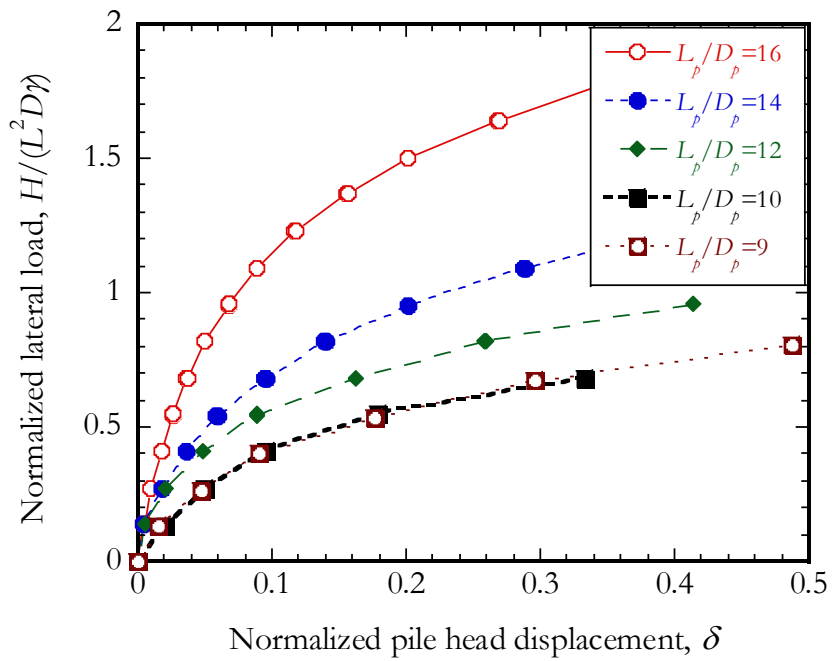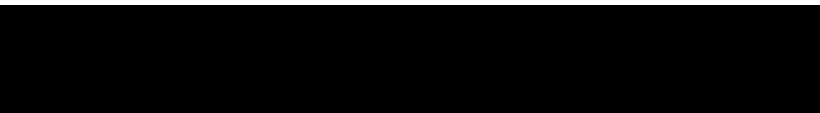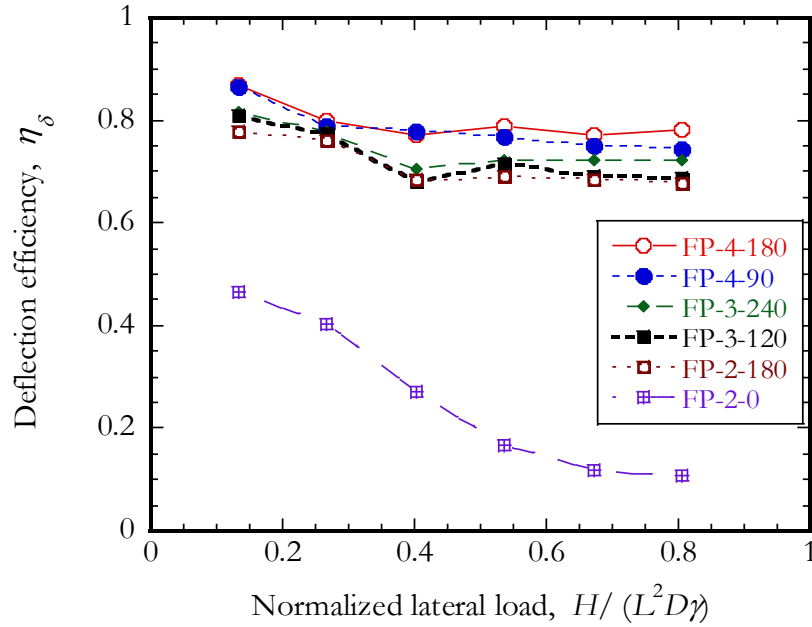
3.4.3 Effect of fins in reducing length of pile length

Lateral load displacement curves for monopiles of different L_p/D_p ratios are as shown in Figure 3-14. Superimposed on this graph are the results presented earlier in Figure 3-11 for L_p/D_p ratio of 9, as well.

Figure 3-15 shows the variation of the normalized lateral load with the normalized length of two-finned (FP-2), three-finned (FP-3) and four-finned (FP-4) pile configurations, as presented in Table 3-2. The lateral load and the length values were normalized by those of the monopiles. It's important to note again that, while the lengths of the finned piles were fixed at L_p/D_p ratio of 9, the length monopile was varied form L_p/D_p ratio of 9 through 16 (as shown in Figure 3-14) in this representation. The lateral loads were normalized by those of the corresponding monopile load at constant deflection of δ=0.1.
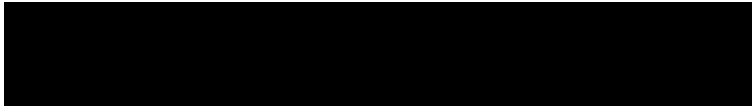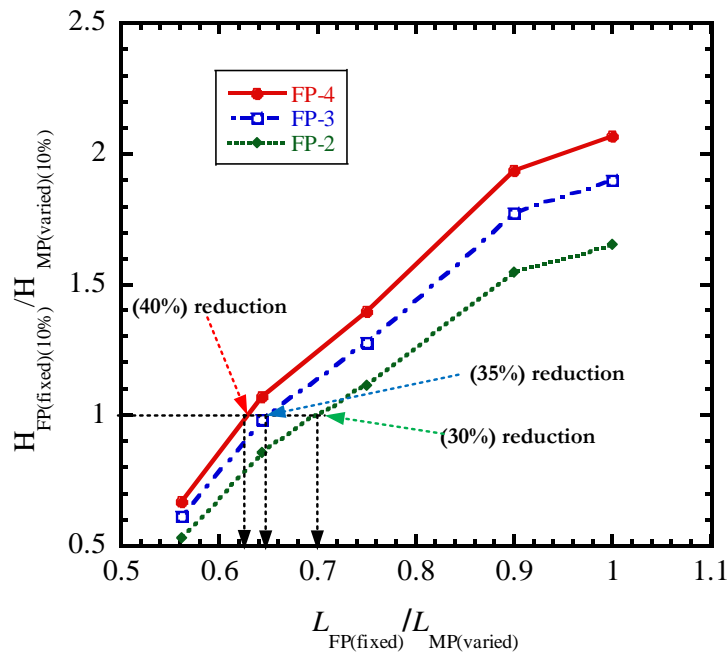
It can be observed from Figure 3-15 that the pile length could be reduced by about 40%, 37%, and 30% for the four-, three-and the two-finned piles, respectively, for the same lateral load capacity demand ($H_{(FP)}/H_{(MP)}$ =1). These results show clearly that fins are effective in reducing the required length of monopile in design, which in turn can translate to reduction in cost. Shorter pile length may also bring about the added benefit of rendering less likely the occurrence pile refusal during driving.

3.4.4 Relationship between fin efficiency and weight of the pile

Figure 3-16 shows the variation of the lateral load efficiency of finned pile at normalized lateral displacement of 10% or $y/D_p = 0.1$ (i.e., serviceability limit state) with the mass of the pile. The notations M_{FP} and M_{MP} stand for the mass of the finned and monopile respectively. In here, $H_{MP(varied)(10\%)}$ correspond to values for the monopiles where L_p/D_p ratios were varied as 16, 14, 12, 10 and 9.

$$\frac{H_{FP(fixed)10\%}}{H_{MP(varied)10\%}} = 0.132e^{\left(\frac{M_{FP(fixed)}}{M_{MP(varied)}}\right)}$$
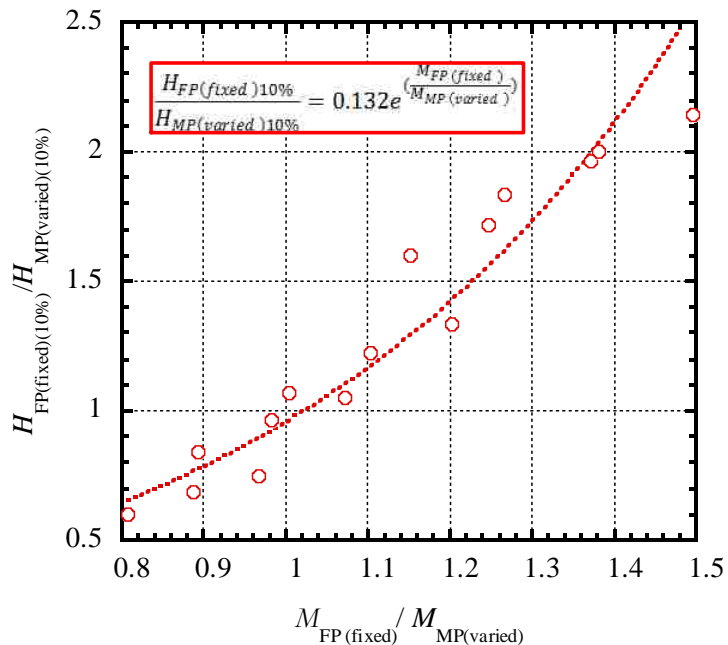
The efficiency increased with mass of the finned piles. This relationship was fitted to an exponential curve, as shown in Figure 3-16. It appears from the data that this empirical model may be valid for M_{FP}/M_{MP} ratio of up to 1.4.

3.4.5   Change in lateral soil pressure during lateral loading of MP and FP

The changes in soil horizontal stresses at various distances away from the pile perimeter were measured using null pressure sensors placed in the soil at the set depth of $2D_p$, as described earlier (see Section 3.3.10). These sensors were initialized to zero prior to application of the lateral loading. The tests were conducted by increasing the lateral load in increments of 10N. The lateral pressure change measured at each sensor was normalized by the overburden stress calculated at $2D_p$ depth of embedment.

Figures 3-17a, 3-17b and 3-17c show the variation of the change in horizontal stress measured during lateral loading of three separate piles of MP, FP-3 and FP-4 type, respectively. The change in horizontal stress was based on the initial value of lateral stress at each sensor location. While Figure 3-17a shows the results for the monopile section, Figures 3-17b and 3-17c show the results for the three- and the four-finned pile section, respectively. It can be observed from the data that horizontal stress evolution in soil is influenced by the pile configuration. Smaller horizontal stresses were observed with the finned pile sections, implying larger area of interaction between the soil and the pile, and potentially wider strain wedges. In all the tests the strain wedges did not extend to the boundary of the soil box for any of the pile sections confirming that the dimensions of the soil box used were sufficient to carry out the lateral loading test for the model piles without any anticipated boundary effects.

69

(a) MP

(b) FP-3

(b) FP-4
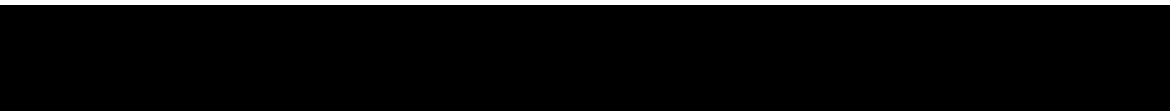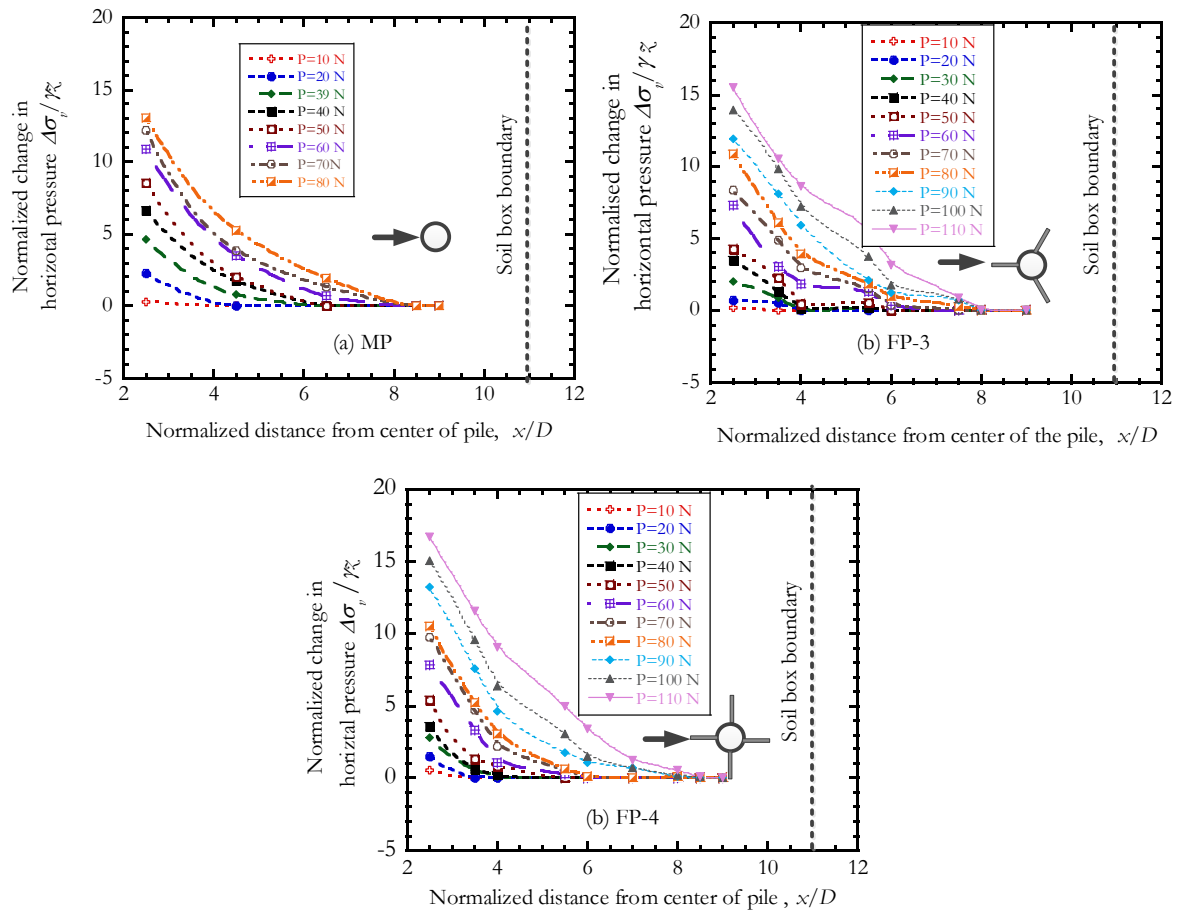
3.4.6 Length of strain wedge for MP and FP

The measured changes of pressure from the sensors were used to estimate the length of the strain wedge formed at $2D_p$ embedment depth during lateral loading. For a given pile head displacement at a constant load of H, the maximum wedge length was assumed to extend to the point where the change in the measured earth pressure was nearly zero. Described as such, the variation of normalized strain wedge length with normalized pile head displacement is shown in Figure 3-18. The data indicate the wedge

length for the four-finned pile section (FP-4) to be about $8.5D_p$ from center of pile, while it is $8.0D_p$ and $6.5D_p$ for the three-finned pile (FP-3) and monopole (MP), respectively.

Although much study has been devoted to understanding the lateral load response of piles, there is little reported in literature that document the length of strain wedge determination for single piles in order to compare with the present results. Hence, the available data for group pile behavior from literature is used to compare with the results obtained in here, as shown in Figure 3-18.
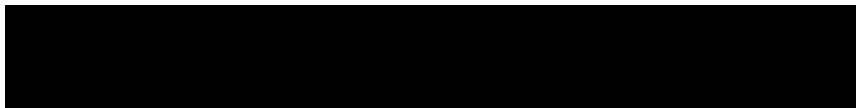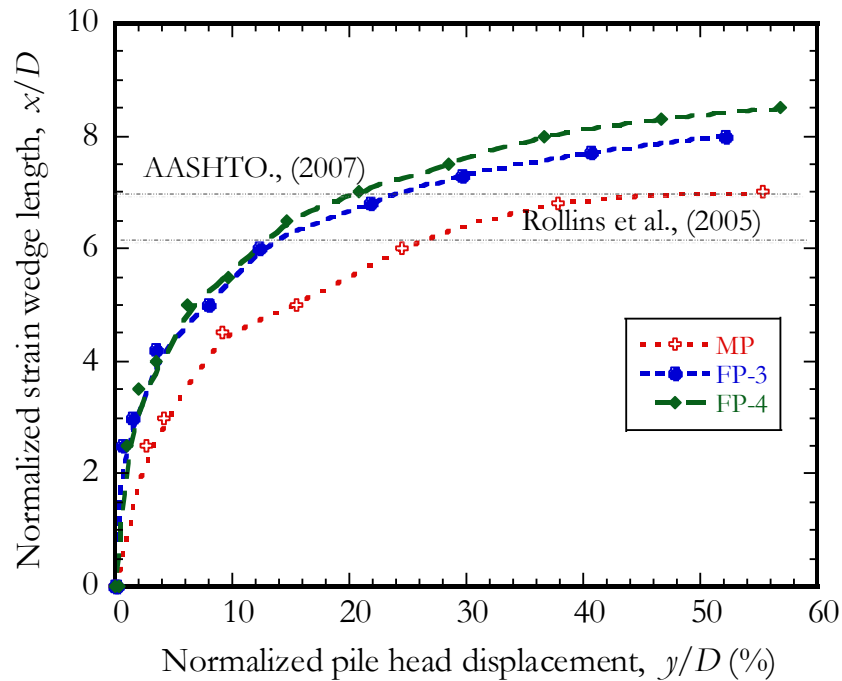
The results from full-scale tests and centrifuge model tests (Rollins et al. 2005, AASHTO, 2007) indicate that piles in groups undergo significantly higher displacement for a given load per pile than a single pile. Although piles in the front row of a group may display load versus deflection curves similar to that of single pile, piles in the trailing rows will exhibit significantly softer load versus displacement curves. As the closely spaced pile groups move laterally, the failure zones for individual piles overlap. The tendency for piles in the trailing row to exhibit less lateral resistance is commonly referred to as "shadowing," or group interaction. Group interaction effects tend to become less significant as the spacing between piles increases. Group interaction effects are often accounted for by using a multiplier (*p-multiplier*) that reduces the load displacement as proposed by Brown et al. (1988).

The comparison of the length of strain wedge obtained by model pile tests in this study is done by comparing the spacing of the trailing piles in a group with the *p-multiplier* of unity. As shown in Figure 3-18, the results for the MP agree well with those reported by AASHTO (2007). For finned pile sections of FP-3 and FP-4, the length of the strain wedge or the zone of influence is larger than those reported for a single pile. If finned piles are to be adopted for use in a group, spacing greater than $8.5D_p$ may be recommended to minimize shadowing effect.

3.5 Summary and conclusion

In this chapter, a comparative study of lateral load capacity and deflection behavior of finned and monopiles using model piles in a floor scale laboratory test set-

72

up is described and discussed. Finned piles of different configurations were tested to determine the effect of fins in reducing the required length of piles compared to monopiles. The effect of the orientation of the fins to loading directions on the lateral load capacity was examined. The suitability of the soil box used in conducting the model pile tests was assessed through measurement of the lateral earth pressure distribution at various distances away from the pile surface to ascertain no intersection of the soil strain wedge with the boundary of the soil box. The same data was used to predict the length of a shear wedge that can form in front of a finned pile and make recommendation of spacing of finned piles for use in groups.

The following conclusions were made from the comparative tests:

(i)   The lateral load efficiency of the finned piles varied greatly from 15%-98% depending on the number of fins and their orientations to the direction of loading. Four-finned piles displayed the largest efficiency. Large variations of lateral load efficiency were observed for the two-finned pile sections depending on the orientation of the fins to the direction of loading.

(ii)   Fins oriented obliquely with respect to direction of loading had lower efficiency than those oriented perpendicular to the direction of loading. This was due to the reduced effective load bearing area available with the fins. Four-finned and three-finned piles did not show as large variations of lateral load efficiency with orientation of fins to loading direction. Piles with three or four fins can meet the load demands best, particularly when the loading directions are anticipated to change with time (i.e., wind and wave loads).

73

(iii)   The deflection was reduced by more than 65% for all finned piles of different fin orientations and loading directions, except for the two-finned section (FP-2-0) for which the reduction was between 15%-45%.

(iv)   Test results also showed that the length of pile could be reduced by 40% for four-finned pile, 37% for three-finned pile and 30% for two-finned piles for the required lateral resistance when compared to monopile.

(v)   The length of the shear wedge for a four-finned pile (FP-4) extended to up a distance of $8.5D_p$ from center of pile, and those of the three-finned pile (FP-3) and monopole (MP) were $8.0D_p$ and $6.5D_p$, respectively. These results also confirmed that the soil box used in the lateral load test was suitable without introducing boundary effects.

3.6 References

1. AASHTO (2007): AASHTO LRFD *Bridge Design Specifications, 4ᵗʰ edition,* AASHTO, Washington, DC.

2. ASTM. (2006a): Standard test methods for maximum index density and unit weight of soils using a vibratory table. *D4253–06*, West Conshohocken, PA.

3. ASTM. (2006b): Standard test methods for minimum index density and unit weight of soils and calculation of relative density. *D4254–06*, West Conshohocken, PA.

4. ASTM. (2012): Standard Test Method for Direct Shear Test of Soils Under Consolidated Drained Conditions. *D3080–12*, West Conshohocken, PA.

5. ASTM. (2014): Standard test methods for specific gravity of soil solids by pycnometer. *D854–14*, West Conshohocken, PA.

6. Bolton, M.G. (1986): The strength and dilatancy of sand. *Geotechnique*, 36(1):65-78.

7. Bransby, P.L. and Smith, I.A. (1975). Side friction in model retaining wall experiments. *Journal of Geotechnical Engineering*, 101(GT7): 615–632.

8. Brown, D.A., Morrison, C., and Reese, L.C. (1988): Lateral load behavior of pile group in sand, *Journal of Geotechnical and Geoenvironemental Engineering*, 114 (11): 1261–1276.

9. Byrne, B. W. and Houlsby, G. T. (2003): Foundations for offshore wind turbines, *Philosophical Transactions of the Royal Society London, Series A (Mathematical, Physical and Engineering Sciences),* 361 (1813): 2909-2930.

10. Duhrkop, J. and Grabe, J. (2008): Improving the Lateral Bearing Capacity of Monopiles by Welded Wings. *Proc. of the 2nd BGA International Conference on Foundations*, 1: 849-860.

11. Franke, E., and Muth, G. (1985): Scale effect in 1g model tests on horizontally loaded piles. *In Proceedings of the 11th International Conference of Soil Mechanics and Foundations*, San Francisco. Vol. 2, pp. 1011–1014.

12. Hajialilue-Bonab, M., Sojoudi, Y., and Puppala, A. J. (2013): Study of strain wedge parameters for laterally loaded piles. *International Journal of Geomechanics*: 143–152

13. Houlsby, G.T. (1991): How dilatancy of soils affects their behavior. Soil mechanics Report No.121/91, Oxford University, UK.

14. LeBlanc, C., Houlsby, G. T. and Byrne, B. W. (2010): Behavior of stiff piles in sand to long term cyclic loading. *Geotechnique,* 60 (2): 79–90

15. Mezazigh, S. and Lavacher, D. (1998): Laterally loaded piles in sand-slope effect on P-Y curves. *Canadian Geotechnical Journal*, 35: 433–441.

16. Nasr, A. M. A. (2013): Experimental and theoretical studies of laterally loaded finned piles in sand. *Canadian Geotechnical Journal*, 51: 381-393

17. Peng, J. (2005): Behavior of finned piles in sand under lateral loading. PhD Thesis, University of New Castle Upon Tyne

18. Peng, J., Clarke, B., and Rouainia, M. (2011): Increasing the resistance of piles subject to cyclic lateral loading. *Journal of Geotechnical and Geoenvironmental Engineering,* 137(10): 977–982.

19. PND Engineers: http://www.pndengineers.com/research-and-development/applied-research-development/spin-fin-piles

20. Rollins, K.M, Lane, D.J. and Gerber, T.M. (2005): Measured and computed lateral response of a pile group in sand. *Journal of Geotechnical and Geoenvironmental Engineering*, 131(1): 103–114.

21. Rosquoet, F., Thorel, L., Garnier, J and Cenepa, Y. (2009): Lateral cyclic loading of sand-installed piles. *Soils and Foundations*, 47 (5): 821-832.

22. TRB (2011): Design Guidelines for Increasing the Lateral Resistance of Highway-Bridge Pile Foundations by Improving Weak Soils. *NCHRP Report 697*.

23. Turner, J.P. and Kulhawy, F.H. (1994): Physical modelling of drilled shaft side resistance in sand. *Geotechnical Testing Journal*, 17(3): 282–290.

24. Songlin, W. (2007): Horizontal Resistance Behavior of Pile with Wings in Sand. *Proceedings of the 32nd Deep Foundations Annual Members Conference* 7:253-259.

25. Vesic, A.S. (1977): Design of Pile Foundation, *National Cooperation Highway Research Programs,* TRB N0. 42

26. Wood, D.M. (2004): Geotechnical modelling. Spon Press, London.

CHAPTER 4

4 SOIL-PILE INTERACTION OF LATERALLY LOADED MONOPILE AND FINNED PILES

4.1 Introduction

When piles are loaded laterally the subgrade reaction of the surrounding soil is mobilized. A large amount of subgrade reaction is desired in the section where large pile deformations are experienced. Due to low overburden pressure near the ground surface the capacity of pile in this section is limited in sand. An improvement of the lateral capacity of the pile can be achieved by welding fins on the pile (Duhrkop and Grabe, 2009).

The important element in estimating the lateral load capacity of a pile is determination of the ultimate resistance that can be mobilized by the surrounding soil on the pile. Several approaches are available in literature for estimating lateral load capacity of piles (Broms, 1964; Fleming, 1992; Meyerhof et al., 1981; Petrovisch and Award, 1972; Prasad and Chari, 1999; Zhang et al, 2005). These methods were developed for circular piles and naturally do not consider the effect of fins on lateral response of a finned pile.

As discussed previously in Chapter 3, the cross-sectional expansion of the pile due to addition of fins results in increase of the overall resistance from the soil with the added benefit of reduction in pile length for the same capacity. As the geometry

78

and configuration of a circular pile change due to addition of fins, there arises a need to investigate the soil pile interaction of the finned pile. In order to study the interaction between a finned pile and the surrounding soil during lateral loading, a series of finned and monopiles were instrumented with strain gauges and miniature earth pressure gauges to measure the bending strains in the piles as well as the mobilized lateral earth pressure at the interface. The measured earth pressures were used to calculate the soil reaction and predict the lateral capacity of the pile by employing a modified form of an existing approach discussed in Section 2.7 of Chapter 2.

4.2 Objective of the study

The main aim of this portion of the study was to:

1) Investigate the effect of fin modification on the bending strain and bending moment along the length of the pile.

2) Investigate the distribution of earth pressure about the perimeter and along the length of the pile to determine the lateral soil resistance.

3) Develop a predictive approach of estimating ultimate lateral capacity of finned piles using the test data from instrumented piles and a modified form of an existing approach used for monopiles.

4.3 Model pile instrumentation

Lateral load tests were conducted on MP, FP-2-180, FP-3-120 and FP-4-180 piles following the same procedure outlined in Chapter 3. These tests were conducted

79

using the same sand substrate prepared at 32% relative density. The elastic modulus and the moment of inertia of the test piles were taken to be 210 GPa and 2.331×10^{-9} m^4, respectively. The piles were each instrumented with 6 pairs of PDA-P type (from Texas Instrument) earth pressure gauges of capacity 200kPa, placed at different positions along the length of the test pile, as shown in Figure 4-1. The earth pressure gauges were installed in the front and the rear side of each pile to ensure full coverage measurement of the passive earth pressure acting on the pile.

MP:Section A-A

FP:Section A-A
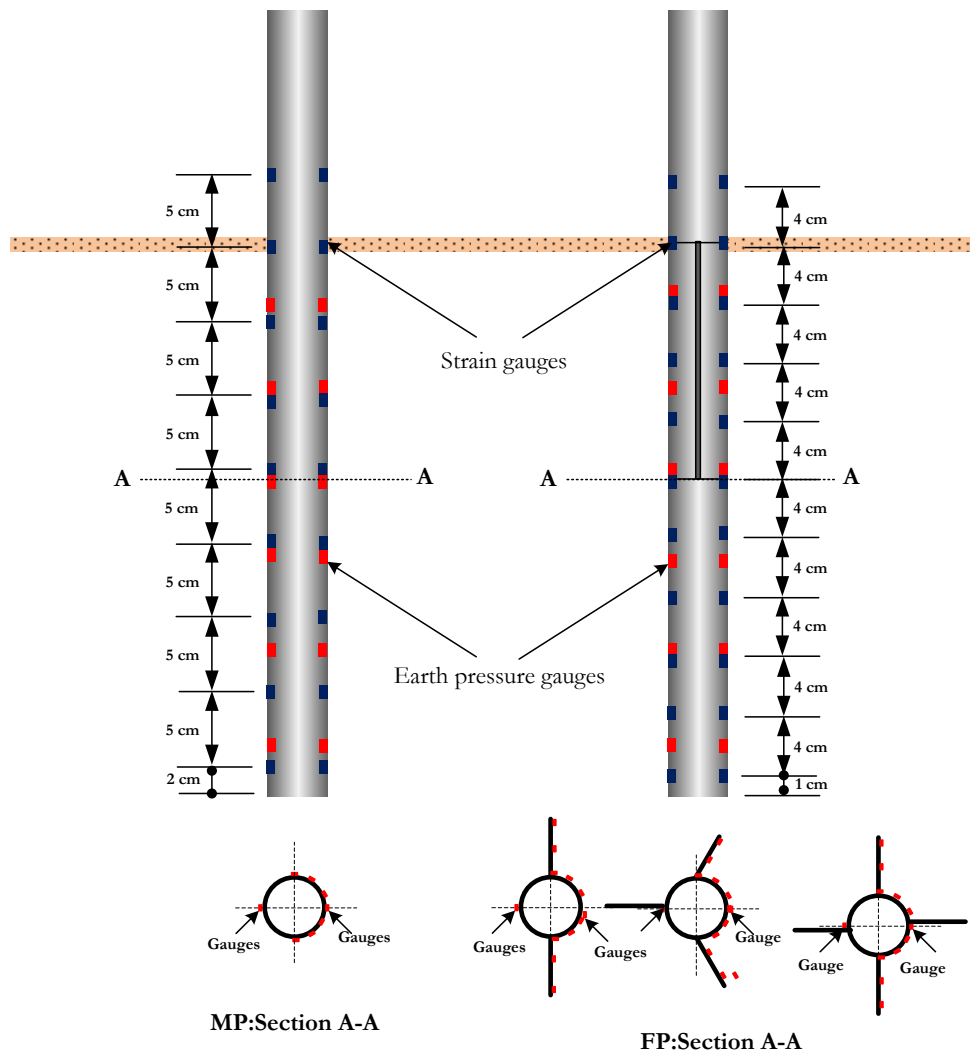
The earth pressure gauges were held in position using multipurpose double-sided adhesive foam tape. The tape consisted of polyurethane foam coated with acrylic adhesive on both sides that attached well to rigid surfaces of the pile providing excellent mount stability of the earth pressure gauges on the pile. The use of double-sided adhesive tape allowed for the re-use of the pressure gauges on other piles and in subsequent tests.

In addition, each pile was instrumented with strain gauges on their both sides perpendicular to the direction of load. Nine pairs of strain gauges were attached on the monopile (eight were buried in the soil and one outside the soil); while eleven pairs of them were attached on the surface of the finned piles (ten were buried in the soil and one outside the soil). They were held in position with epoxy glue. The main purpose of using the strain gauges was to adequately compare the measured bending strains and the calculated bending moment of finned piles relative to those of monopile and to deduce the efficiency of the fin in reducing the bending moment during lateral loading.

All the earth pressure gauges and strain gauges were covered by foil tape to protect them from damage during pile installation and testing.

4.4 Test Results

4.4.1 Static lateral load carrying capacity

Load-deformation criteria to define the ultimate load capacity for axially loaded piles have been well established by others (Chin, 1970 and Davisson, 1972). In these methods, the ultimate lateral load criteria is often related to the specific structure type

81

(Fleming et al.,1992; GAI consultants,1982; Hu et al., 2006; Lee et al.,2013 Meyerhof et al.,1981;). Fleming et al., (1992) suggested a lateral load deflection equal to 10% of pile diameter for a circular pile to define the ultimate load state of the pile. Hu et al. (2006) defined the ultimate lateral capacity for traffic pole structures at pile head rotation of 1.5°. Meyerhof et al (1981) set criteria for defining the lateral load capacity of a pile by observing the point on the load-deflection curve where the curve becomes approximately linear with increasing lateral load. GAI consultants (1982) and Lee et al. (2013) specified the ultimately lateral capacity at pile head rotation of 2°. Other researchers have defined the lateral capacity of monopiles to correspond to a load where the pile head rotated from its vertical alignment by 1.5° producing a lateral displacement between 0.1 D_p to 0.2 D_p at the ground surface (Peng et al., 2011 and Sawwaf, 2006). Lee et al. (2010) estimated the lateral capacity of the pile using the criteria set by Meyerhorf et al. (1981) and GAI consultants (1982) and the two results were in good agreement. In this thesis principles outlined by GAI consultants (1982) were used to define the ultimate lateral pile load capacity, due to its simplicity.

Figure 4-2 shows the normalized lateral load and deflection curves for the monopile and the finned piles. The ultimate lateral load was defined at pile head rotation of 2°. The pile rotation angle was computed from displacement measurements of the two LVDTs attached to the pile. The intersection between the horizontal dashed lines and the *y*-axis in Figure 4-2 indicates the lateral load capacity for each pile, the normalized magnitudes of which are annotated on the graph.

Subsequently, the normalized ultimate load capacity for MP, FP-2-180, FP-3-120 and FP-4-180 were determined as 0.75, 0.99, 1.30 and 1.43, respectively giving computed fin efficiencies of 32% for FP-2-180, 73% for FP-3-120 and 91% for FP-4-180, at the pile head rotation of 2˚. The fin efficiencies were computed from Equation 3-2 given in Chapter 3.

4.4.2 Depth of pile rotation

Rigid piles subjected to lateral load rotate about a certain point as shown in Figure 4-3. Several methods such as those proposed by Petrasovits and Award (1972) and Prasad and Chari (1999) and Rutledge (1956) can be used to estimate the point of rotation for a rigid pile undergoing lateral loading. The method proposed by Petrasovits and Award (1972) is somewhat complex since the depth of pile rotation is computed through a series of numeric iterations until a point of equilibrium in established.
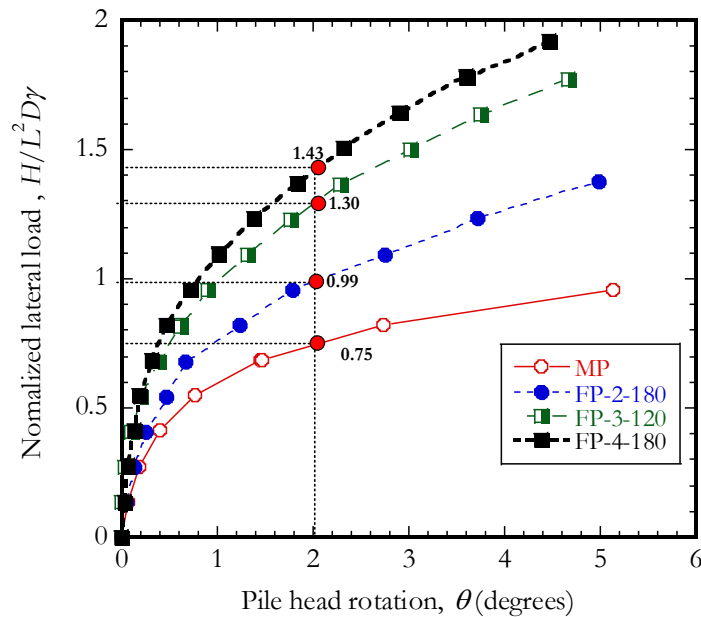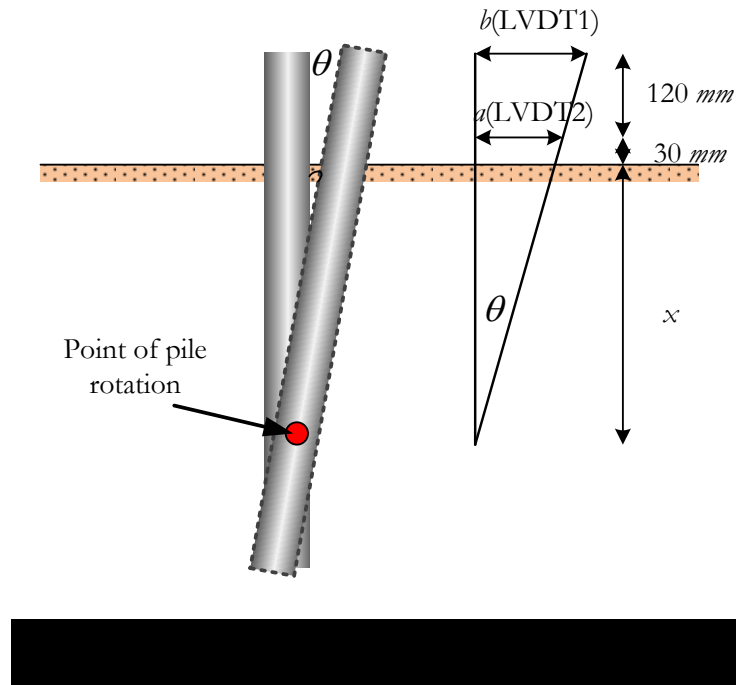
Method proposed by Prasad and Chari (1999) is straight forward, as the depth of pile rotation, *x,* can be calculated from known pile load eccentricity (*e*) and the embedded length of the pile (L_p) using an empirical expression as given in Equation 4-1 below.

$$\frac{x}{L_p} = \frac{\sqrt{7.29\left(\frac{e}{L_p}\right)^2 + 10.541\left(\frac{e}{L_p}\right) + 5.307} - 2.7\left(\frac{e}{L_p}\right) + 0.567}{2.1996} \qquad (4\text{-}1)$$

Two LVDTs (i.e *b*(LVDT1) and *a* (LVDT2)) were installed on the test pile at the heights of 30mm and 150mm, respectively, above the prepared sand surface to measure the lateral deflection of the pile, as shown in Figure 4-3. Using the two LVDT readings of *a* and *b*, the depth of pile rotation and rotation angle were calculated using equations 4-2 and 4-3 (Uchida et al., 2006).

84

$$\frac{x}{L_p} = \frac{30b - 150a}{L_p(a-b)} \qquad (4\text{-}2)$$

$$\theta = atan\frac{(a-b)}{120} \qquad (4\text{-}3)$$

Figure 4-4 shows the variation of depth of rotation with pile head rotation. For values less than 2°, the depth of pile head rotation fluctuates, while for values equal to or greater that 2° the depth of pile rotation point, x, approached to $0.7L_p$ below the ground surface for all piles. This indicates that global mode of failure is independent of the geometry of the pile. The experimentally determined depth of pile head rotation point agreed fairly well with that observed by Prasad and Chari (1999) as $0.72L_p$ and Rutledge (1956) as $0.68 L_p$.
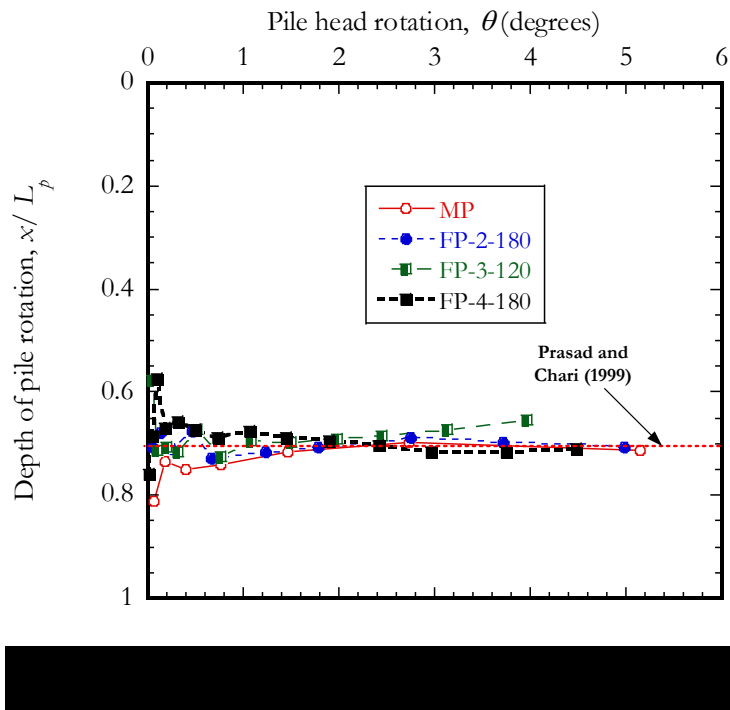
4.4.3   Bending moment distribution

The measured strains during lateral loading are as shown in Figure 4-5 below. In all the cases, bending strains measured on the fin section was smaller than those on monopile at same depth. The bending moment values at the location of strain gauges were calculated from the strain measurements, which were then used in Equation 4-4 (Rollins, 2006).

$$M = \frac{E_p I_p \left(\varepsilon_C - \varepsilon_T \right)}{D_p} \qquad (4-4)$$
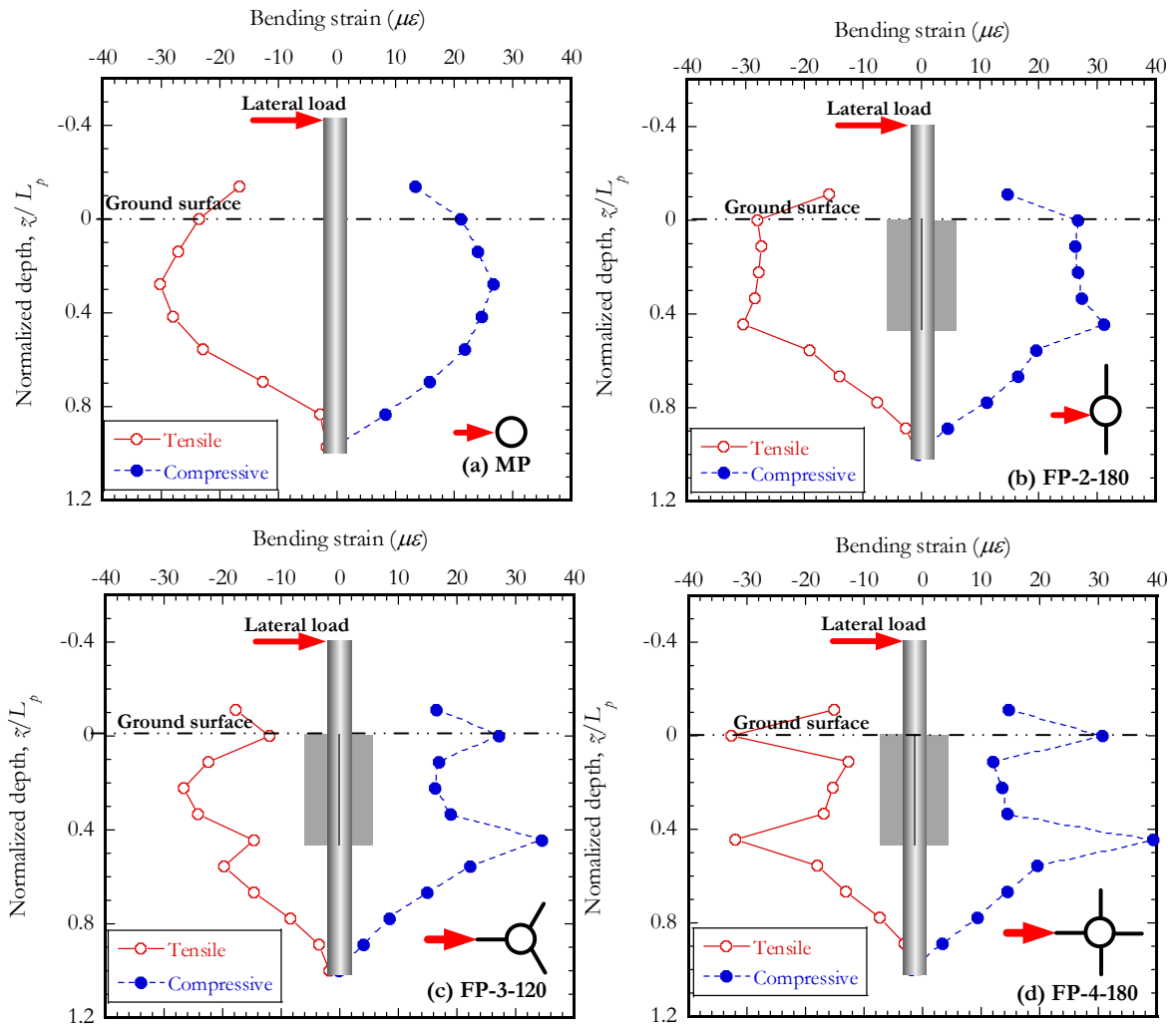
Where, ε_T and ε_C are measured tensile and compressive strains from the strain gauges. E_p and I_p are pile's elastic modulus and moment of inertia, respectively.

The distribution of bending moments along the length of piles for various normalized lateral loads is shown in Figure 4-6. Note that the normalized load is represented simply as (H) on these figures, instead of its dimensionless form ($H/L^2D\gamma$) to be able to fit the annotations on the same figure. The maximum bending moment for the monopole occurred at a depth of $0.3L_p$ while for the finned piles the maximum bending moment occurred at a depth of $0.44\ L_p$, just below the tip of the fin, indicating that the fins modified the location of the maximum bending moment.

4.4.4 Bending efficiency of the fin piles

The effect of the added fins on the response of a pile can be observed from the calculated bending moment distributions from strain gauge measurements. Bending strain is directly related to the applied load and the displacement of the pile. In order to understand the influence of the fin on the bending moment, comparisons to the calculated bending moment distributions at the normalized static lateral load of $H/L^2D\gamma = 0.84$ was made as shown in Figure 4-7.

Three distinct regions can be observed in Figure 4-7. For all the finned piles, the section of the pile above the ground surface and the section of pile below the fins had almost similar bending moment profiles to that of monopole. Large reduction in the bending moments was observed in the finned section of the piles. This reduction

87

is presented in Figure 4-8 in terms of moment efficiency, η_M, expressed as in equation 4-5:

$$\eta_M = \frac{M_{MP} - M_{FP}}{M_{MP}} \qquad (4\text{-}5)$$

Where, M_{MP} and M_{FP} are the bending moments of monopole and finned piles, respectively.

Bending Moment, $M/L^3D\gamma$
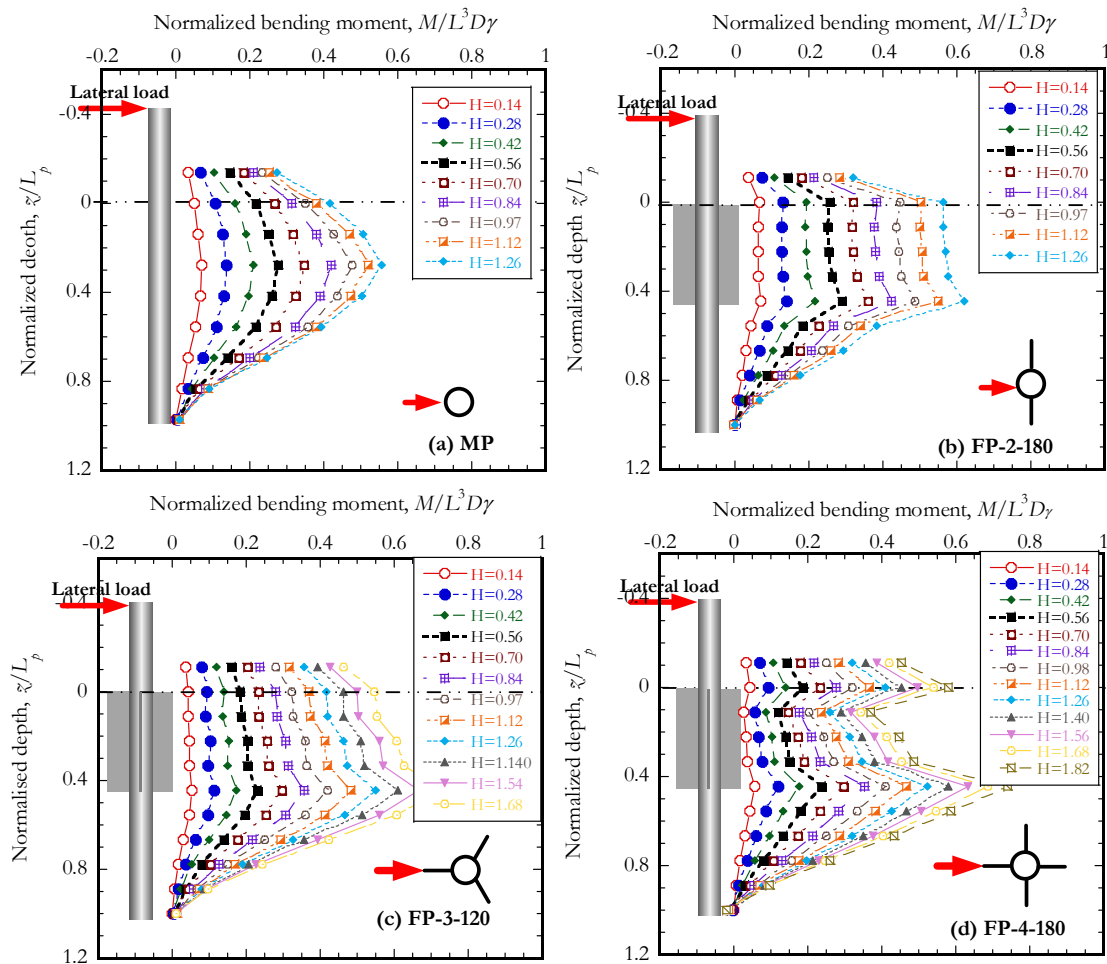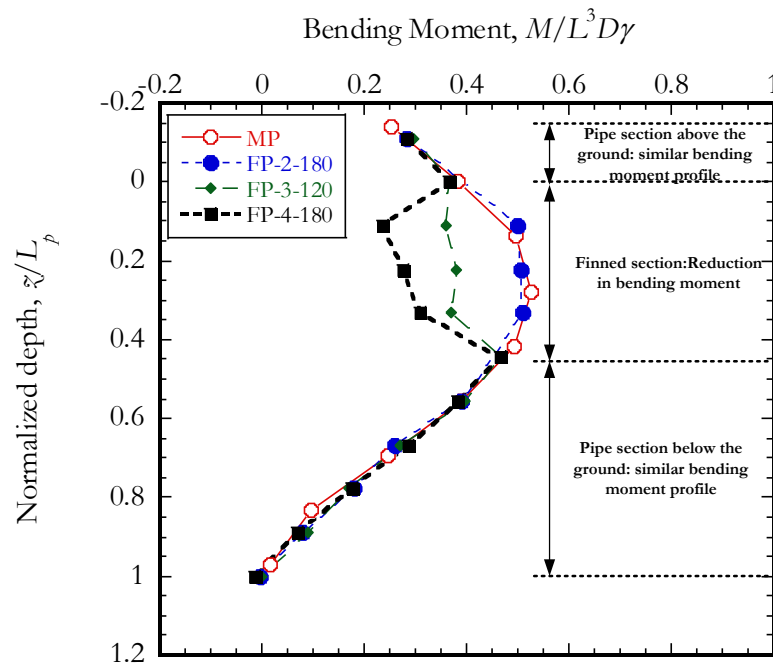
As shown in Figure 4-8, significant reduction in bending moment were observed for three- and four-finned piles which gave efficiencies of 29% and 50% respectively. The two-finned pile showed efficiency of up to 5%. Using finite element modelling, Peng (2006) reported an efficiency of 15% for four-finned pile of L_p/D_p ratio of 9 with L_f/L_p of 0.25 and W_p/D_p of 0.50. Similarly, tests by Nasr (2013) on two-finned piles of L_p/D_p of 15 with L_f/L_p of 0.4 and W_p/D_p of 1 showed efficiency up to 39%. An experimental study by Songlin (2007) on two-finned flexible piles of L_p/D_p ratio of 30 and different finned sizes and different soil densities indicated efficiency ranging from 2% to 44%. These results show that fins can significantly reduce the bending moment of the pile and the results reported in this work agree well with the range of values reported by other researchers on similar systems.

89
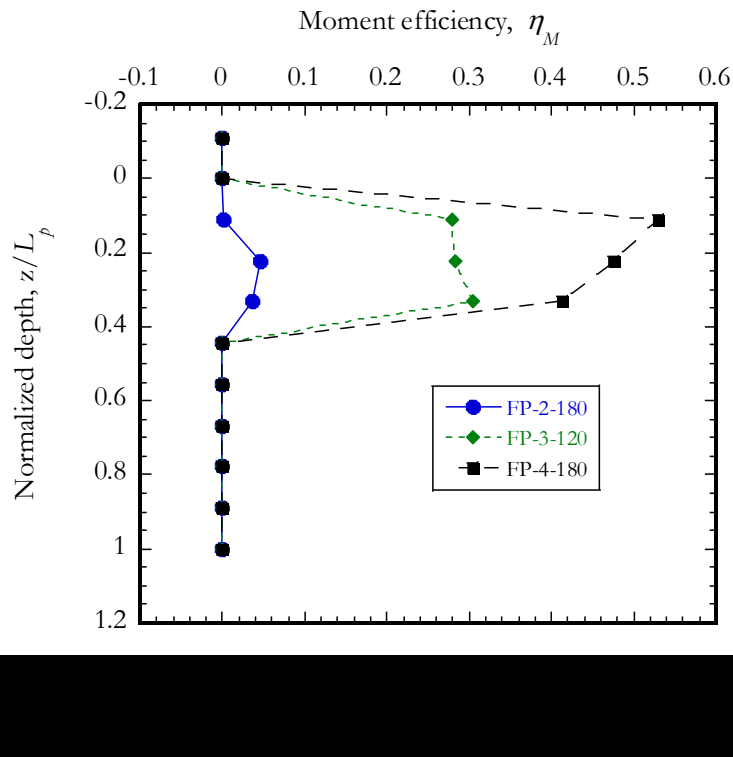
4.4.5   Lateral deflection of the pile inside the soil

Lateral deflection of the piles inside the soil was computed from the readings of the LVDTs attached to the pile. The slope of the pile head at each loading stage was calculated from the LVDT readings and the deflection of the piles at various depths below ground surface was computed assuming linear deflection along the pile length.

Figure 4-9 shows the distributions of lateral deflections of the piles at different lateral loadings expressed as the normalized H (= $H/L^2D\gamma$). The lateral displacements increased with the applied lateral loads, as expected. Small lateral displacements were determined at the tip of the piles. The depth of pile rotation ranged between $0.72L_p$ - $0.75L_p$, which were in good agreement with $0.72L_p$ reported by Prasad and Chari (1999).

90

Figure showing four graphs (a) MP, (b) FP-2-180, (c) FP-3-120, (d) FP-4-180 of Normalized lateral deflection, y/D versus Normalized depth, z/L_p.
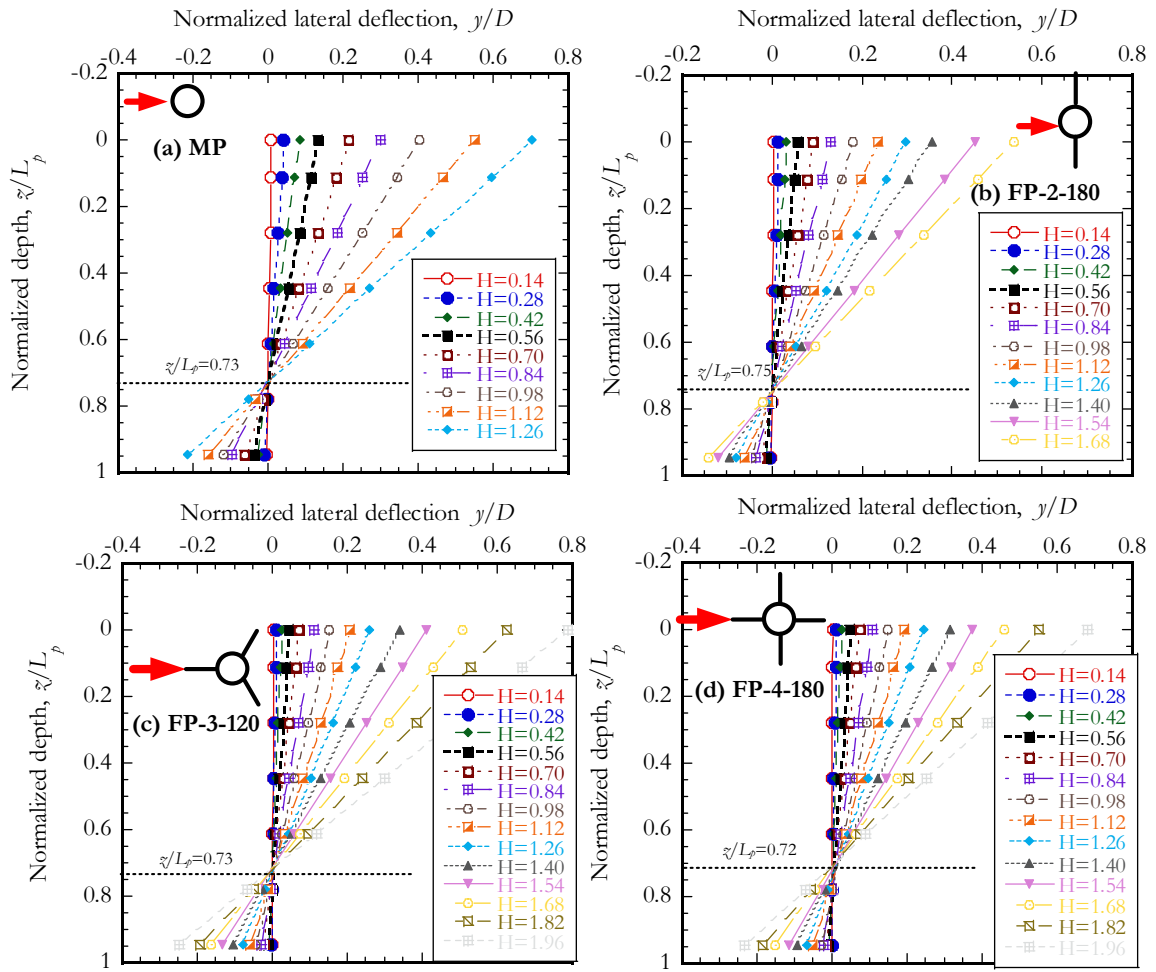
4.4.6   Lateral soil pressure along the length of the pile

Pressure cells, attached on the surface of the piles at various depths, were used to measure the lateral soil pressure during lateral loading. Figure 4-10 shows the measured earth pressure profiles. Increase in lateral load resulted in an increase in lateral soil pressure in front of the pile repeating the similar shape of pressure distribution with each load increment. The depth of maximum lateral soil pressure was found to be at $0.45L_p$. The presence of the fin had no influence on the depth where the maximum pressure occurred. The depth of stress reversal (i.e., depth of pile

91

rotation point) was found to be in the range of $0.7L_p$ to $0.75L_p$. Similar pressure distribution profiles were observed by Prasad and Chari (1999) for circular piles in sand.

4.4.7   Earth pressure distribution around the perimeter of the pile

Lateral soil pressure distribution around the perimeter of the pile at the point of maximum pressure along the pile length (i.e., on section **A-A** of Figure 4-1) is presented in Figure 4-11 below. The pressure measurements made both on the pile and the fins are represented on linear expansions of the curved and the flat surfaces at the points marked as sensor points on section **A-A** in Figure 4-1.
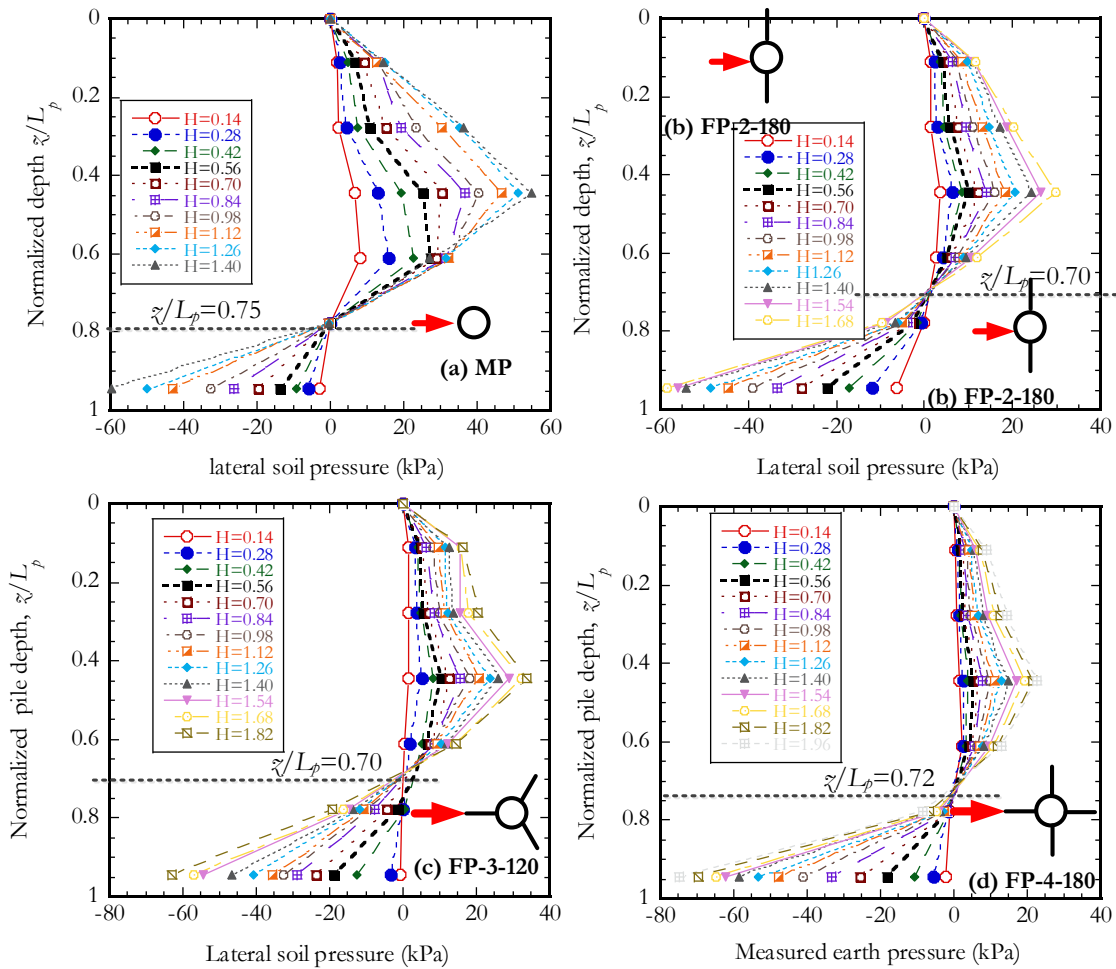
Smith (1987) suggested that the soil resistance to lateral movement of a pile can be expressed in two components: (i) frontal normal bearing pressure and, (ii) side friction. For small diameter piles, the effect of side friction on the periphery of the piles is minimal and can be neglected (Smith, 1987; Ashour et al., 2008). The component of soil resistance to lateral pile movement considered in here will be only the frontal normal bearing pressure. The distribution of the lateral pressure for MP was symmetric about the pile circumference and exhibited similar distribution as those reported by Prasad and Chari (1999) and Smith (1987) for a pipe pile.
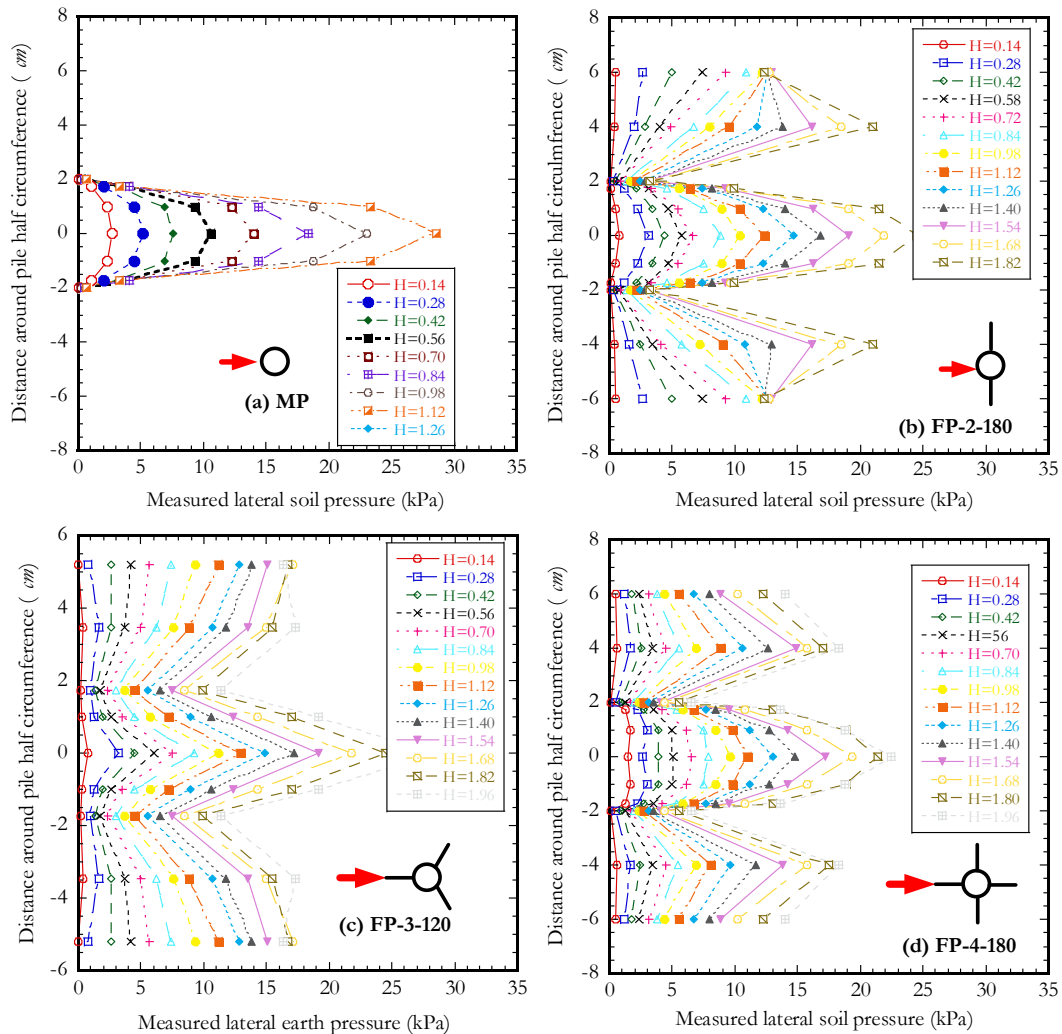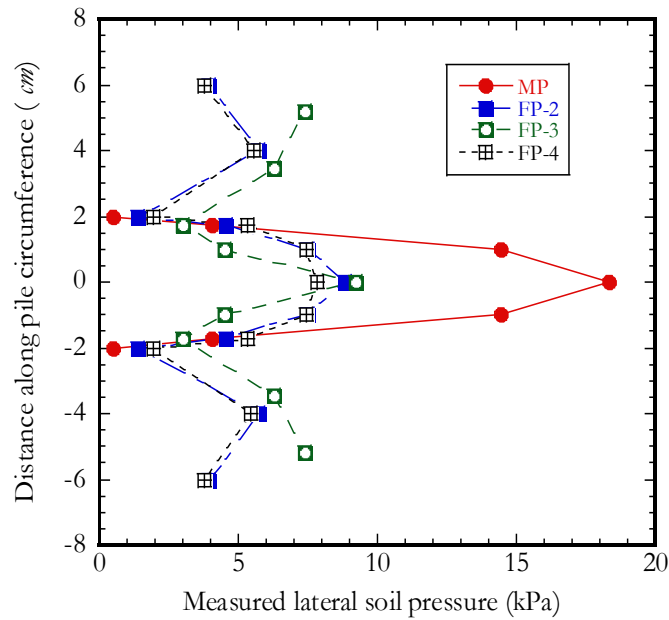
Comparison of lateral soil pressure distributions at the same applied lateral load (Figure 4-12) shows that the pressure acting on monopile is larger than that acting on finned piles. This is attributed to the fact that finned piles have a large surface area than monopile hence smaller pressure in the shaft section of the finned pile. For a finned pile, pressure on the shaft section was larger than the pressure in the finned section for all fin configurations.

4.5 Bulge factor of finned piles

Rudolph and Grabe (2013) suggested that the effectiveness of the fins on a pile can be assessed by calculating separately the amount of pressures that act on the fin and on the pile shaft using the proposed mechanical system shown in Figure 4-13,

94

where the pile shaft is represented as a beam element with length $L_1 = D/2$ and the fin is represented as a beam element with a length $L_2 = W_f$ (Figure 4-13(b)).

Defining the total load as Q_r and the load acting on the fin as Q_w, the pressure on the wing can be defined as:

$$p_w = \frac{Q_w}{W_f} \qquad (4\text{-}6)$$

The pressure on the shaft is then defined as:

$$p_{sh} = \frac{(Q_r - Q_w)}{W_f} \qquad (4\text{-}7)$$

(a) Pressure distribution
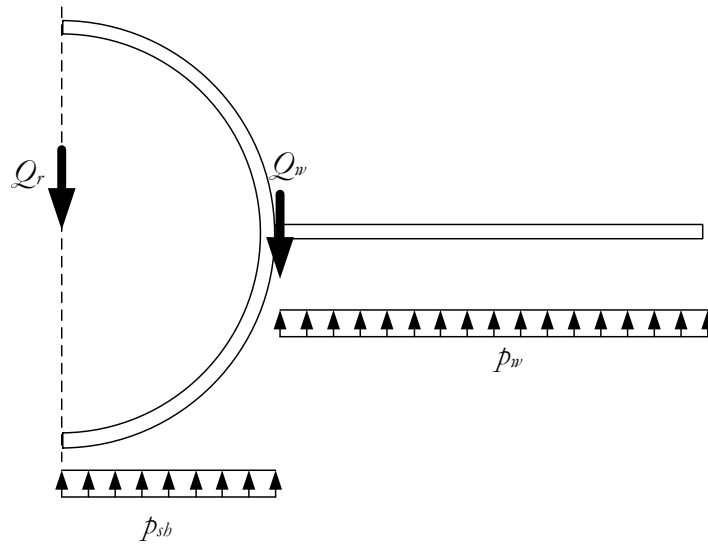
(b) Idealized beam section

EI_1, L_1 EI_2, L_2

$L_1 = D/2$ $L_2 = W_f$

95

The efficiency of the fin can then be expressed as the ratio of the two pressures:

$$R_p = \frac{p_w}{p_{sh}} \leq 1.0 \qquad (4\text{-}8)$$

R_p is used to calculate the bulge factor, κ_w, which is described as the ratio of the resistance provided by the pile and the fins at the same depth.

$$\kappa_w = \frac{\left(D + 2R_p W_f\right)}{D} \qquad (4\text{-}9)$$

In the experiments reported here, both the p_{sh} and p_w were measured directly during lateral loading. The values of p_{sh} and p_w obtained at each loading stage from earth pressure sensors attached at the mid axis of the shaft section and mid axis of the fin section (see Section A-A in Figure 4-1) at a depth, z of $0.45L_p$ were used to compute the fin efficiency, R_p as given in Equation 4-8. The variation of the computed fin efficiency, R_p with applied lateral load for the three finned piles are shown in Figure 4-14. Although the data shows increasing efficiency with load for each pile, the measured ultimate load state was selected for each pile in order to effectively compare the R_p values. At the normalized ultimate lateral load state (i.e., 2° pile head rotation) for each pile type the fin efficiency R_p was found to be 0.76 for FP-2, 0.65 for FP-3 and 0.78 for FP-4. Values of R_p obtained for FP-2 and FP-4 were similar. The R_p for FP-3 was lower than those calculated for FP-2 and FP-4 partly due to the oblique orientation of the fins hence smaller area available to resist lateral movement when compared to FP-2 and FP-4.

96
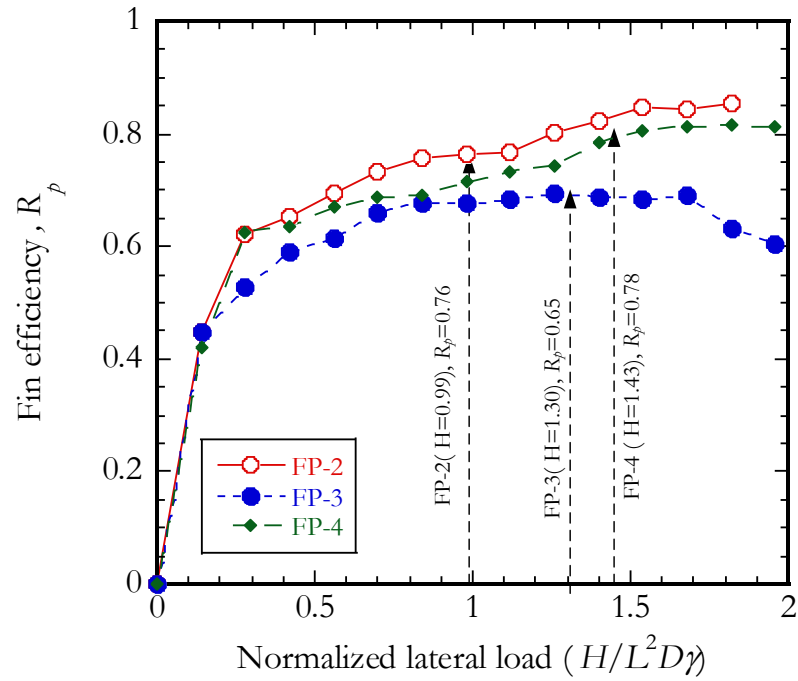
4.6 Maximum lateral soil pressure (p_{max})

Accurate determination of the maximum soil pressure is critical in estimating the lateral pile capacity. Lateral soil resistance of a finned pile can be compared to that of monopile by incorporating the bulge factor, κ_w in the finned section of the piles.

Considering the fins on a pile, the effective diameter of the finned pile can be expressed as $D^*=D_p\ \kappa_w$ while that of the monopile it is $D^*=D_p$. The bulge factors, κ_w were calculated from equation 4-9. A bulge factor of 2.56 was used for FP-2 and FP-4, while a value of 2.30 was used for FP-3 to compute the maximum soil resistance in this study. The ultimate soil pressure was considered to correspond to the pressure reading taken at 2° pile head rotation. The measured earth pressure values were non-

97

dimensionalized by multiplying each quantity by coefficient $(D^*/L^2\gamma)$. In this process, D^* incorporated the effect of the fins, while $L^2\gamma$ incorporated the effect of pile length and soil density. The ultimate lateral soil resistance along the length of the piles measured from earth pressure gauges were then compared to those proposed by other researchers as show in Figure 4-15.

The tests agreed well with the empirical method proposed by Prasad and Chari (1999) with 2%-9% deviation. The data did not agree well with empirical determinations proposed by Broms (1964) and Fleming (1992), as these two empirical methods were developed in absence of actual pressure data. Furthermore, the ultimate soil resistances in these latter methods were assumed to occur at the pile tip at the displacement level of 0.1*D,* which in most cases is less than that of the ultimate state.

Normalized lateral soil pressure ($P_{max}D^*/L^2\gamma$)
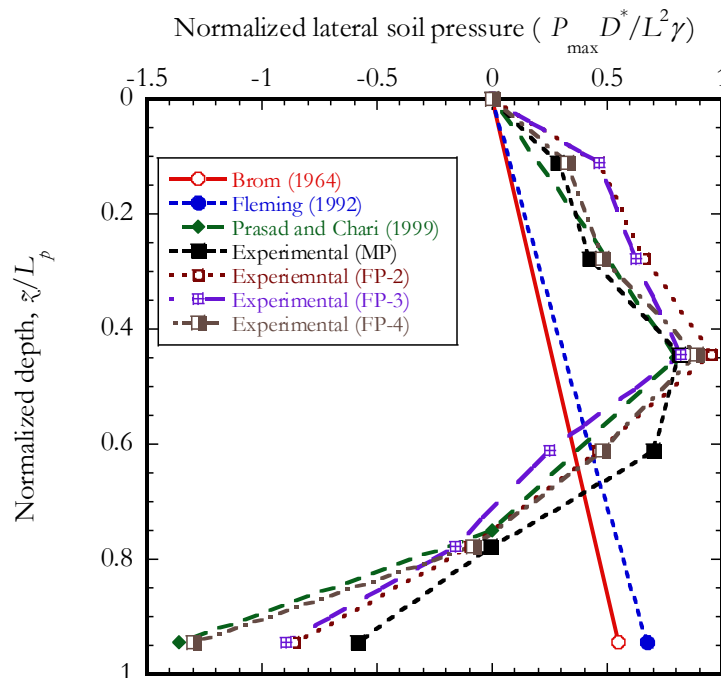
In the experiments the maximum pressure occurred at $0.45L_p$, as observed in Figure 4-15. The ratios of the maximum earth pressures at $0.45L_p$ and the earth pressures at the pile tip were all less than 1.7, as suggested by Prasad and Chari (1999).

4.7 Soil pile interaction: Force-displacement (p-y curves)

The measured lateral earth pressure profiles along the length of the piles (Figure 4-10) were used to directly determine the soil reaction during lateral loading. The soil reaction (force/unit length) was determined by multiplying the measured earth pressure with the effective pile diameter, D^*. The effective pile diameter for the finned section of the pile was the taken as the product of the diameter, D_p of the monopile and the bulge factor κ_w, as described earlier.

Earlier, the lateral displacement of each pile at different depths along the length of the pile was computed from two LVDTs readings at the pile head, assuming a linear variation of displacement throughout the length as shown in Figure 4-9. The lateral displacement profiles of the piles in Figure 4-9 and the calculated soil reaction profiles in Figure 4-10 were used to develop the *p-y* curves along the length of each pile. These *p-y* curves were then compared with theoretical *p-y* curves developed using two separate methods: (i) API (1993) method ;(ii) Zhang (2009) method.

4.7.1 *p-y* curves from methodology developed by Zhang

Zhang (2009) proposed a nonlinear method for estimating *p-y* curves for rigid piles in sand. The method assumed a linear variation of the ultimate soil resistance and modulus of horizontal subgrade reaction with depth. Furthermore, it assumed that the

99

modulus of subgrade reaction decreases with pile displacement. The process is described as below.

i. The lateral soil resistance, p at any depth, z is expressed

$$p = k_h y = \frac{n y_0 (a-z) z}{a} \qquad (4\text{-}10)$$

Where k_h is the horizontal subgrade reaction, a is the depth of pile rotation below the ground surface (seeFigure 4-16), y_0 is the lateral pile displacement at the ground surface.

ii. The constant, n can be expressed as function of normalized pile displacement at the ground surface, y_o by equation (4-11)

iii. The maximum horizontal subgrade reaction, n_{max} can be obtained from Figure 4-17 as proposed by Murchison and O'Neil (1983) and Zhang (2009).

$$n = 0.066 n_{max} \left(\frac{y_o}{D} \right) \qquad (4\text{-}11)$$
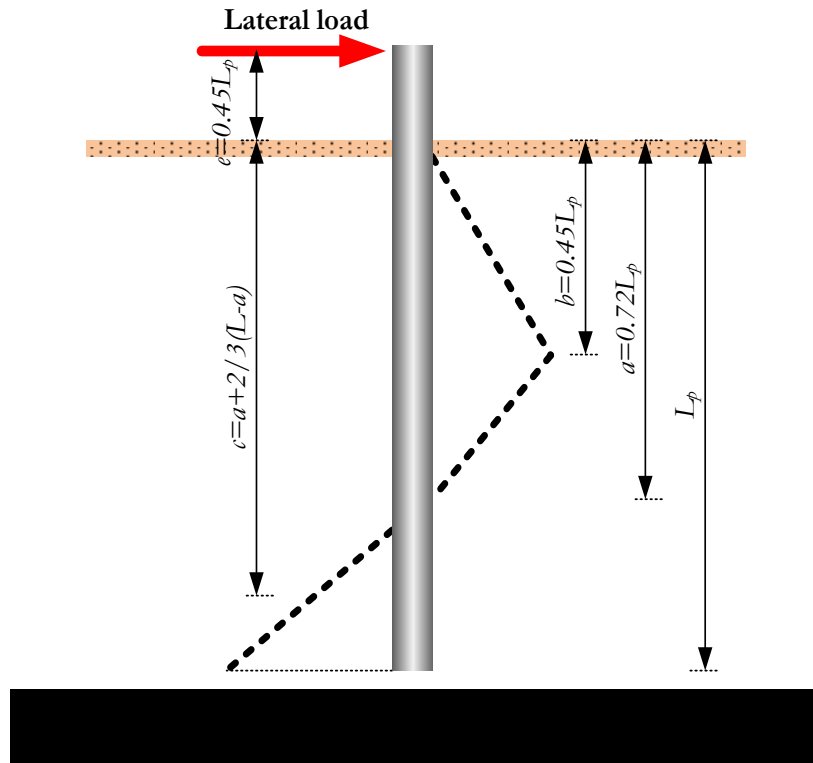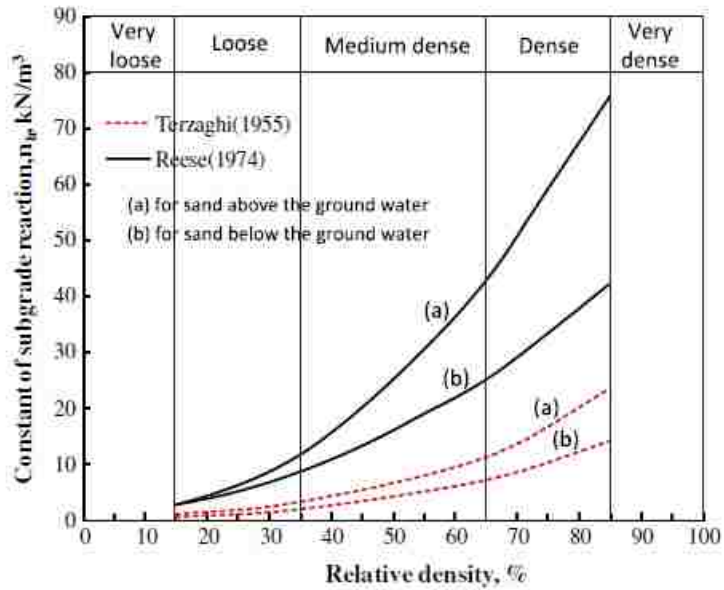
Using this method, for sand of ϕ =35.2˚, and relative density of 32% the value of the constant n_{max} was estimated as 10 kN/m². The parameters *a*, *b* and *c* (as described in Figure 4-16) were directly obtained from the earth pressure distribution profiles along the length of the piles. Values of $a=0.72L_p$, $b=0.45L_p$ and $c=a+2/3(L_p-a)$ were used in appropriate computations, as will be discussed later in this Chapter. The bulge factor, K_w was incorporated when describing the finned section of the pile.

The *p-y* curves developed using Zhang (2009) method were compared with the experimentally determined *p-y* curves as shown in Figure 4-18. The experimental and the computed *p-y* curves proposed by Zhang (2009) showed similar trends, but the stiffness from the method by Zhang (2009) were systematically higher than those obtained experimentally by about 20-35%. The empirical method overestimated the experiment at and above $z=0.44L_p$, point at the maximum lateral soil pressure for all

101

finned piles. Below $z=0.44L_p$ the empirical curves underestimated the experiment. Regardless, the experimental and the empirical p-y curves displayed similar initial stiffness, which was also the same for all piles at $z=0.44L_p$.
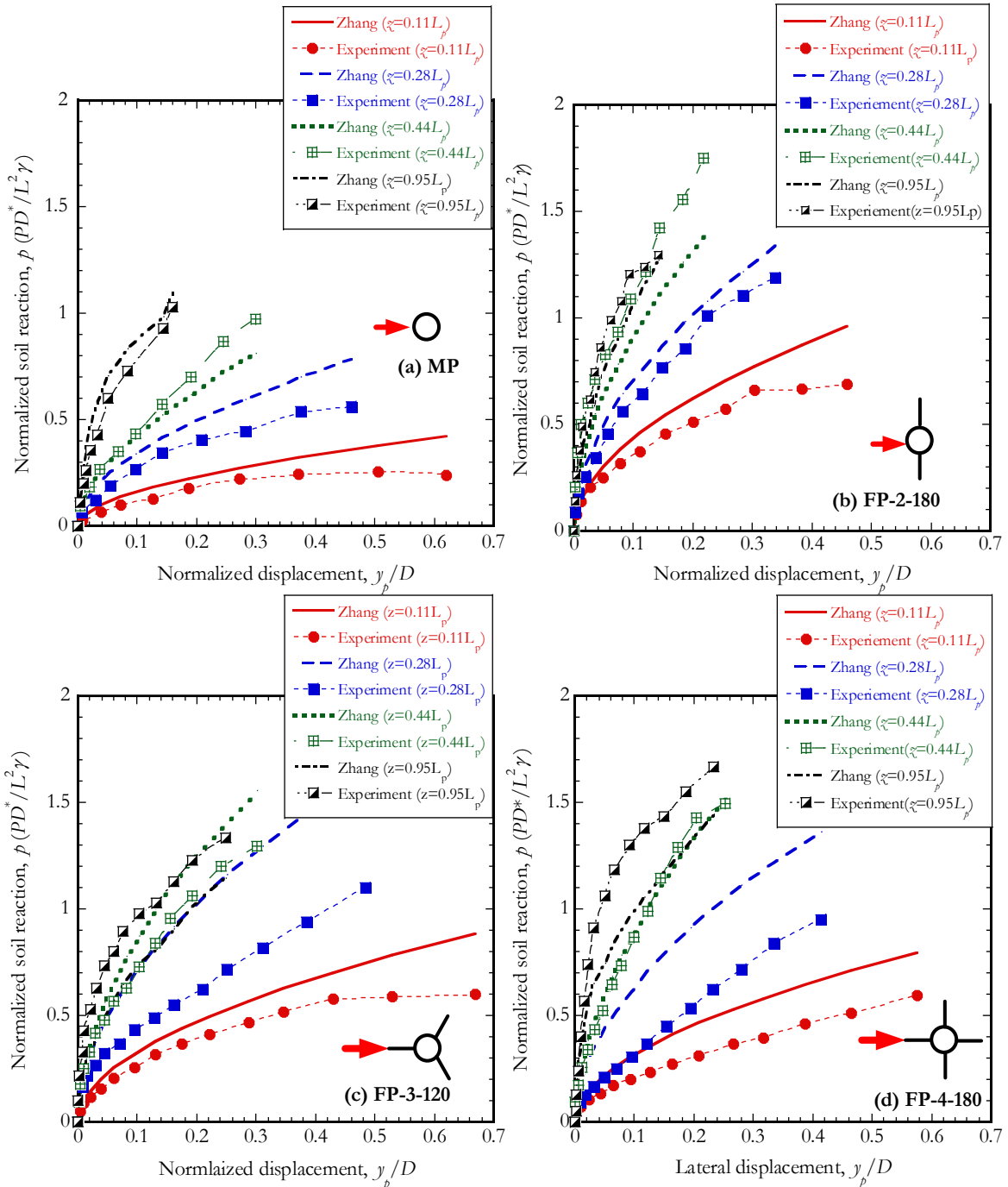
4.7.2 *p-y* curves from methodology developed by API (1993)

In order to determine *p-y* curves using the method proposed by API (1993), first the ultimate soil resistance, p_u was calculated using equation 4-12:

$$p_u = (C_1 z + C_2 D)\gamma z \qquad (4\text{-}12)$$

Where D is the diameter of the monopile and z is the depth below the ground surface. The coefficients C_1 and C_2, which depend on the friction angle, were obtained from Figure 4-19 (API, 1993).

A hyperbolic function given by equation 4-13 below was used to determine the soil pressure, *p* at various displacements, *y*.

$$p = A p_u \tanh\left(\frac{n_{\max} z y}{A p_u}\right) \qquad (4\text{-}13)$$

The coefficient A was calculated from equation 4-14.

$$A = 3.0 - 0.8\frac{z}{D} \qquad (4\text{-}14)$$

In this work, estimation of the *p-y* curves for finned piles from API approach followed again the incorporation of the bulge factor in the finned section of the pile when computing the pressures. Equation 4-12 was modified my multiplying the soil reaction by the bulge factor for section of the pile with fin. Therefore, for soil of $\phi = 35.2°$ the value of coefficients C_1 and C_2 were determined 3.2 and 2.5, respectively from Figure 4-19. The value of the constant $n_{\max}$ was determined as 10kN/m² from Figure 4-17.

103
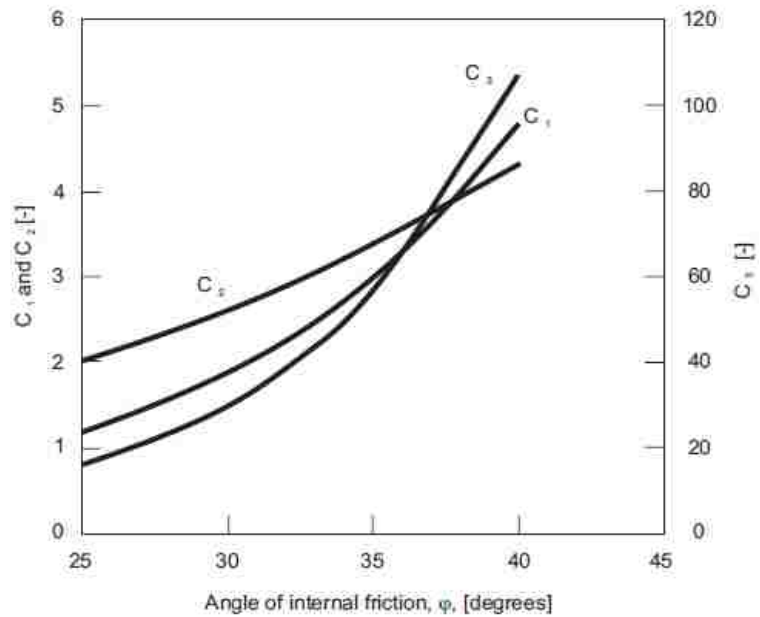
Figure 4-20 shows the *p-y* curves computed for different depth using the API method compared to those obtained experimentally. Stiffer response of the initial tangent of the *p-y* curves were observed from *p-y* curves from API method. In addition, the experimental and empirical plots displayed marked differences in the shape of the *p-y* curves. One of the major reasons for the discrepancy may be attributed to the fact that the API method was developed for flexible piles and its application in rigid piles has not been verified by any past work.

104
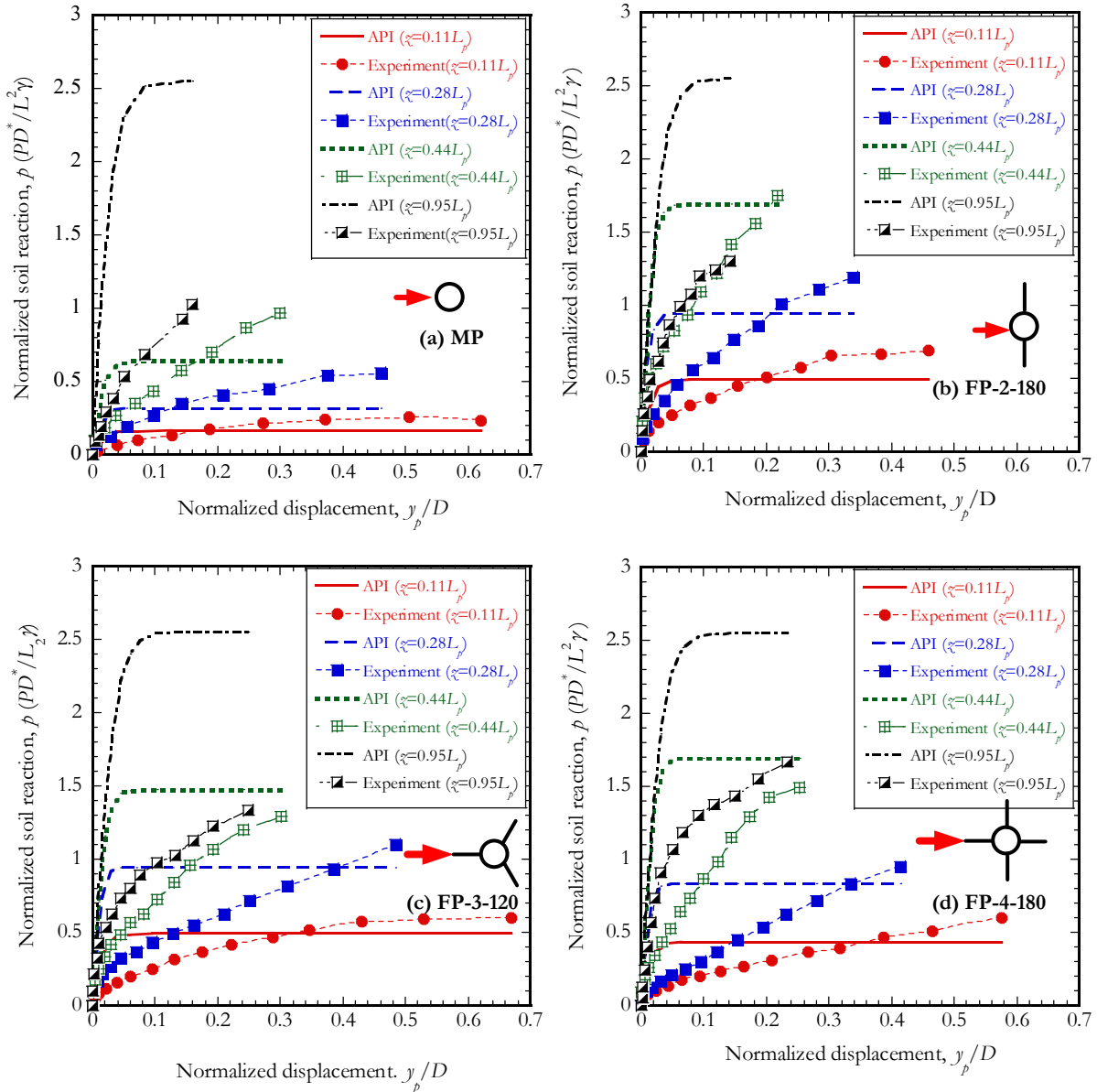
4.8 Estimation of ultimate lateral capacity of finned pile

In order predict the ultimate capacity of laterally loaded finned pile, the method proposed by Zhang (2009) for estimating the lateral capacity of rigid piles was modified to take into account the effect of fins. Zhang's approach assumed that both the

moment and horizontal loads were large enough to cause yielding of the soil in the region above and below the rotation point. Accordingly, the ultimate lateral load capacity, H_u, was expressed as:

$$H_u = \frac{mb^2}{2} - \frac{ny_0}{a}\left[\frac{a}{2}(b^2 - L^2) - \frac{1}{3}(b^3 - L^3)\right] - m(L^2 - c^2) \qquad (4\text{-}15)$$

The parameters *a, b* and *c* were described earlier in Figure 4-16. They were directly inferred from the experimental test data of Figure 4-10. The two other parameters, *m* and *n* in equation 4-15 must be determined in order to solve the equation. The parameter *n* can be calculated from equation 4-10 and Figure 4-17 (Murchison and O'Neil, 1983). The parameter *m* can be obtained from the assumption that the ultimate soil resistance varies linearly with depth, therefore $m = p_u/z$, which is a constant.

The ultimate lateral soil resistance, p_u is calculated using equation 4-16 (Prasad and Chari, 1999) where it is equal to the maximum pressure, P_{max}, multiplied by the diameter of the monopile, *D* (Note that *D** is used instead of *D* in equation 4-16)

$$p_u = P_{max} D \qquad (4\text{-}16)$$

Where,

$$P_{max} = 10^{(1.3\tan\phi + 0.3)}\gamma z \qquad (4\text{-}17)$$

The method by Prasad and Chari (1999) was selected to determine the variation of p_u because the method considered the ultimate soil resistance at the point of rotation to be zero. This assumption agreed with the conditions of the experimental study in here. Lateral displacement of the pile at the ground surface is a function of the stiffness of the pile assembly and the soil density. The number and orientation of the fins will modify the stiffness of the pile and lower the magnitude of the displacement at the

106

ground line when compared to that of a monopile. In order to apply equation 4-15 to a finned pile, a displacement factor, δ_w is introduced which compares the ground line deflection of a monopile to that of a finned pile at the same pile head rotation, as in Equation 4-18.

$$\delta_w = \frac{y_{o(MP)}}{y_{o(FP)}} \qquad (4\text{-}18)$$

Equation 4-15 was modified to take into account the effect of the fin by multiplying the ground line deflection of monopile by the displacement factor. Thus, the equation for determining the ultimate lateral capacity of finned pile was expressed as Equation 4-15b:

$$H_u = \frac{mb^2}{2} - \frac{ny_0}{a\delta_w}\left[\frac{a}{2}(b^2 - L^2) - \frac{1}{3}(b^3 - L^3)\right] - m(L^2 - c^2) \quad (4\text{-}15b)$$

With the known ground line deflection of the monopile at ultimate load, the ultimate lateral load of a finned pile can then be estimated from Equation 4-15b. Figure 4-21 shows the variation of the displacement factor, δ_w with the pile head rotation of a monopile. At 2° rotation which correspond to ultimate load state of the pile, the δ_w values were obtained as 2.3, 2.8 and 3.0 for FP-2, FP-3 and FP-4 piles, respectively.

The measured and the predicted ultimate lateral load of the piles from Equation 4-15b is correlated in Figure 4-22. It can be observed that the predicted ultimate lateral capacity is in good agreement with the measured capacity with errors ranging from 4%-17%.

107
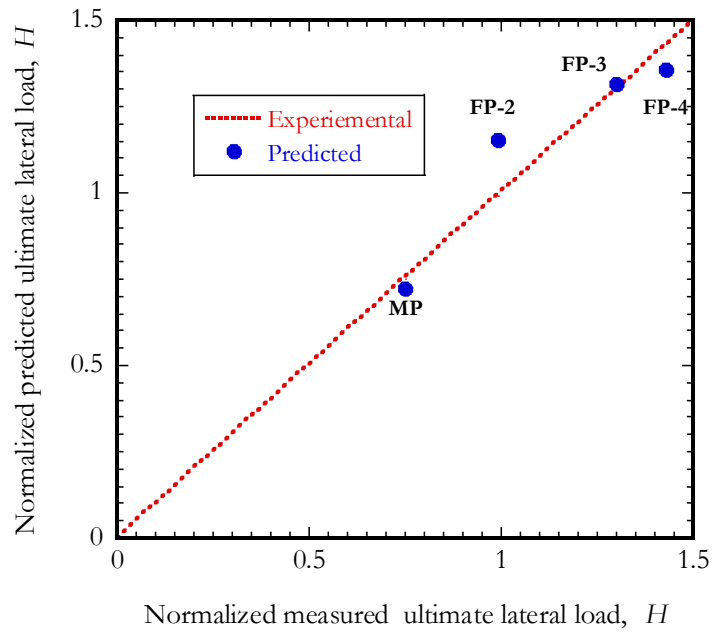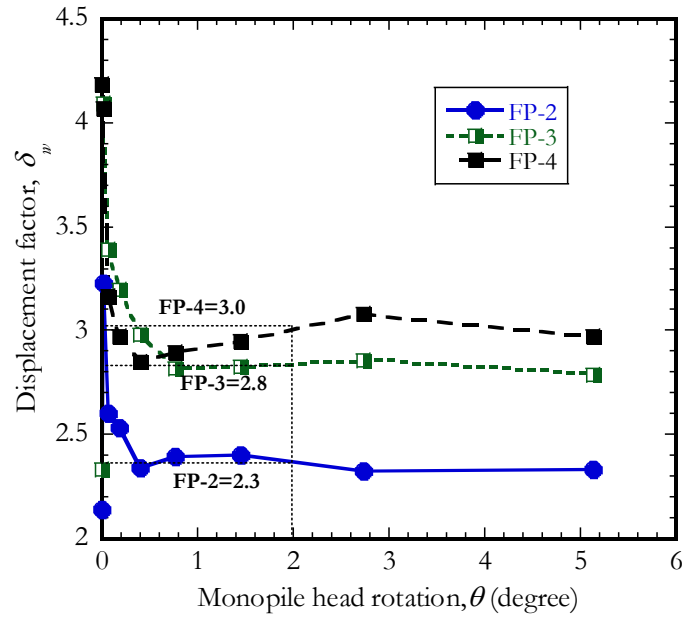
4.9 Summary and conclusion

The interaction between finned pile and the surrounding soil was investigated through static load model pile tests. The model piles and surrounding soil were instrumented with LVDTs, strain gauges and earth pressure sensors. The measured lateral earth displacements and the pile head rotation at the ground line, the lateral earth pressure and pile strain profiles along the length of the piles were used to predict the load-displacement response and soil-pile interaction. The following conclusions were drawn from the results of the work presented in this chapter:

(i)   Addition of fins modified the bending moment distribution of the pile. The maximum bending moment of a monopile occurred at a depth of $0.31L_p$ while that of finned piles occurred at a depth of $0.45L_p$ from ground surface. Fins reduced the bending moment profile of a pile within the finned section significantly. The reduction in bending moment at the finned section ranged from 8%-55% depending on the number of fins in a pile. The bending moment distribution of the sections above and below the fins was similar to that observed for monopile.

(ii)   The depth of pile rotation point below the ground surface calculated from measured pile displacements above ground line ranged from $0.72L_p$ -$0.75L_p$ and the point of stress reversal from measured earth pressure data also ranged between $0.72L_p$-$0.75L_p$. The estimated depth of pile rotation point and the measured point of stress reversal were in good agreement with that observed by Prasad and Chari (1999). For all the piles, the maximum soil pressure occurred at

109

0.45L_p below the ground surface. This depth was similar to that reported by Prasad and Chari (1999). The presence of fins did not modify the point where the maximum soil pressure occurred.

(iii) Lateral soil resistance of a finned pile was compared to that of monopile by incorporating the bulge factor κ_w in the finned section of the piles. Considering the fins, the new diameter of the finned piles was expanded to $D^*=D_p\,\kappa_w$ while that of the monopile was $D^*=D_p$. Bulge factor of 2.56 was used for FP-2 and FP-4 while a value of 2.30 was used for FP-3 to compute the ultimate soil resistance of finned pile. Comparison of the ultimate soil resistance measured and the computed soil resistance from a method developed by Prasad and Chari (1999) was in good agreement.

(iv) Comparison of the soil resistance and displacement curves (*p-y* curves) of finned piles and of monopile were made possible by introduction of the budge factor κ_w. Experimental *p-y* curves were compared with *p-y* curves from methods proposed by Zhang (2009) and API (1993). Empirical method by Zhang delivered better agreement with the experimental *p-y* curves while the predictions from API method resulted in large discrepancies with the experimental trends. The large deviation between the API method predictions and the experimental curves was attributed to the fact that API method was developed for flexible pile and its applicability to rigid piles has not been adequately verified.

(v) Estimation of the ultimate lateral pile capacity was obtained by modifying an equation proposed by Zhang (2009). Introduction of displacement factor, δ_w

110

made it possible to estimate the lateral capacity of a finned pile using Zhang (2009) approach. Displacement factor values of 2.3, 2.8 and 3.0 were determined and used in ultimate lateral pile capacity estimations for FP-2, FP-3 and FP-4, respectively. The calculated and measured lateral capacities of piles at pile head rotation of 2° were in very good agreement.

4.10 References

1. API (1993): Recommended practice for planning, designing, and constructing fixed offshore platform: Working stress design, RP2A-WSD. 20th edition.

2. Ashour, M., Norris, G., and Elfass, S. (2008): Analysis of laterally loaded long or intermediate drilled shafts of small or large diameter in layered soil, Univ. of Nevada, Reno, NV.

3. Broms, B.B. (1964): Lateral resistance of piles on cohesionless soils. Journal of Soil Mechanics and Foundation Division, ASCE, (SM3), Vol. 90, No. 3, pp. 123–156.

4. Chin, F. V. (1970): Estimation of the Ultimate Load of Piles not carried to Failure, Proceedings of 2nd Southeast Asian Conference on Soil Engineering, Southeast Asian Society of Soil Engineering, Singapore: 81–90.

5. Davisson, M. T. (1972): High Capacity Piles," Proceedings, Lecture Series, Innovation in Foundation Construction, Vol. 52, ASCE, Chicago, Illinois: 81–112.

6. Duhrkop, J. and Grabe, J. (2008): Improving the Lateral Bearing Capacity of Monopiles by Welded Wings. Proceedings of the 2nd BGA International Conference on Foundations, Vol. 1, pp. 849-860.

7. Fleming, W. G. K., Weltman, A. J., Randolph, M. F., and Elson, W. K. (1992). Piling engineering, Wiley, New York.

8. GAI Consultant Inc., 1982, "Laterally Loaded Drilled Pier Research, Vol. 2, Research Documentation," *GAI Report EL-*2197*, Research project* 1280–1*, EPRI*, Monrocville, PA.

9. Hu, Z. H., McVay, M., Bloomquist, D., Herrera, R., and Lai, P. (2006): Influence of Torque on Lateral Capacity of Drilled Shafts in Sands. *Journal of Geotechnical and Geoenvironmental Engineering*, 132 (4): 456–464.

10. Lee, J., Paik, K., Kim, D., and Park, D. (2012): Estimation of ultimate lateral load capacity of piles in sands using calibration chamber tests. *Geotechnical Testing Journal*, 35(4): 1–12.

11. Meyerhof, G. G., Mathur, S. K. and Valsangkar, A. J. (1981): Lateral resistance and deflection of rigid wall and piles in layered soils. *Canadian Geotechnical Journal*, 18: 159–170.

12. O'Neill, M., and Murchison, J. (1983): An evaluation of p-y relationships in sands. A report to the American Petroleum Institute, *PRAC 82-41-1*, University of Texas, Huston.

13. Peng, J., Clarke, B.G. and Rouainia, M. (2011): Increasing resistance of piles subjected to cyclic lateral loading. *Journal of Geotechnical and Geoenvironmental Engineering*, 137 (10): 977-982.

14. Petrasovits, G., and Award, A. (1972): Ultimate lateral resistance of a rigid pile in cohesionless soil. *Proceedings of 5th European Conference on Soil Mechanics and Foundation Engineering*, Madrid, Vol.3, pp. 407-412.

15. Prasad, Y. V. S. N. and Chari, T. R. (1999): Lateral capacity of model rigid piles in cohesionless soils. *Soils and Foundations*, 39 (2):21–29.

16. Rollins, K. M., K. G. Olsen, D. H. Jensen, B. H. Garrett, R. J. Olsen, and J. J. Egbert (2006): Pile Spacing Effects on Lateral Pile Group Behavior: Analysis. *Journal of Geotechnical and Geoenvironmental Engineering, ASCE*, 132(10):1272-1283.

17. Rudolph, C and Grabe, J. (2013): Laterally loaded piles with wings- Insitu testing with cyclic loading from varying directions. *Proceedings of ASME, 31th International Conference on Ocean, Offshore and Arctic Engineering*, Nantes, France

18. Rutledge, P. C. (1956): Design monographs for pole structure.

19. Sawwaf, M. (2006): Lateral resistance of single pile located near geosynthetic reinforced Slope. *Journal of Geotechnical and Geoenvironmental Engineering*, 132(10): 1336-1347

20. Smith, T. D. (1987): Pile horizontal soil modulus values. *Journal of Geotechnical Engineering* 113 (9): 1040–1044.

21. Uchida, K., Kawabata, T. and Aki Ohara, K. (2006): Lateral load capacity for pile with multi-stepped two diameters embedded in sand. In the *Proceedings of the*

Sixteenth International Offshore and Polar Engineering Conference, San Francisco, California, USA.

22. Zhang, L., Silva, F. and Grismala, R. (2005): Ultimate lateral resistance to piles in cohesionless soils. *Journal of Geotechnical and Geoenvironmental Engineering,* 131 (1): 78-83.

23. Zhang, L, (2009): Nonlinear analysis of laterally loaded rigid piles in cohesionless soil. Computer and Geotechnics, 36 (5): 718–724.

<div align="right">

CHAPTER 5

</div>

5 CYCLIC RESPONSE OF LATERALLY LOADED MONOPILE AND FINNED PILES

5.1 Introduction

During its lifetime, the monopile foundation of an offshore wind turbine is unavoidability subjected to long-term cyclic loading, originating from waves and wind. This can lead to accumulated rotation and change in stiffness of the monopile and seriously impact the strict operation criteria and standards of the offshore wind turbine. The allowable accumulation of pile head rotation at mudline is limited between 0.25° to 0.30° according to DNV standards (Malhotra,2009), and to 0.50° according to API (1993).

Lateral capacity of pile is a function of the pile geometry, soil properties and type of loading. Therefore, improving the capacity of a pile may require either improving the properties of the near soil surface layers or changing the pile geometry. It can be prohibitively expensive or virtually impossible to improve the soil properties at the seabed hence the better alternative is to change the pile geometry. At sites where water depths are greater than 30m the monopile diameter may be increased to provide additional stiffness. However large cross section area may attract larger wave and current loading and incur significantly higher manufacturing and handling costs, thus reducing the potential benefit of increase size (Murphy et al., 2015).

Alternative to increasing the monopile diameter is using finned-piles, which involves incorporation of plates attached to monopiles to increase their lateral load capacity, increase pile-soil stiffness and minimize the accumulated pile head rotation. At present, little or no research has focused on cyclic response of finned piles. It is challenging to carry out full model test or field test on finned piles with large diameters thus model test can be used to produce intuitive results. This chapter explores the potential of using of finned monopile for offshore wind turbine foundation though 1 g model test.

5.2 Cyclic response of piles

Cyclic response of pile can be described in terms of pile head displacement, y or rotation θ, and the applied lateral load H. Four parameters are necessary to describe the cyclic loading process, the maximum applied cyclic load H_{max}, the minimum applied cyclic load H_{min}, the period of a cycle, T and the number of cycles, N. The difference between H_{max} and H_{min} is the loading amplitude, ΔH.

A schematic of typical load-displacement response of a pile under constant-amplitude cyclic loading is shown in Figure 5-1. In each loading cycle, the maximum and minimum value of load ($H_{max, N}$ and $H_{min, N}$) and displacement ($y_{max, N}$ and $y_{min, N}$) can be obtained. Pile stiffness can be evaluated as defined in Figure 5-1, as either "pile equivalent stiffness" or "pile secant stiffness".

The characteristic of the cyclic load must be uniquely defined. Two independent parameters are defined to characterize the applied sinusoidal loading (Leblanc, 2010).

116

$$\zeta_b = \frac{H_{\max}}{H_u} \qquad\qquad (5\text{-}1)$$

$$\zeta_c = \frac{H_{\min}}{H_{\max}} \qquad\qquad (5\text{-}2)$$

Cyclic load magnitude ζ_b, expresses the magnitude of loading as the ratio of applied cyclic load to the ultimate lateral load in static test. The cyclic load ratio ζ_c, defines the direction of loading on the basis of minimum and maximum applied cyclic load and will take maximum value of 1 for static loading, 0 for one-way loading and -1 for two-way loading.
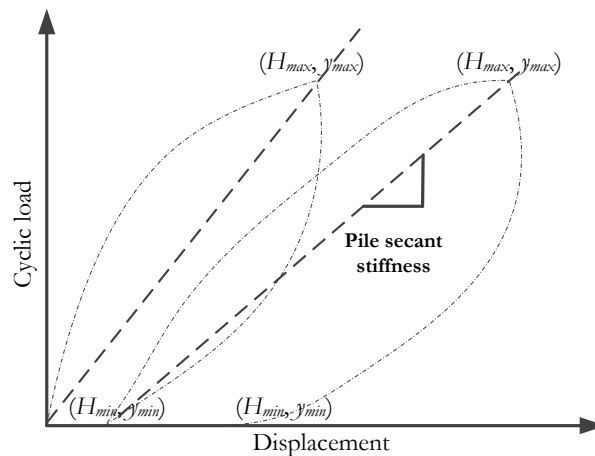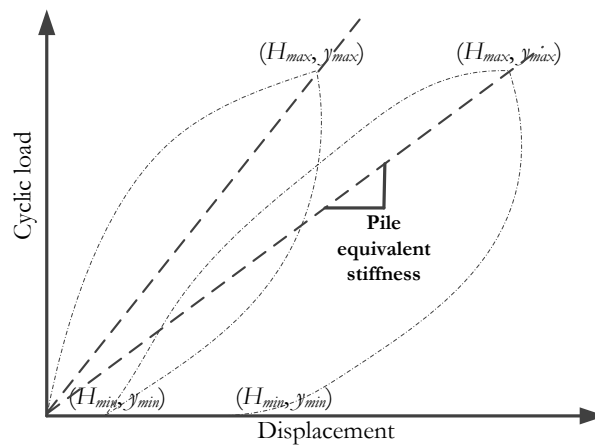
5.3 Cyclic accumulated deflection and rotation models

Cyclic lateral loading is often investigated using static pile analysis, where the pile head displacement or rotation under static condition are modified to account for the effect of cyclic loading using degradation laws (Garnier, 2013). The most common procedure for predicting accumulated displacement or rotation for constant amplitude cyclic loading involves modelling the accumulated displacement, y_N or rotation θ_N, after N number of loading cycles as a function of number of cycles, N. The displacement y_1 or rotation θ_1 in the first loading circle is incorporated as:

$$y_N = f(N, y_1) \tag{5-3}$$

Centrifuge model tests and 1g model tests have been used to study the response of piles under cyclic loading which have led to the development of a logarithmic function, as given in Equation 5-4 (Peralta and Achimus, 2010) and power law equation, as given in Equation 5-5 (Klinkvort et al., 2012; Long and Vennester, 1994; Peralta and Achimus, 2010). These equations have been used widely in modelling the accumulated pile head displacement and rotation.

$$y_N = y_1 (1 + b \ln(N)) \tag{5-4}$$

$$y_N = y_1 N^{\alpha} \tag{5-5}$$

Where, b and α are model parameters.

Using results from centrifuge test on monopile and finned piles, Bienen et al., (2012) modified the logarithmic expression (Equation 5-4) and developed the following equation for pile head displacement.

118

$$y_N = y_1\left[1 + 0.05\frac{N-1}{N}\ln\left(\frac{N}{2}+1\right)\right] \qquad (5\text{-}6)$$

Based on results from 1g test on stiff piles, Leblanc et al., 2010 proposed a model for calculating the accumulated pile head rotation as:

$$\theta_N = \theta_1\left(1 + T_b T_c N^\alpha\right) \qquad (5\text{-}7)$$

The model parameters T_b and T_c are functions of ζ_b and ζ_c respectively.

5.4 Aim of the study

This research aims at understanding the advantage of fins in improving the cycling response and load capacity of the piles through 1 g model test. The study will seek to clarify:

i.   Effect of fins in reducing the accumulated pile head rotation during cyclic loading.

ii.   The effect of fins in improving the soil pile stiffness.

iii. Predicting the long-term response of mono and finned piles at fatigue limit state.

5.5 Cyclic loading device

Figure 5-2 shows a schematic depiction of the cyclic lateral loading system used in this study, which is an improved version of a similar device used by LeBlanc et al., (2010). Figure 5-3 shows a photograph of the actual test set-up.

119

The system consisted of a rectangular soil box of 0.9m length by 0.7m width and 0.7m depth, equipped with a steel loading frame. The cyclic loading is controlled simply using a leaver arm, weight hangers, applied masses m_1, m_2 and m_3 and an electric motor. The leaver is attached to the steel frame through a pivot and carries electric motor which rotates mass m_1. Cables and electric motor controls the rotation of m_1. The rotation causes oscillating motion of the leaver translated as cyclic load on the pile. The loading to the pile is applied through the steel cable attached to the pile and connected to the leaver arm. A load cell is attached to the leaver arm to measure the load on the pile head.
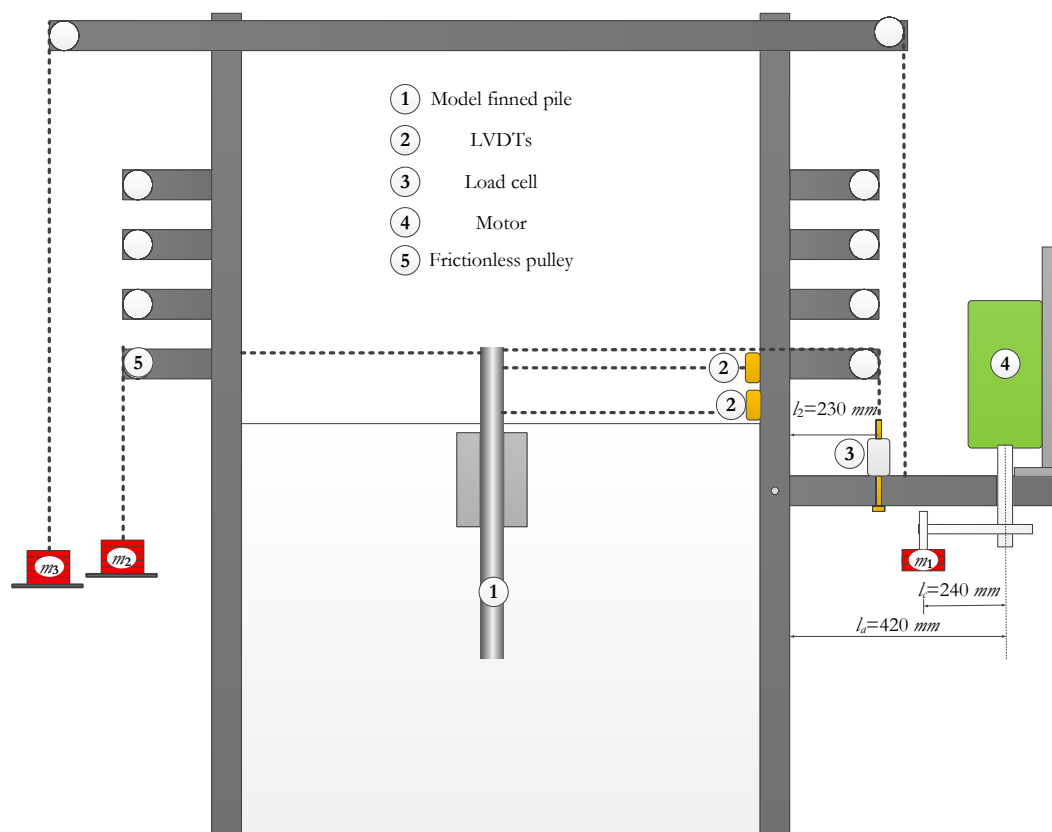
5.6 Generation of cyclic lateral load

The cyclic device worked based on the following principles. Initially when mass $m_1 = m_2 = 0$, mass m_3 is chosen to counterbalance the system. The mass of m_3 needed to counter balance the loading system in here was 8 kg. The masses m_1 and m_2 are then carefully selected to provide the desired cyclic loading.

When the motor rotates the mass $m_{1, a}$ sinusoidal load is produced on the pile head. The equation of this load can be given as following:

$$H(t) = H_0 + H_a \sin(\omega t) \tag{5-8}$$

$$\omega = 2\pi f \tag{5-9}$$

Where ω is the angular rotation frequency of the electric motor.

The mass, m_1 required to produce the desired cyclic load and corresponding counter balance mass m_2 are calculated as follows

$$m_1 = \frac{l_2 H_a}{l_a g} \tag{5-10}$$

$$m_2 = \frac{\dfrac{l_c}{l_a} H_a - H_o}{g} \tag{5-11}$$

Parameters H_0 and H_a for computing the cyclic loading has defined by Leblanc et al (2010) can be estimated from equations 5-10 and 5-11 respectively.

The rotation frequency of the motor was set to 0.1 Hz. This frequency was selected to simulate pile subjected to long term wave loading according to Peng et al., (2011). The dimensions l_a and l_c used in these calculations are provided in Figure 5-2.

121

5.6.1 Model piles and cyclic load application

Previously reported results from cyclic lateral load tests of piles conducted in the centrifuge showed that one-way loading produced the greatest accumulation of displacement at the pile head (Klinkvort and Haidebal, 2013). Also reported is when an offshore wind turbine structure is loaded by water waves the resultant load eccentricity can change between approximately $2D_p$ to $25D_p$ (Klinkvort et al., 2012).

Following the previous findings, one-way cyclic lateral load tests were selected and conducted on MP, FP-2-180, FP-3-120 and FP-4-180 piles. They were all

122

embedded in packed dry sand of relative density 32%. Cyclic load was applied at a distance of 160mm from the sand surface which provided an eccentricity of about $4D_p$. This load eccentricity fell within the range suggested by Klinkvort et al., (2012). The cyclic load applied on the pile head was directly measured using load cell attached to the device. Lateral pile head rotation was measured from displacement transducers attached to pile at 30mm and 150mm from the surface of the sand bed.

5.6.2   Lateral cyclic load ratio

Cyclic load magnitudes, ζ_b of 0.2, 0.3, 0.5, 0.8 and 1.0 of the ultimate load capacity H_u were chosen for the tests. The ultimate load capacity was obtained from static lateral load test on the piles at a pile head rotation of 2° (GAI consultants, 1982), as discussed in Chapter 3. The cyclic load magnitudes of 0.2 and $0.5H_u$ were considered to reflect realistic loading conditions of fatigue limit state and serviceability limit state loading, respectively. Cyclic load magnitude of $0.8H_u$ and above were considered cyclic loading near the ultimate pile capacity. All the cyclic load test was conducted under one-way constant amplitude up to N=1000 cycles.

5.7 Test Results

5.7.1   Characteristics cyclic loads

Different mass combinations of m_1 and m_2 were selected to provide the desired cyclic loading as shown in Table 5-1 below. Theoretical loading calculated from Equation 5-8 was compared with the cyclic load measured from the load cell. Figure 5-4 shows the variation of the experimental and theoretical cyclic loading with time.

123

Loading up to the initial 30s are shown for comparison. The theoretical and experimental cyclic load for each load magnitude agreed fairly well error ranging from 0.6% to 15.1%.

Pile	ζ_b	m_1 (kg)	m_2 (kg)	H_{max} (Expt.)	H_{max} (Theori.)	% Error
	0.2	0.6	0.5	0.167	0.158	5.1
	0.3	1.0	0.8	0.287	0.264	8.7
MP	0.5	1.5	1.25	0.423	0.396	6.8
	0.8	2.5	2.0	0.584	0.660	11.5
	1.0	3.0	2.5	0.749	0.792	5.4
	0.2	0.8	0.7	0.213	0.211	0.95
	0.3	1.2	1.0	0.365	0.317	15.1
FP-2	0.5	2.0	1.5	0.545	0.528	3.2
	0.8	3.0	2.5	0.802	0.792	1.3
	1.0	3.6	3.0	1.000	0.950	5.3
	0.2	1.0	0.8	0.347	0.304	14.4
	0.3	1.5	1.25	0.50	0.45	11.1
FP-3	0.5	2.5	2.0	0.656	0.660	0.6
	0.8	4.0	3.3	0.985	1.056	6.7
	1.0	4.8	3.9	1.224	1.267	2.1
	0.2	1.1	0.9	0.50	0.316	14.4
	0.3	1.6	1.3	0.504	0.480	5.0
FP-4	0.5	3.0	2.5	0.727	0.792	8.2
	0.8	4.5	3.8	1.158	1.214	4.6
	1.0	5.5	4.5	1.457	1.478	1.4

124
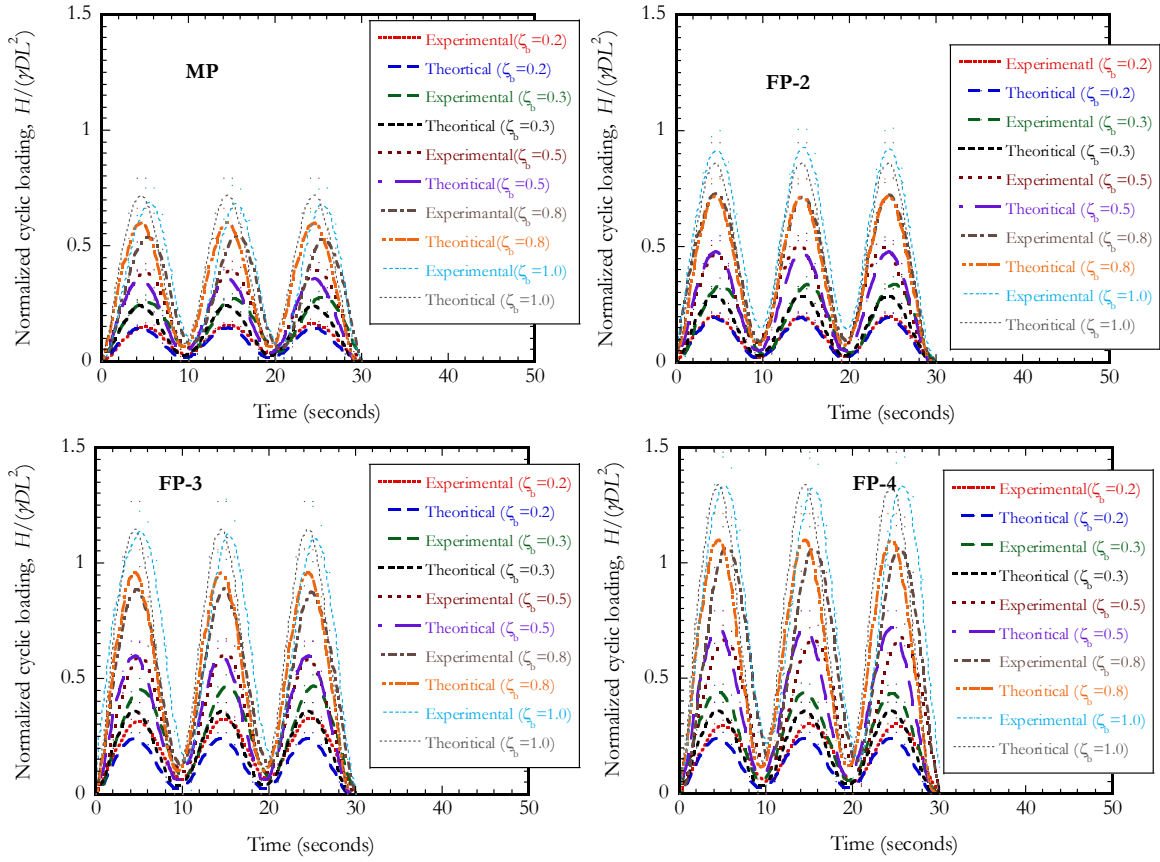
5.7.2 Lateral cyclic load- rotation curves

The static and cyclic lateral load pile head rotation obtained for monopile and the finned piles are shown in Figures 5-5 through 5-8, respectively. All the tests were conducted under same relative density and same cyclic load ratio of ζ_t =0. On a typical cyclic load-rotation curve the first load cycle followed the static curve to seat the selected load magnitude ratio, as expected. Hence, the first cycle pile secant stiffness was significantly lower than the subsequent ones with increasing number of cycles. The secant stiffness did not change appreciably with number of cycles of loading, but the accumulated pile head rotation increased with the number of cycles of loading, N and the cyclic load magnitude ζ_b.

125
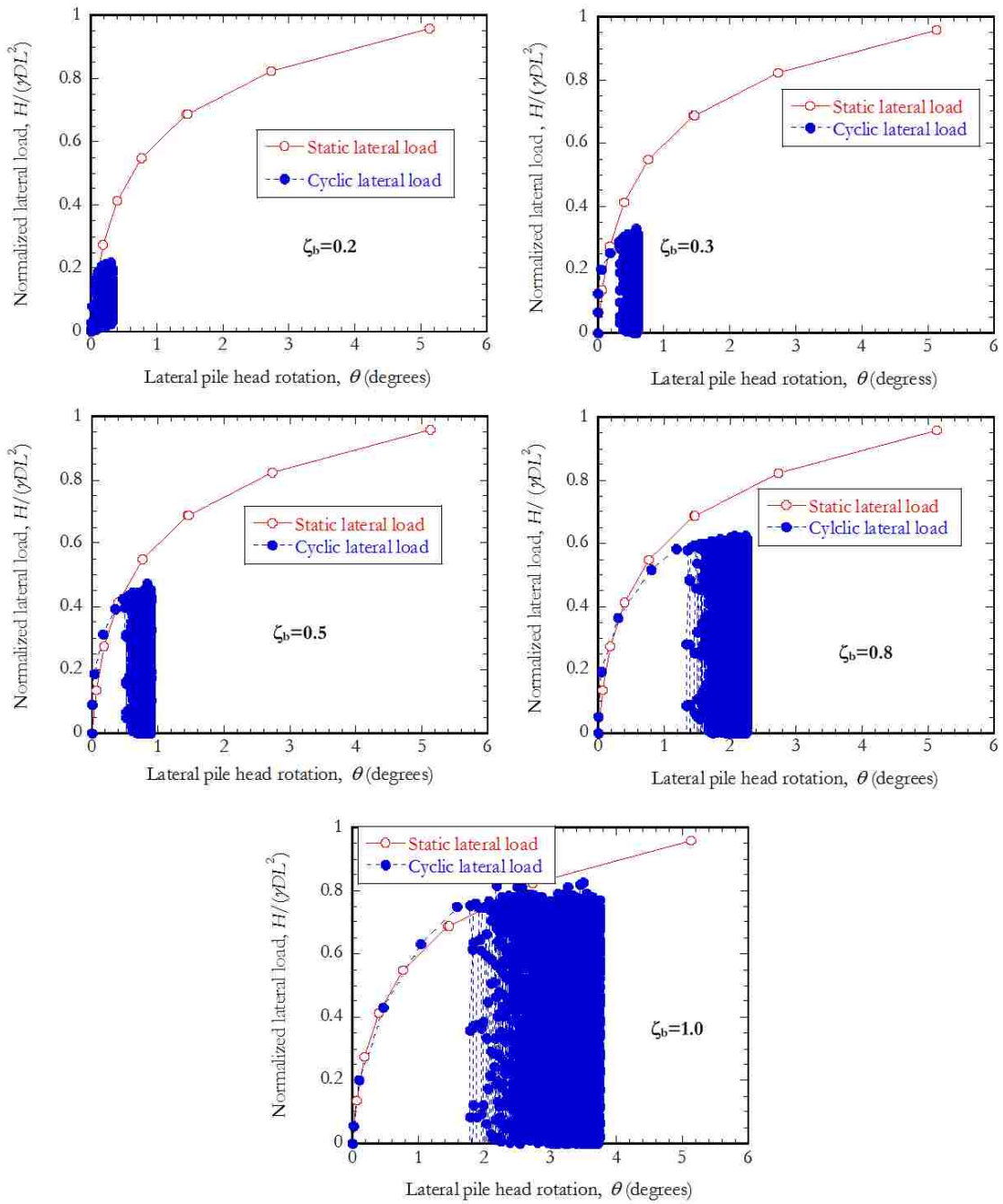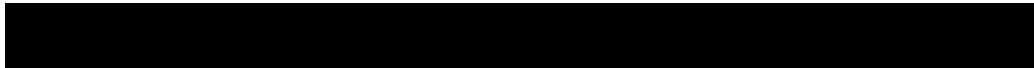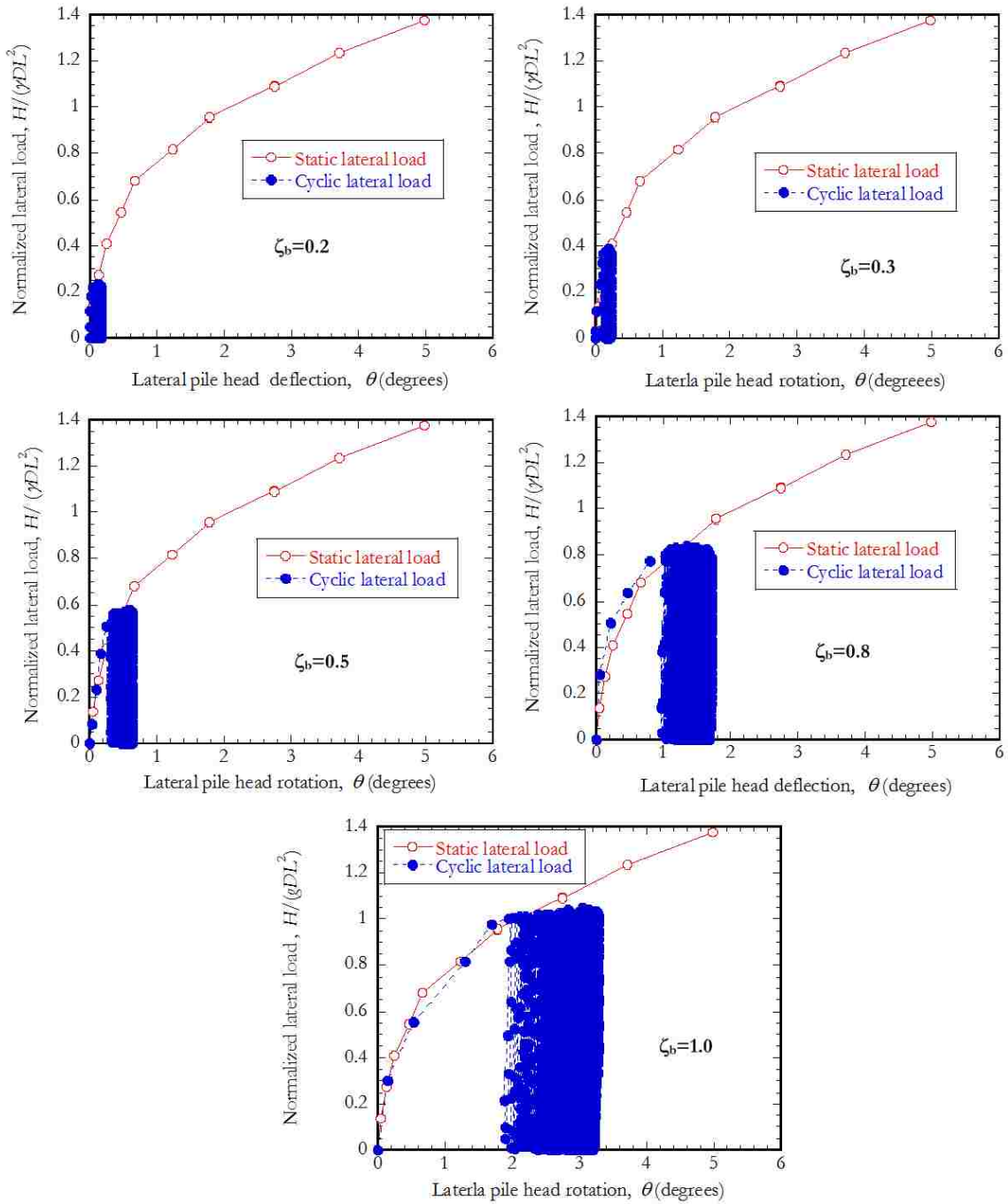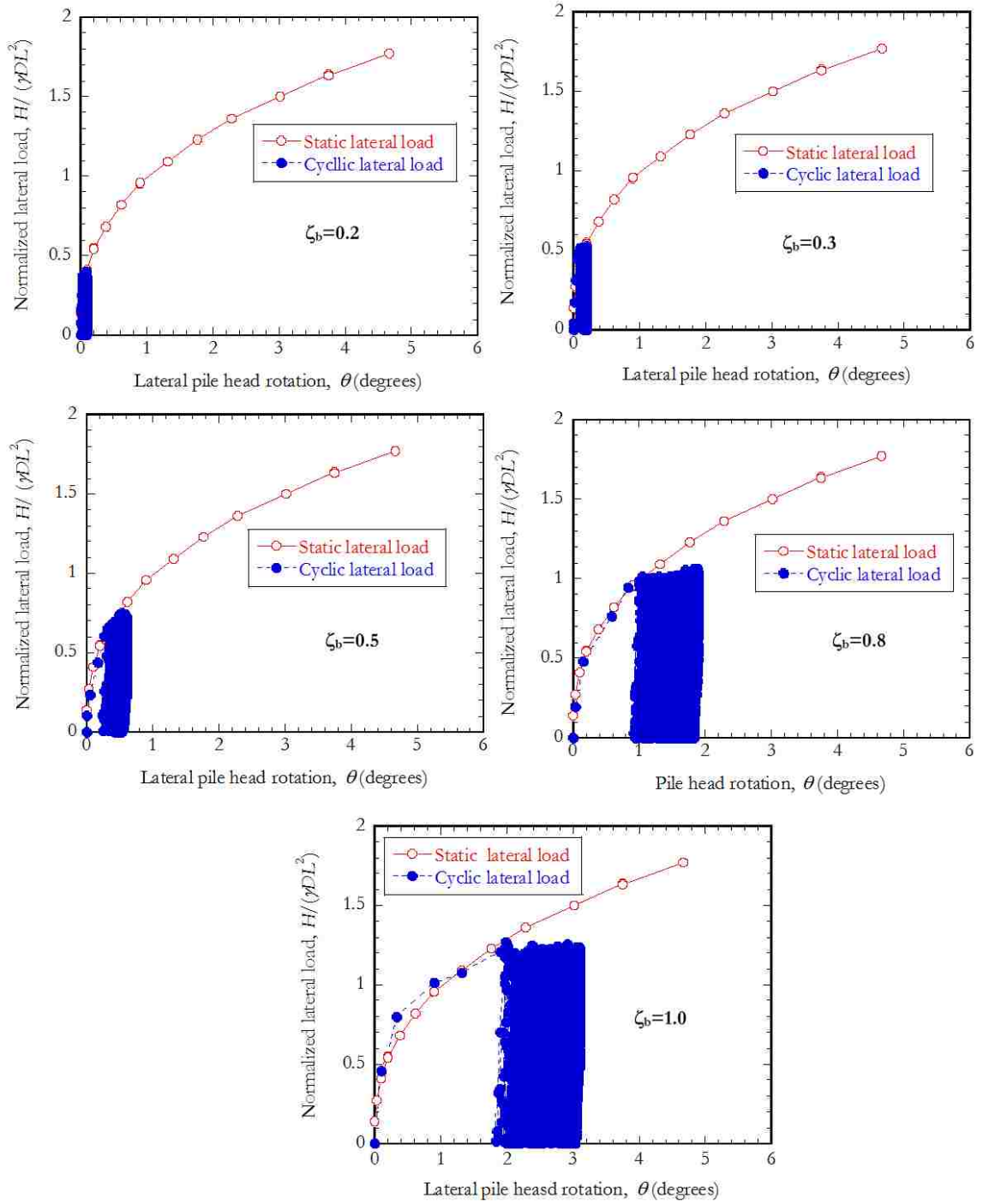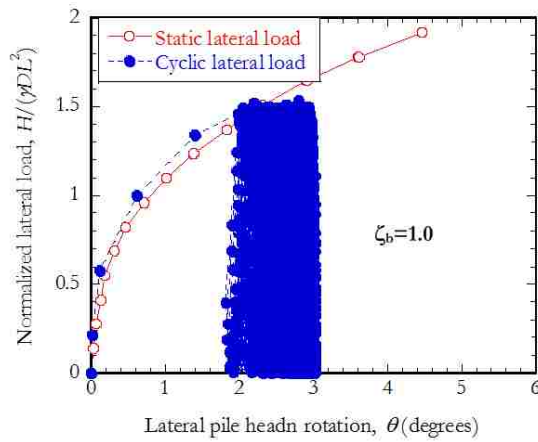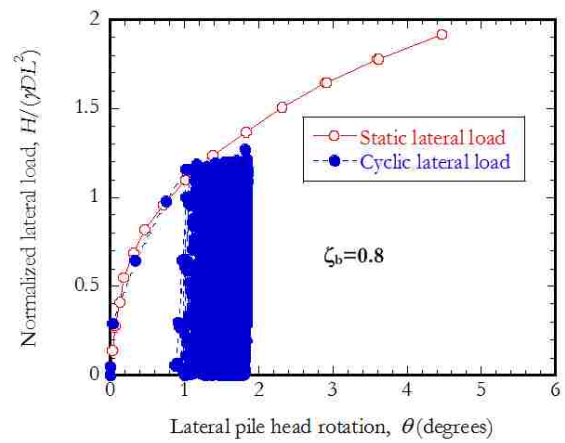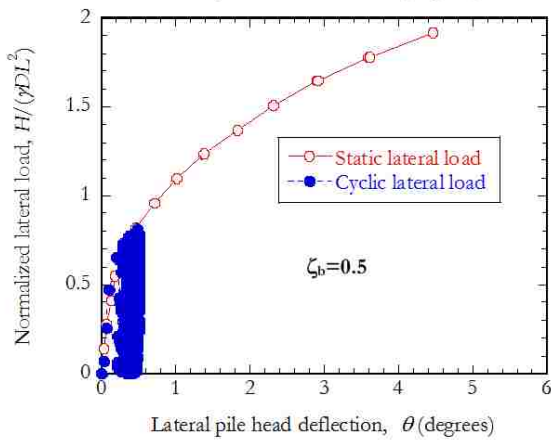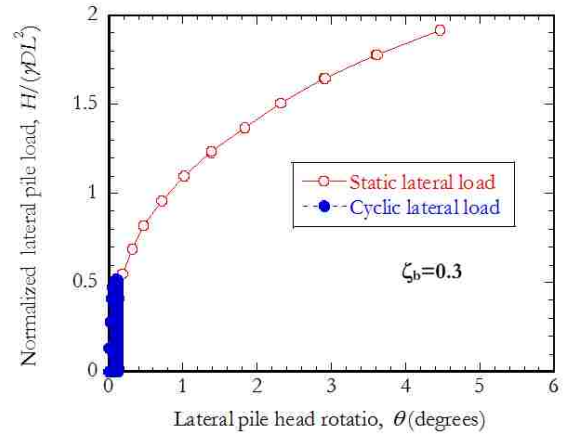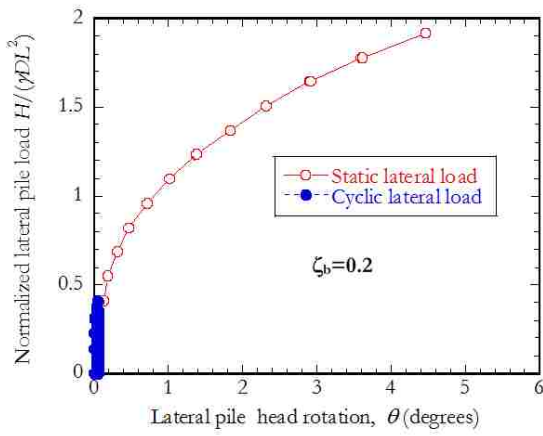
5.7.3   Accumulated pile head rotation

Figure 5-9 shows the accumulated piled head rotation with the number of cycles. The accumulated rotation increases rapidly for initial 100 cycles, after which the rates of increase diminish for all cases. For a given cyclic load magnitude ζ_b, the accumulated pile head rotation decreased with the number of fins. Monopile showed larger accumulated rotation than finned piles implying that the fins affect reduction of accumulated pile rotation.

The efficiency of finned piles in reducing the accumulated pile head rotation under cyclic loading can be better understood by plotting the rate of change in rotation with change in number of cycles, $d\theta/dN$ as shown in Figure 5-10. The rate of change of pile head rotation $d\theta/dN$ reduced significantly within the first 100 cycles after which it stabilized to a constant rate. Comparing the monopile behavior with the finned ones, it is observed clearly that finned piles showed lower rate of change than monopile or the first 100 cycles.

The pile head rotation was fitted using a power function as suggested by several authors (Long and Vennester, 1994; Peralta and Achimus, 2010) and as given by Equation 5-5. These power functions are annotated on the figures in Figure 5-9. The value of the power coefficient, α, was found to range between 0.07 and 0.23. In a similar analysis, Rosen et al., (2012) reported values of α ranging from 0.11 to 0.18 on 1 g scale test under one-way cyclic loading of monopiles. Nicolai and Ibsen, (2014) concluded values of α depended on the relative density of sand hence should not be considered as a constant.

130

$\theta = 0.079539\ N^{0.16929}$
$\theta = 0.34736\ N^{0.081217}$
$\theta = 0.52414\ N^{0.080576}$
$\theta = 1.3498\ N^{0.07307}$
$y = 1.7632\ N^{0.10986}$

(a) MP

$\zeta_b=0.2$
$\zeta_b=0.3$
$\zeta_b=0.5$
$\zeta_b=0.8$
$\zeta_b=1.0$

$\theta = 0.068409\ N^{0.13729}$
$\theta = 0.12564\ N^{0.077885}$
$\theta = 0.30386\ N^{0.1044}$
$\theta = 0.95136\ N^{0.081007}$
$\theta = 1.9412\ N^{0.076832}$

(b) FP-2

$\zeta_b=0.2$
$\zeta_b=0.3$
$\zeta_b=0.5$
$\zeta_b=0.8$
$\zeta_b=1.0$

$\theta = 0.024902\ N^{0.23487}$
$\theta = 0.089663\ N^{0.11586}$
$\theta = 0.3401\ N^{0.083216}$
$\theta = 0.89662\ N^{0.09916}$
$\theta = 1.8387\ N^{0.077414}$

(c) FP-3

$\zeta_b=0.2$
$\zeta_b=0.3$
$\zeta_b=0.5$
$\zeta_b=0.8$
$\zeta_b=1.0$

$\theta = 0.033762\ N^{0.095172}$
$\theta = 0.063183\ N^{0.14661}$
$\theta = 0.30405\ N^{0.074332}$
$\theta = 1.0087\ N^{0.089251}$
$\theta = 1.8886\ N^{0.059687}$

(d) FP-4

$\zeta_b=0.2$
$\zeta_b=0.3$
$\zeta_b=0.5$
$\zeta_b=0.8$
$\zeta_b=1.0$

Pile head rotation, θ

Number of cycles, N

(a) MP

(b) FP-2

(c) FP-3

(d) FP-4

5.7.4 Estimation of pile head rotation at fatigue limit state

Fatigue limit state corresponds to the design life time of an offshore pile and it is usually taken as 20-25 years. During this time the pile is expected to experience up to 10^7 loading cycles. Offshore piles design guidelines such as API standards and DNV code have strict limitation on the allowable pile head rotation during the life of a wind turbine foundation. The rotation of the pile at fatigue limit state was estimated using the pile head rotation reached at 1000 cycles of loading. The accumulated pile head rotation was fitted logarithm functions as shown in Figure 5-11 to linearize the relation

between rotation and number of cycles. These equations were then used to estimate the accumulated rotation at $N=10^7$ cycles for each cyclic load magnitude.

Figure 5-12 shows the estimated accumulated pile head rotation at $N=10^7$ cycles for different cyclic magnitudes for the four pile types. The allowable values of accumulated pile head rotations for monopiles at fatigue limit state according to API (1993) and DNV (2013) codes are superimposed on the figures (15-12a and 5-12b), where API demands a maximum rotation of the pile head of 0.5° and DVN code specifies 0.25°.

Comparing the experimental data with the two criteria as shown in Figure 5-12, it's clear that the finned piles display lower accumulated pile head rotation than monopiles at the same cyclic magnitude. Based on API standards that sets the maximum pile head rotation at 0.5°, corresponding cyclic load magnitudes that produced this rotation were found to be 0.22, 0.30, 0.36 and 0.39 for MP, FP-2, FP-3 and MP-4 respectively. This implies that FP-2, FP-3 and FP-4 can take 36%, 63% and 77% more cyclic lateral load than MP at a pile head rotation of 0.5° at fatigue limit state.

Considering the DNV codes that limit the accumulated pile head rotation to 0.25°, the corresponding cyclic load magnitudes that produced rotation of 0.25° were 0.09, 0.14, 0.18 and 0.25 for MP, FP-2, FP-3 and FP-4 respectively. These numbers correspond in increase in cyclic load capacity of 55%, 100% and 177% for FP-2, FP-3 and FP-4 respectively.

133

$\theta = 0.060209 + 0.060891\log(N)$
$\theta = 0.33663 + 0.08664\log(N)$
$\theta = 0.50746 + 0.12985\log(N)$
$\theta = 1.3114 + 0.32719\log(N)$
$\theta = 1.6071 + 0.48991\log(N)$

$\theta = 0.061946 + 0.035113\log(N)$
$\theta = 0.12019 + 0.030891\log(N)$
$\theta = 0.2791 + 0.11112\log(N)$
$\theta = 0.90549 + 0.24676\log(N)$
$\theta = 1.8727 + 0.45989\log(N)$

(a) MP

(b) FP-2

$\theta = 0.015165 + 0.03229\log(N)$
$\theta = 0.080308 + 0.038177\log(N)$
$\theta = 0.32751 + 0.088423\log(N)$
$\theta = 0.82305 + 0.31065\log(N)$
$\theta = 1.7624 + 0.44661\log(N)$

$\theta = 0.0316 + 0.010801\log(N)$
$\theta = 0.054529 + 0.036892\log(N)$
$\theta = 0.29735 + 0.067156\log(N)$
$\theta = 0.95758 + 0.29215\log(N)$
$\theta = 1.8429 + 0.33005\log(N)$

Pile head rotation, θ

Number of cycles, N

$\zeta_b=0.2$
$\zeta_b=0.3$
$\zeta_b=0.5$
$\zeta_b=0.8$
$\zeta_b=1.0$

134

5.7.5 Pile-soil stiffness

The pile equivalent stiffness ratio was used to investigate further the change in soil-pile stiffness, as defined in Figure 5-1. The equivalent rotational stiffness is defined as the slope from the origin of the load-rotation curve to the peak load point of each cycle. Figure 5-13 shows the equivalent rotation stiffness for the piles determined at different cyclic load magnitudes. It can be seen that the equivalent stiffness decreases with the load magnitude and the number of cycles. Finned piles showed lower equivalent stiffness than monopile. The decrease in equivalent rotational stiffness can be correlated with the accumulation of pile head rotation. The equivalent stiffness of finned piles decreased faster than that of monopile implying that finned piles showed lower accumulated pile head rotation, or smaller θ. The rate of decrease was sensitive to cyclic load magnitude.

Normalized equivalent rotational stiffness variations with number of cycles of loading are shown in Figure 5-14. The normalization is done by dividing the stiffness of the finned piles with that of the monopile at a given cycle, N for a given cyclic load magnitude. The normalized rotational stiffness increased with the number of fins, but decreased with the cyclic load magnitude. FP-4 showed equivalent rotational stiffness as high as 6 times that of monopile at ζ_b=0.2, and as low has 2.5 times for ζ_b=1.0. The equivalent stiffness for FP-3 was about 3.8 times of MP for ζ_b=0.2 and, 2.2 times for ζ_b=1.0. FP-2 had equivalent rotational stiffness multiplier ranging from about 1.8 for ζ_b=0.2 to 1.7 for ζ_b=1.0 with respect to that of MP. These results highlight clearly the

136

benefits of using finned piles in reducing the accumulation of pile head rotation due to cyclic loading.
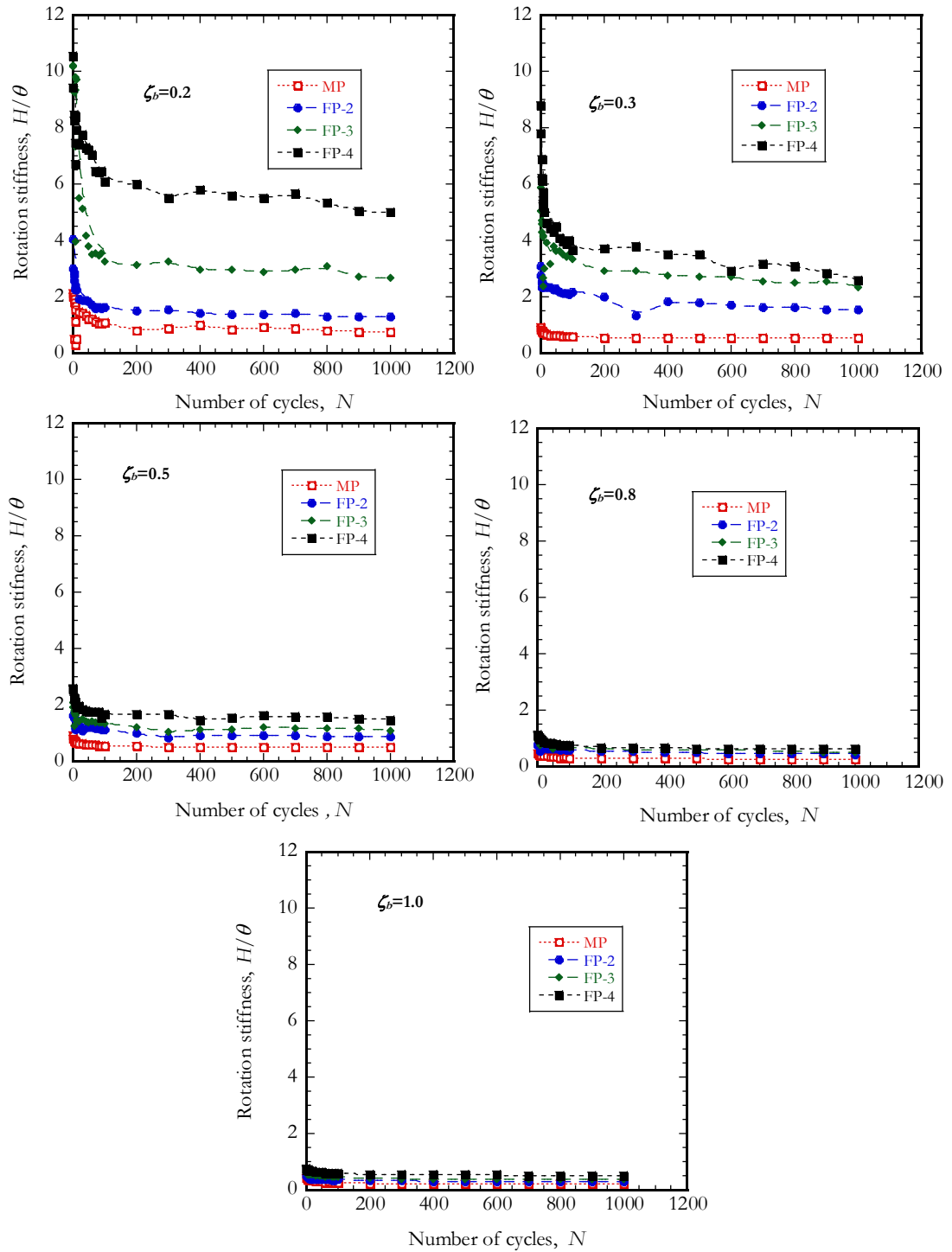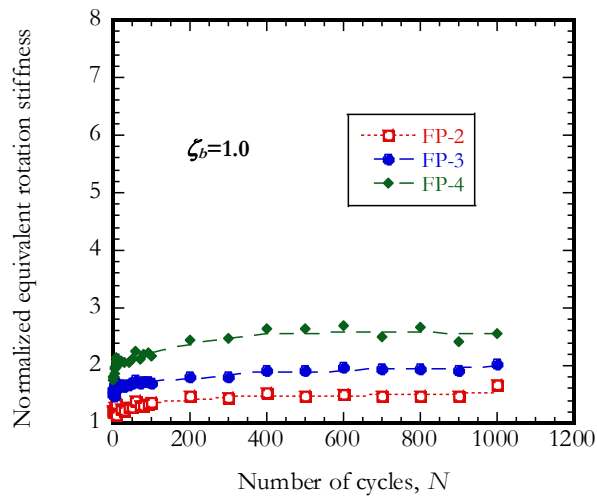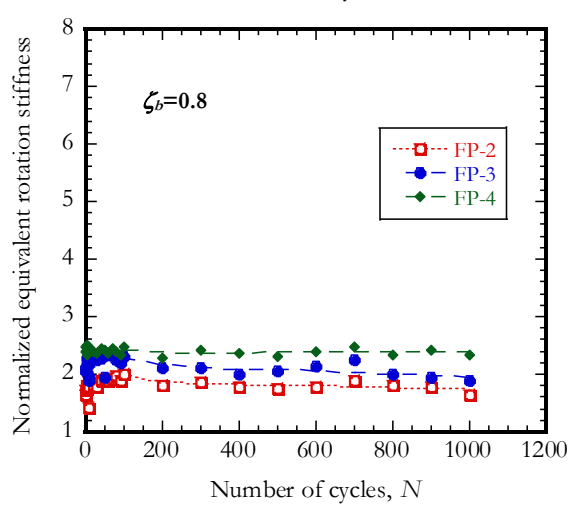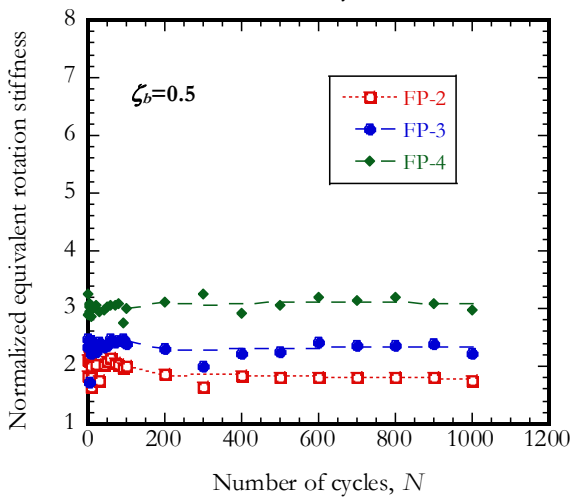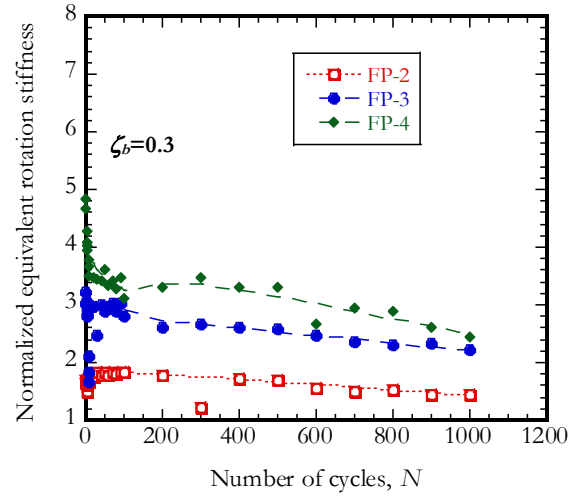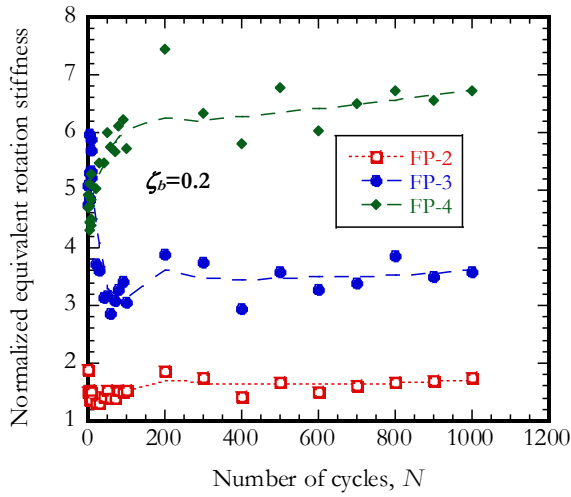
According to Leblanc et al., (2010), Peng et al., (2011) and Qin and Guo, (2014) long-term cyclic loading can change the properties of soil around a pile, which can then affect the dynamic response (i.e. system frequency) of the foundation structure. In all the tests conducted in this study, increase in pile-soil stiffness was observed as the number of fins increased, but the finned piles showed significantly lower change in stiffness than monopiles with cyclic loading. Therefore, finned piles may offer less variability in the overall system response with long-term cyclic loading.

5.8 Conclusion

The 1g study was aimed at determining the response of finned piles under cyclic loading. The following conclusions could be drawn:

(i) The accumulated rotation increases rapidly for initial 100 cycles of loading after which the increment becomes smaller with the number of cycles, N. For a given cyclic load magnitude ζ_b, the accumulated pile head rotation decreased with the number of fins. Monopile had significantly larger accumulated rotation than finned piles at the same ζ_b.

(ii) At extrapolated fatigues limit state ($N=10^7$) that sets maximum pile head rotation at 0.5° based on API standards, the corresponding cyclic load magnitudes that produced this rotation were found to be 0.22, 0.30, 0.36 and 0.39 for MP, FP-2, FP-3 and MP-4 respectively. This finding implies that FP-2, FP-3 and FP-4 can take 36%, 63% and 77% larger in magnitude the cyclic lateral load than MP. Considering the DNV codes that limit the accumulated pile head rotation to

139

0.25°, the cyclic load capacity increase was predicted at 55%, 100% and 177% for FP-2, FP-3 and FP-4 respectively compared to MP.

(iii) Finned piles showed equivalent rotational stiffness that depended on the number of fins and the cyclic load magnitude. The equivalent stiffness of FP-4 for example, was as high as 6 times that of monopile. Those piles that started with high stiffness showed the least degradation of stiffness with cycles of loading. Similar results for all finned piles showed the benefit of using finned piles to reduce the potential changes in the system response that can come about with sustained cycles of loading.

5.9 References

1. API (1993): Recommended practice for planning, designing, and constructing fixed offshore platform: Working stress design, RP2A-WSD. 20th edition.

2. Bienen, B., Duhrkop, J., Grabe, J., Randolph, M.F., and White, D. (2012): Response of piles with wings to monotonic and cyclic lateral loading in sand. *Journal of Geotechnical and Geoenvironmental Engineering*, 138(3): 364–375.

3. GAI Consultant Inc., 1982, "Laterally Loaded Drilled Pier Research, Vol. 2, Research Documentation," *GAI Report EL*-2197, *Research project* 1280–*1*, EPRI, Monrocville, PA.

4. Garnier, J. (2013) : Advances in lateral cyclic pile design: Contribution of the SOLCYP project. Proceedings, TC 209 Workshop, 18th ICSMGE, Paris, France.

140

5. Klinkvort, R.T. Leth, C. T. and Hededal, O. (2010): Centrifuge modelling of a laterally cyclic loaded pile. *In the 7th International Conference on Physical Modelling in Geotechnics.*

6. LeBlanc C., Houlsby G.T. and Byrne B.W. (2010): Response of stiff piles in sand to long-term cyclic lateral loading. *Géotechnique* 60 (2): 79-90.

7. Long, J. H. and Vanneste, G. (1994): Effects of cyclic lateral loads on piles in sand. Journal of Geotechnical Engineering, ASCE, 120(1): 225–244.

8. Malhotra, S. (2009): Design and construction considerations for offshore wind turbine foundations in North America. Civil Engineering Practice, Spring/Summer: 7-42.

9. Murphy, G., Doherty, P., Cadogan, D. and Gavin, K. (2016): Field experiments on instrumented winged monopiles. *ICE Proceedings of Geotechnical Engineering*, 169: 227-239

10. Nicolai, G. and Ibsen , L.B. (2014): Small-Scale Testing of Cyclic Laterally Loaded Monopiles in Dense Saturated Sand. *In the Procedding of The Twenty-fourth International Ocean and Polar Engineering Conference*, Busan, Korea.

11. Peng, J., Clarke, B.G. and Rouainia, M. (2011): Increasing resistance of piles subjected to cyclic lateral loading. *Journal of Geotechnical and Geoenvironmental Engineering*, 137 (10): 977-982.

12. Peralta, P. and Achmus, M, (2010): An Experimental Investigation of Piles in Sand Subjected to Cyclic Lateral Loads. *Proceedings of the 7th International Conference on Physical Modelling in Geotechnics*. Zurich, Switzerland: 985–990.

13. Roesen, H. R., Ibsen, L. B. and Andersen, L. V. (2012): Small-Scale Testing Rig for Long-Term Cyclically Loaded Monopiles in Cohesionless Soil, *Proceedings of the 16th Nordic Geotechnical Meeting*, Copenhagen :435-442

14. Qin, H., and W. Guo. (2014): Response of static and cyclic laterally loaded rigid piles in sand. *Marine Georesources and Geotechnology* 34 (2):138–53.

CHAPTER 6

6 NUMERICAL STUDY ON THE LATERAL RESPONSE OF MONOPILE AND FINNED PILES

6.1 Introduction

Compared to different pile foundations like monopile, tripod or tapered foundations for offshore wind farms, finned piles appear to offer the best option to increase lateral static and cyclic resistance of these structures as suggested in Chapters 3, 4 and 5.

Optimization of fin dimensions is necessary in order achieve both economic as well as structural advantage over monopile in terms of increasing lateral capacity and minimize pile lateral deflection or rotation. Finite element computer codes such as LPILE™, PLAXIS™ and ABAQUS™ have been used successfully in the study of laterally loaded finned piles (Peng, 2005; Peng et al., 2010; Babu and Viswanadham, 2018). Some of the earlier studies, focusing on the geometric shape of the fins, mainly triangular and rectangular shaped fins of same surface area, reported that rectangular fins were more effective in resisting lateral loads compared to triangular shape fins (Duhrkop and Grabe 2007; Nasr, 2013). Three-dimensional numerical analysis of laterally loaded finned piles was presented by Peng et al. (2010). Correlating the lateral resistance versus displacement of the pile head with fins situated close to the pile head,

143

the numerical analysis showed that increasing the fin length had significant effect on increasing the lateral capacity of pile. The optimum fin efficiency was obtained when the fin length equaled half the pile length. Other numerical modeling focusing on the optimum number and positioning of the fins concluded that when fins were placed at the top of the pile immediately below the ground surface and in the middle of the pile, they produced grater resistance to lateral load than when they were placed at the bottom of the pile (Babu and Viswanadham, 2018).

In this study the lateral response of piles embedded in sand was investigated numerically by varying fin length, width and position of the fins by way finite element analysis using PLAXIS 3D (Ben™tley Inc., 2018). PLAXIS 3D™ provided a versatile tool that is capable of modelling soil continuity, soil nonlinearity and soil-pile interface behavior (Nasr, 2013). The numerical study was aimed to verify the experimental work as well as examine the outcome of various configurations of fins that have not been modelled experimentally. The performance of the finned piles was studied numerically to determine their optimum dimensions.

6.2 Materials and method

6.2.1 Model piles

The numerical model was first built based on laboratory model test model and validated by the lab experimental results. Relationship developed by Wood and Crewe (2002) was followed to select the dimension of the model piles.

144

$$\frac{E_m I_m}{E_p I_p} = \frac{1}{n^5} \tag{6-1}$$

The dimensions of model finned piles were approximately 1/100 in scale with reference to current offshore monopile foundations in UK and in other European countries (Peng, 2004). The physical model parameters used in lab experiments is summarized in the Table 6-1 below. The same parameters listed in Table 6-1 were used in the numerical analysis in here.

6.2.2 Soil modelling

Sand with similar properties as the one used in the experimental study presented in Chapters 3, 4 and 5 were used in the numerical analysis. The sand was assumed to be linear elastic perfectly plastic material. A non-associated Mohr-Coulomb constitutive model was assumed to govern the soil behavior, because of its simplicity, reasonable number of model parameters, and reasonable accuracy in modeling the behavior of laterally loaded piles (Peng, 2010; Nasr, 2013).

Property	Model pile	Prototype Pile
Diameter, D_p	40 mm	4 m
Inner Diameter, D_i	38 mm	3.8 m
Embedded length, L_p	360 mm	36 m
Thickness, t	1 mm	10 cm
Load eccentricity, e	160 mm	16 m
Young's modulus, E	200 GPa	200 GPa
Moment of Inertia, I	2.33x10^{-12} m^4	2.33 m^4
Density, γ	78 kN/m^2	78 kN/m^2

Mohr-Coulomb model has a fixed yield surface which is not affected by plastic straining. The analysis of laterally loaded piles is conducted under drained conditions to simulate the model scaled piles. The elastic-plastic Mohr-Coulomb model involves five basic input parameters: elastic modulus (E), Poisson's ratio (ν), internal friction angle (ϕ), cohesion (c) and dilatancy angle (ψ). The parameters used for the Mohr-Coulomb model is summarized in Table 6-2.

Name	Symbol	Sand	Unit
General			
Parameter model	-	Mohr-Coulomb	-
Drainage Type	-	Drained	-
Soil total unit weight	γ_{unsat}	16	kN/m^3
Soil saturated unit weight	γ_{sat}	19	kN/m^3
Initial void ratio	e_0	0.5	-
Parameters			
Effective Young's modulus	E	40	kN/m^2
Effective Poisson's ratio	ν	0.33	-
Cohesion	c	0	kN/m^2
Friction angle	ϕ	35	°
Dilatancy angle	ψ	0	°
Increase in your modulus per unit depth	E_{inc}	2000	$kN/m^2/m$
Reference depth	z_{ref}	0	m
Interfaces			
Interface strength type	-	Manual	-
Strength reduction factor	R_{inter}	0.65	-
Initial			
K_0 determined	-	Auto	-

In order to account for the variation in soil properties with depth, Young's modulus was assumed to increase linearly as follows according to Peng (2010):

$$E'(z) = E'_0 + E'_{inc}(z - z_{ref})$$ (6-2)

Where, E'_0 is the Young's modulus at the reference soil depth, z_{ref} and E_{inc} is the increase of Young's modulus per unit of depth. When Mohr-Coulomb model is used to describe soil behavior, the Young's modulus implies the soil's compression modulus (i.e., constrained modulus). All the parameters were determined by appropriate lab tests except the E'_0 and E_{inc} values. These two parameters were determined by fitting numerical model to the physical data of monopile from lab experiments. The values that gave close match were adopted for the subsequent analysis.

6.2.3   Interface element between soil and pile

Modelling the interaction between the sand and the pile required creating an interface element along the circumference of the pile. A decreased value of shear modulus was assigned to the interface element when a slip mode occurred. The decrease of strength for the interface element is represented by a strength reduction factor (R_{inter}) in the PLAXIS material input. The strength reduction factor of the interface (R_{inter}) along the pile was set to 0.65 which is typical of sand steel interfaces. This factor relates the interface properties to the strength properties of a soil layer as follows:

$$\begin{cases} \tan\varphi_i = R_{inter}\tan\varphi' \\ c_i = R_{inter}c' \\ \psi_i = 0 \quad \text{if} \quad R_{inter} < 1 \text{ otherwise } \psi_i = \psi \end{cases}$$ (6-3)

147

Where, φ_i, c_i, ψ_i are the friction angle, cohesion and dilatancy angle of the interface respectively.

6.2.4 Meshing

Rectangular soil boundary with the same dimension as the laboratory soil box (1.0m x 0.7 m x 0.7m) was used to model piles in series 2 and 3 (see Table 6-3 below). However, in series 1, due to the larger sizes of fins to be analyzed, the soil boundary was increased three times (3m x 2.1 m x 2.1 m) the laboratory model to minimize the boundary effects. The soil boundary was fixed against movements in all directions, whereas the 'ground surface' was free to move in all directions. The vertical boundaries were fixed against movement in the orthogonal directions. The geometry of a three-dimensional soil model and the embedded pile in soil is shown in Figure 6-1. The pile is set in the middle of the soil. The coarseness factor for soil mesh and pile are set at 1.0 and 0.5, respectively. The mesh used 10-node elements, automatically generated by the software. The entire model consisted of 11000 elements and 18000 nodes.

6.2.5 Construction of model and loading sequence

Finite element calculations were divided into several sequential calculation phases. Each calculation phase corresponded to a loading or a construction stage. These phases are described as following:

a) Initial phase

This phase entails building the soil geometry. In the initial phase, the pile, interface and lateral loads are not present. The corresponding pile geometry is deactivated in

148

the initial phase. The K_0 procedure, a special calculation method available in PLAXIS is used to define the initial stresses for the model, which considers the loading history of the soil.

(a)

(b)　　(c)　　(d)　　(e)

149
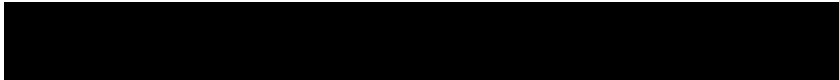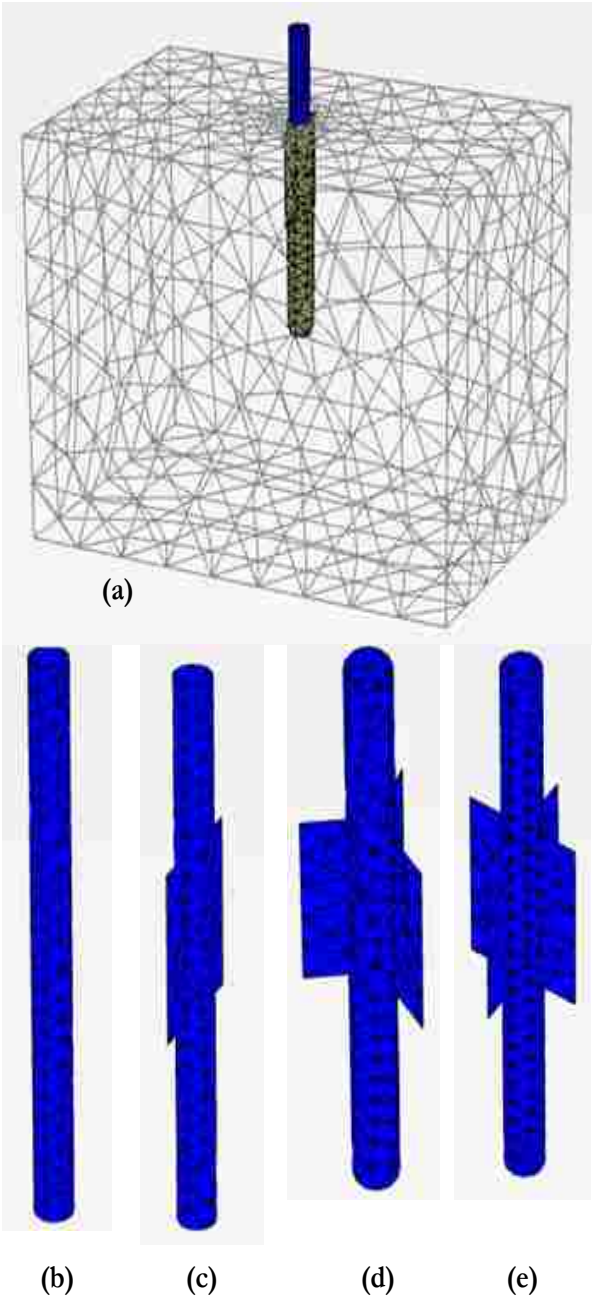
b) Phase 1

This phase is set to simulate the pile installation in the soil. In the lab, when the piles were driven into the soil, soil plug is formed inside the hollow pipe. The height of the soil plug was set at 12 cm lower than the ground surface to simulate this condition.

c) Phase 2

This phase is the loading phase. The displacement is initially set to zero. The loading phase is activated, and the initial load value set to 0.01kN.

d)   Phase 3

This phase involved increasing systematically the lateral load on the pile head. The load increment in each phase was 0.01kN, similar to the laboratory experiment where the loading was added in increments of 0.01 kN and the pile head displacement measured for at each load increment.
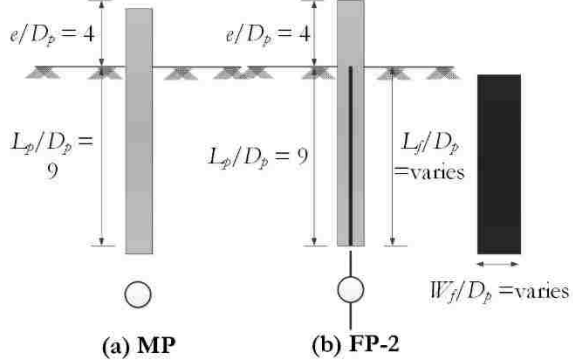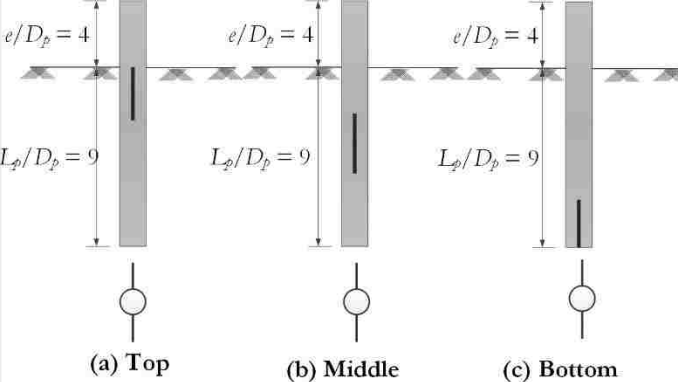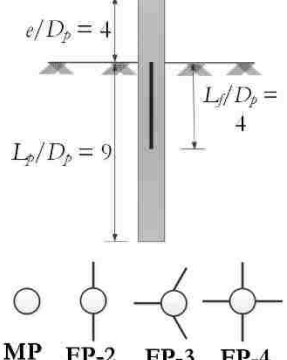
6.3 Numerical analysis series

6.3.1   Test series

Three test series were analyzed as shown in Table 6-3. These test simulation series are summarized below.

- Series 1: Involved varying the length and width of the fin. In this series, two test configurations were adopted. The first configuration entailed varying the width of the fin with the fin length extending the entire pile length. The second configuration involved constant width of the fin while varying the

150

length of the fin along the pile. These tests were conducted to optimize the fin dimensions. The simulations used FP-2 piles (two-finned piles) fins oriented perpendicular to the loading direction.

Series	Test Description	Test Detail
①	(a) MP (b) FP-2	<u>Aim is to optimize fin length and width</u> 1. Varying normalized fin width (W_f/D_p) and keeping ratio of fin length to pile length constant (fin length extend entire pile embedded depth). W_f/D_p =0.1,0.2,0.3,0.4,0.5,1.0,2.0,5.0 L_f/L_p =9 2. Varying the ratio of length of fin to length of pile while keeping normalized fin width (W_f/D_p) constant. L_f/L_p =,0.1,0.2,0.45,0.6,0.8,1.0 W_f/D_p =1.0
②	(a) Top (b) Middle (c) Bottom	<u>Aim is to find the ideal fin position</u> For the optimized fin geometry from series 1 above, the position of the fin inside ground will was varies to determine the most ideal position on the pile.
③	MP FP-2 FP-3 FP-4	<u>Aim is to study the influence of number of fins and direction of loading on lateral pile</u> 1. Series 3 will involve varying number of fins based on fin dimensions from series 1. 2. Compare numerical and laboratory test results. 3. Determine the effect of loading direction with respect to fin orientation.

151

- Series 2: This series involved using the optimum fin dimensions obtained from series 1 above. The number of fins and the loading direction was the same as Series 1 above However, fin position along the pile length was varied.

- Series 3: Using the optimum fin dimensions obtained from Series 1 above, the number of fins and loading directions with respect to fin orientation were varied in series 3. The simulations were carried for piles with two, three and four fins.

In all the test series above, the embedded pile length was kept constant at $L_p=9D_p$.

6.3.2 Specific objectives of the study

The main objective of the numerical work was to validate the experimental findings and study behavior of finned piles that could not me modeled experimentally. The specific objectives were:

i. Study the effect of fin length and width in improving the lateral capacity of a pile and to determining the optimum fin dimensions.

ii. Determine the best positioning of the fins along the pile length that will most enhance the pile's lateral capacity.

iii. Determine the effect of number of fins and direction of loading with respect to fin orientation on the efficiency of finned piles.

6.4 Tests Results

6.4.1 Boundary Effects

Figure 6-2 shows the distribution of horizontal stresses during loading of FP-2. The stress distribution was generated for a normalized lateral loading of 1.68, which was larger than the experimental normalized ultimate lateral loading for MP, FP-2, FP-3 and FP4 at 0.75, 0.99, 1.30 and 1.43, respectively, as shown in Figure 4-3 in Chapter 4. Maximum stress value of 15.4kN/m² was concentrated around the vicinity of the pile. At the edge of the soil boundary the stress distribution was at around 1.0kN/m² which was about 6% of the stress on the pile. The stress distribution shows that the assumed strain wedge did not extend to the soil boundary hence little or no interference are expected from the soil boundary.

Cartesian total stress σ_{xx}
Maximum value = 0.5416 kN/m²
Minimum value = -15.40 kN/m²
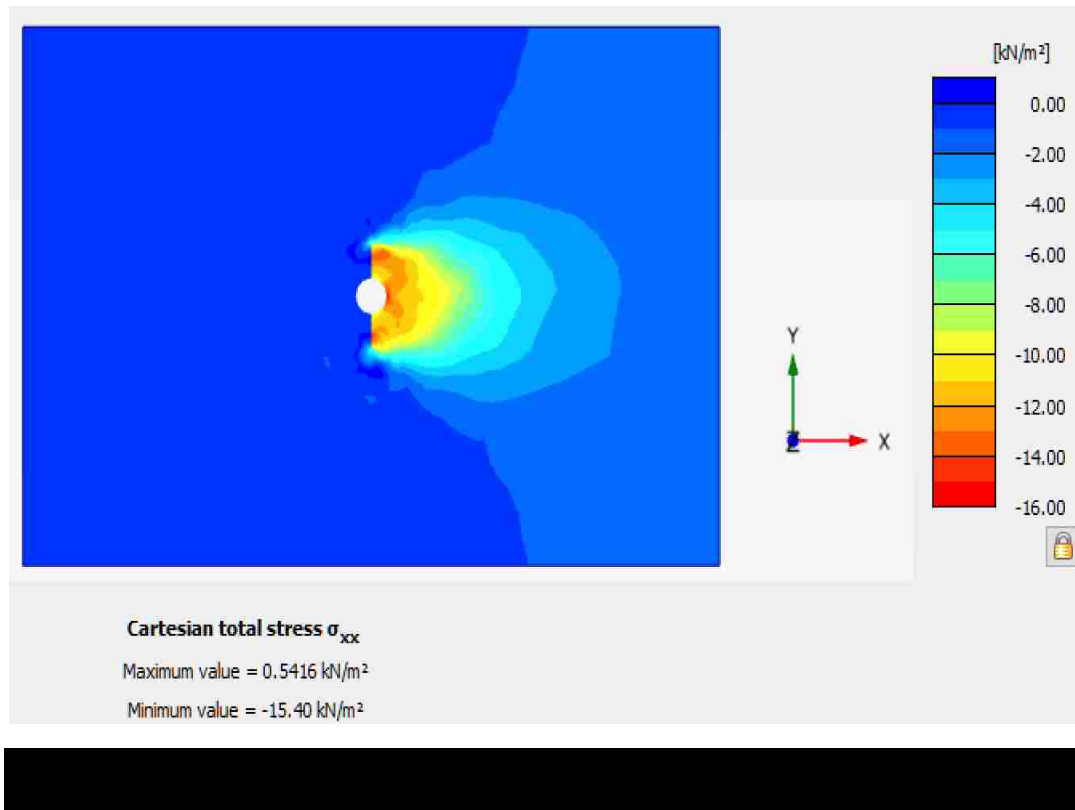
6.4.2 Validation of the FEM model

Validation of the FEM model was done by comparing the experimental and the numerical results. Figure 6-3 compares the load vs pile head deflection obtained from experimental and numerical models for MP and FP-2 with W_f/D_p=1 and L_f/L_p=4.5. As observed, the load-deflection curves were in close agreement implying that the model selected is suitable to predict soil pile interaction with some degree of accuracy.

6.4.3 Optimum fin width

Normalized fin length L_f/L_p was kept constant while varying the normalized fin width W_f/D_p. In the initial analysis, the fin length extended the entire depth of pile embedment (L_f/L_p = 9). Fin widths were varied at W_f/D_p = 0.1, 0.2, 0.3, 0.4, 0.5, 1.0, 2.0 and 5.0. Two finned pile was used in the analysis with the loading direction perpendicular to the orientation. The load was applied at the top of the pile at a load eccentricity of e=0.4 D_p.

The pile lateral rotation efficiency versus normalized pile width for various loadings is show in Figure 6-4. The lateral rotation efficiency is defined as the decrease in lateral pile head rotation for a particular load for a finned pile in comparison to a monopile (MP) equation 6-4 below.

$$\eta_\theta = \frac{\theta_{MP} - \theta_{FP}}{\theta_{MP}} \qquad (6.4)$$

Where θ_{MP} and θ_{FP} are the rotation of monopile and finned pile respectively.

154
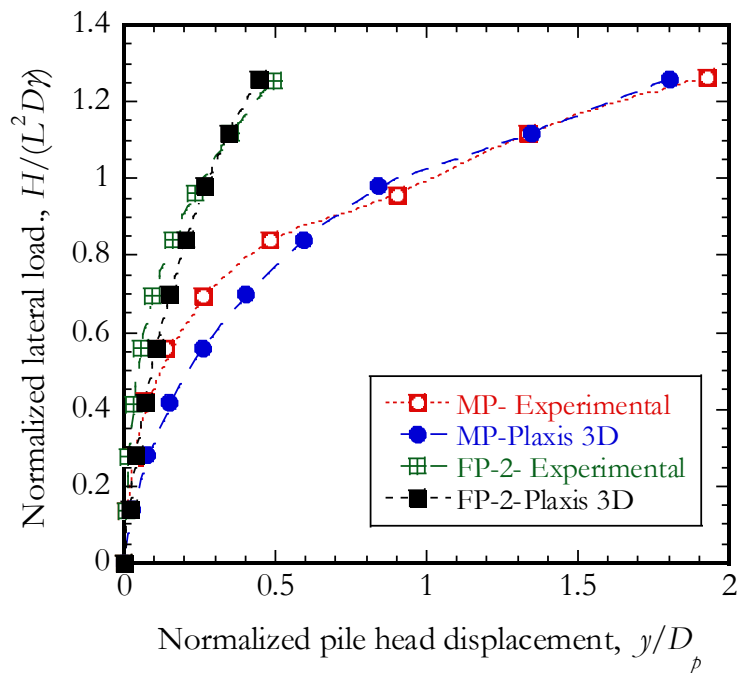
The results clearly indicate that the rotation efficiency increases with increase in fin width, W_f/D_p. As shown in Figure 6-4, there is a sudden increase in rotation efficiency from $W_f/D_p = 0$ (Monopile) to $W_f/D_p = 0.1$. This shows that fins have a significant effect on increasing the lateral capacity and reducing the lateral pile head deflection. It is evident in Figure 6-4 that there is a significant increase in rotation efficiency up to $W_f/D_p = 1.0$. Increasing the fin width beyond $W_f/D_p = 1.0$ resulted in an increase rotation efficiency at a reduced rate. This can be attributed to the fact that piles with fins width $W_f/D_p > 1.0$ had portion of the fin outside the range of influence zone of pile horizontal resistance, as was also suggested by others (Stewart, 1999; Ashour, 2002; Otani et al., 2006). Using reconstructed 3D images from X-ray CT scan, Otani et al. (2006) concluded that the failure pattern of sand around of the laterally

155

loaded piles was almost like an inverted cone. The depth of the failure surface decreased along the pile length. Stewart (1999) concluded that the failure zone extended to about three times the pile diameter. Normalized pile width larger than $W_f/D_p > 1.0$ yielded no significance increase in lateral pile resistance since most of the fin was outside the influence zone of the inverted cone. Based on these previous observations and the current findings in this study the normalized width $W_f/D_p = 1.0$ is suggested to be the optimum fin width.

Figure 6-5 shows the variation of the load efficiency with normalized pile width at 0.5° and 2° pile heads rotations. The pile head rotation at 0.5° is considered the limiting pile head rotation value per API, (1993) guidelines while 2° is taken as pile head rotation corresponding to the ultimate load as defined and practiced by GAI Consultants (1982).
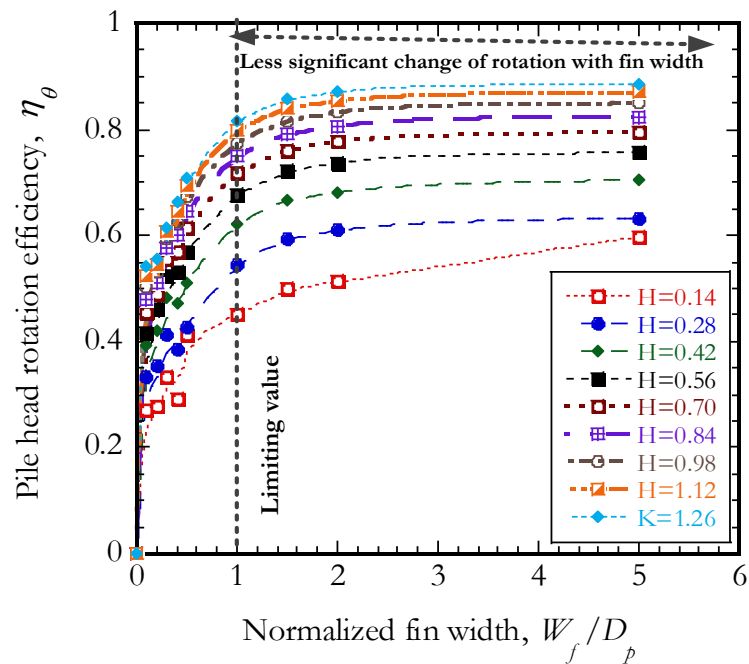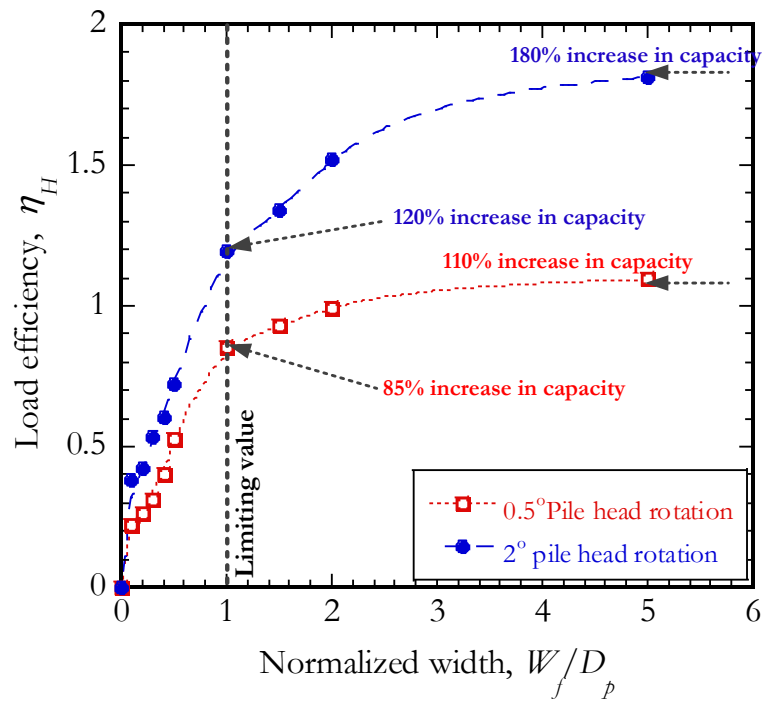
Defining the limiting W_f/D_p = 1.0, FP-2 showed 85% and 110% increase in lateral load capacities in comparison to those of the monopile at the 0.5˚ and 2° pile head rotations, respectively, as depicted in Figure 6-5. At 0.5° rotation, normalized fin width W_f/D_p > 1.0 yielded no significant increase in lateral load capacity of the pile. The increase in lateral load efficiency at W_f/D_p =5.0 was only 25% more than that at W_f/D_p = 1.0. Even though a marked increase in lateral load capacity for normalized fin width W_f/D_p > 1.0 was observed at 2° pile head rotation, the increase in capacity was not proportional to the increase in fin width.

157

6.4.4   Optimum fin length

The fin length was varied at the limiting normalized width of W_f/D_p =1.0 to determine its optimum value. Normalized fin length ranged from L_f/L_p = 0 to 1.0 (L_f/D_p =0, 1, 2, 4, 6, 8 and 9). Figure 6-6 shows the variation of lateral rotation efficiency with the normalized fin length. As expected, all finned piles showed an increase in efficiency due to the higher stiffer response of the finned structure compared to monopile. The rotation efficiency increased with increasing fin length. The lateral load efficiency increased rapidly from L_f/L_p = 0 to L_f/L_p =0.45 as shown in Figure 6-7. The load efficiency at 0.5° and 2° pile head rotations were similar for normalized L_f/L_p <0.22. For L_f/L_p = 0.45 the lateral load efficiency increases ranged between 65%-85% while for L_f/L_p > 0.45, the additional increase in load efficiency ranged between 20 % to 35%. Based on this finding L_f/L_p = 0.45 is suggested as the limiting fin length.
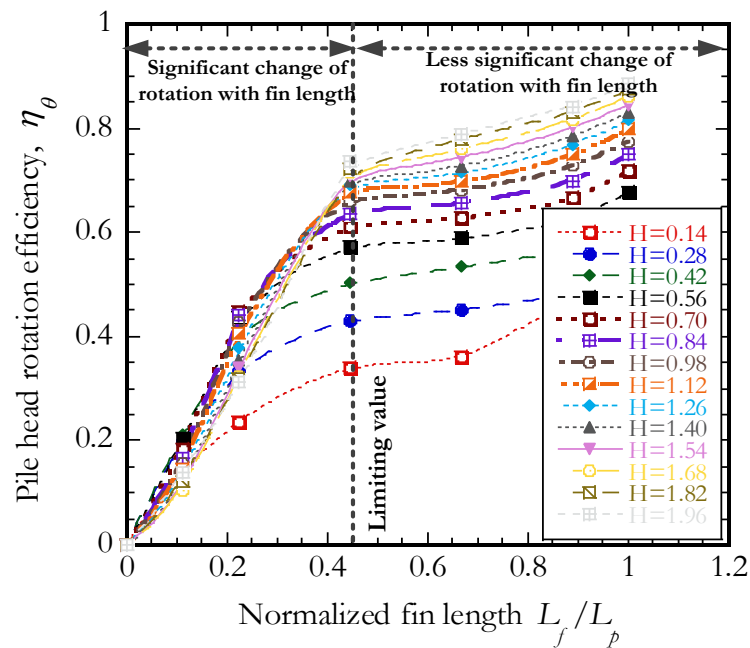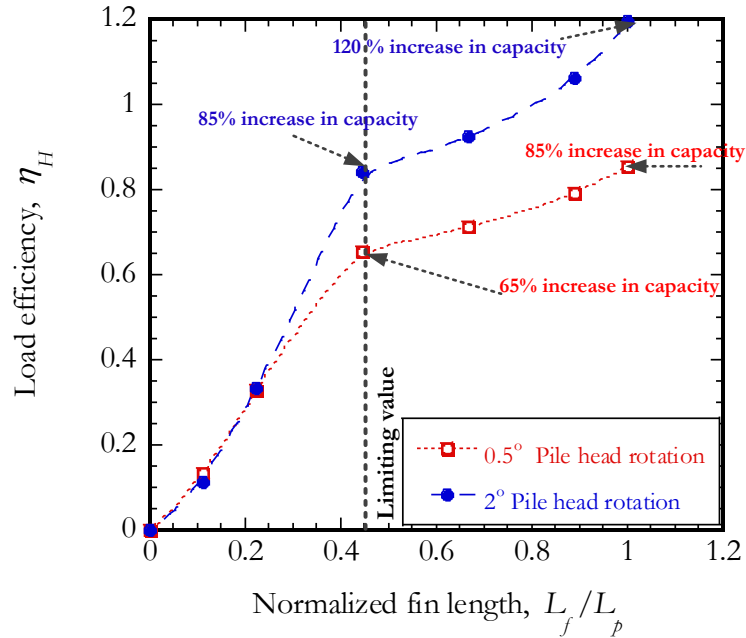
6.4.5 Effect of fin area on pile load efficiency

The length, width and effective area of pile are key factors in resisting the lateral load on a pile. The effective area to resist the lateral load is the area perpendicular to the loading direction. The effective area for a monopile can be considered as the embedded pile length multiplied by the pile diameter while for a two-finned pile the effective area is the monopile area plus the area of the two fins. The area of each fin is the width of the fin multiplied by the length of the fin.

From test simulation series 1 and 2 on two-finned piles, the following three configurations were derived: (i) $L_f/L_p = 1$ and $W_f/D_p < 1$, (ii) $L_f/L_p < 1$ and $W_f/D_p = 1$ and (iii) $L_f/L_p = 1$ and $W_f/D_p > 1$. The variation of fin efficiency with increase in pile effective area is shown in Figure 6-8. Clearly, the efficiency increased with increasing effective bearing area.

159

For configuration where $L_f/L_p = 1$ and $W_f/DL_p > 1$, the effect of the fin was less significant in increasing the lateral pile capacity. However, for fin configurations where $L_f/L_p = 1$ with $W_f/L_p < 1$ and $L_f/L_p < 1$ with $W_f/L_p = 1$, the area of the fin had significant effect on the capacity. Two different configurations with almost same effective area produced nearly same lateral resistance. For fin width, $W_f/D_p > 1$, the effect of fins in improving the lateral resistance of pile was less significant due to much of the fin area falling outside the influence zone of the inverted cone in front of the pile. Between the values of limiting fin length ($L_f/L_p = 0.45$ and $W_f/D_p = 1$) and the extended fin length ($L_f/L_p = 1$ and $W_f/D_p = 1$), the load efficiency increased from 67% to 85% while the increase in effective bearing area was 90% and 200% respectively. In this latter observation, even with doubling of the effective bearing area, the increase in load efficiency was only 17%. These results implied that increase in fin length beyond $L_f/L_p = 0.45$ produces little additional gain to the pile resistance.
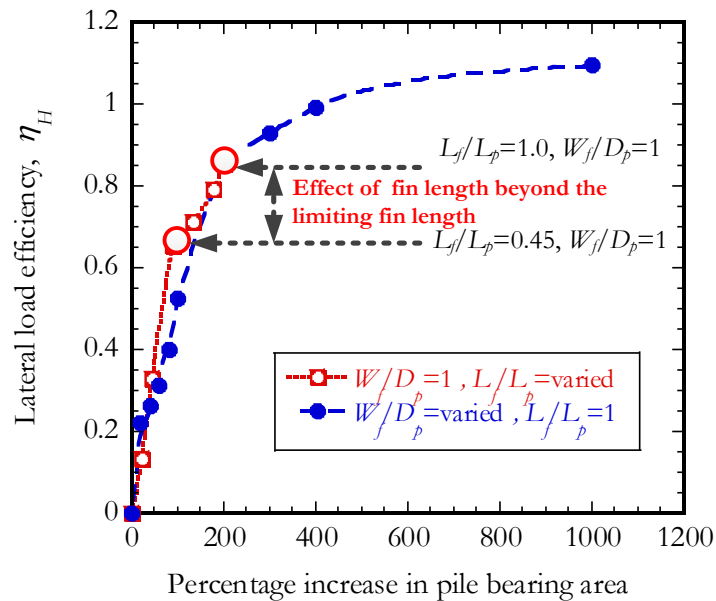
6.4.6 Optimum fin positioning

Figure 6-9 shows the lateral load versus pile head rotation curves for finned piles with fins at the top, the middle and the bottom of the FP-2 piles. The FP-2 pile with normalized fin width, W_f/D_p =1.0 and normalized fin length, L_f/L_p =0.45 was used in the analysis. The pile with fin at the top exhibited the largest lateral resistance whereas the one with fin at the bottom showed the smallest resistance.

Fin placed at the top of the piles carried more load due to maximum mobilization of passive resistance compared to middle and bottom pile, as shown in Figure 6-9. The load efficiencies of the pile with fin at the bottom, middle and top were 30%, 58% and 65% respectively. Furthermore, fins placed at the bottom of the pile would not be a viable option in practice owing to drivability constraints. Irrespective of the fin position, finned piles carried more load than monopile at 0.5° pile head rotation.
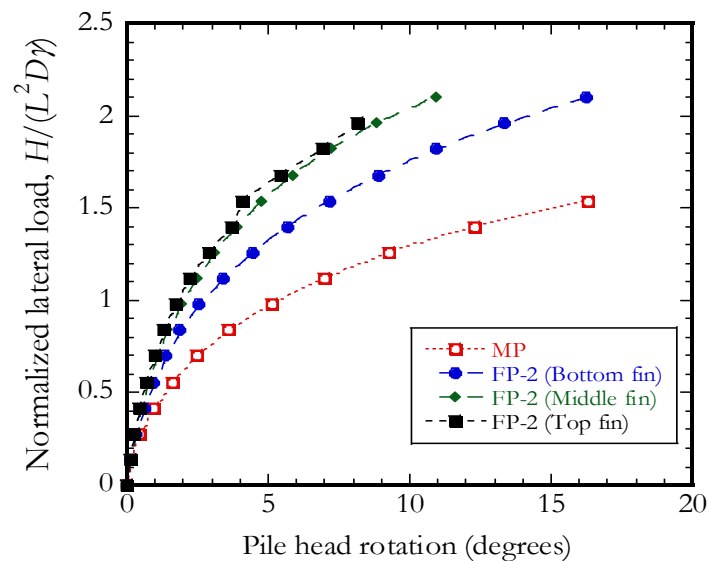
6.4.7 Effect of fin orientation

Due to varying direction of potential lateral loads on wind farm piles from waves or wind, it was suggested to use multiple fin piles with more than two fins, as per experimental results presented earlier in Chapter 3.4.1. In order to simulate the effect of directional load, numerical analysis was performed only on three- and four-finned piles as recommended earlier. The normalized length and width of the fins were selected as $L_f/L_p = 0.45$ and $W_f/DL_p = 1$ in these simulations.

Figures 6-10 and 6-11 show the variation of normalized lateral load with normalized lateral deflection obtained from the numerical simulations Superimposed onto graphs in these figures are the results from the experimental simulations. The results show clearly that the experimental and numerical behaviors are in close agreement.

Figure showing Normalized lateral load, $H/(L^2 D \gamma)$ versus Normalized pile head displacement, y/D_p

Legend:
- FP-4-0°-Experiment
- FP-4-0°-Plaxis 3D
- FP-4-15°-Plaxis 3D
- FP-4-30°-Plaxis 3D
- FP-4-45°-Plaxis 3D

FP-4-0°   FP-4-15°   FP-4-30°   FP-4-45°
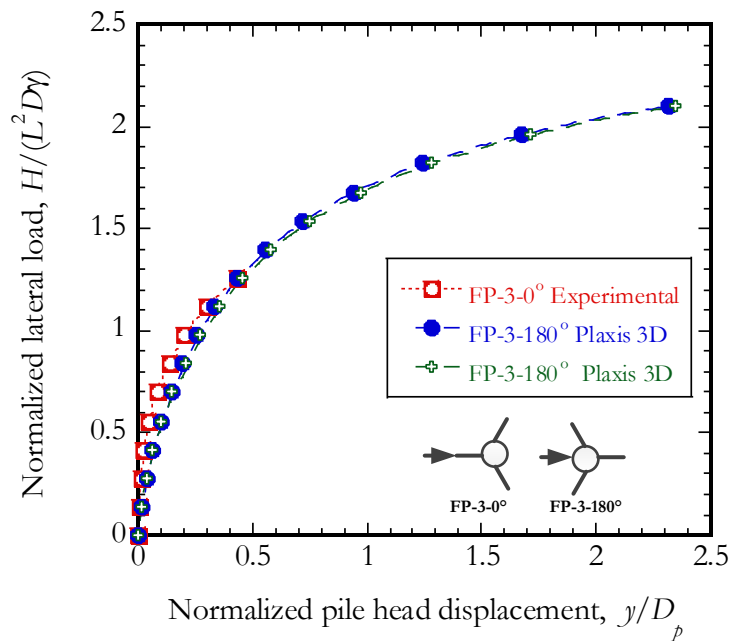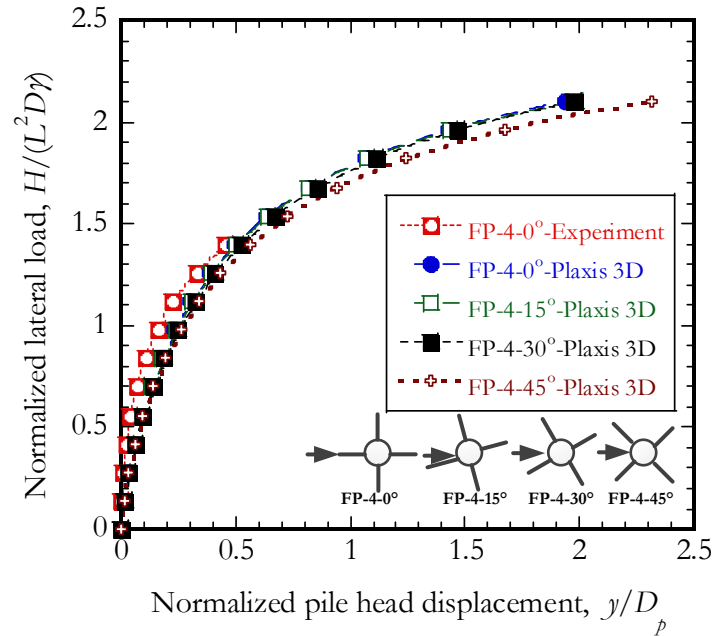
The four-finned pile showed slightly higher lateral capacity than the three-finned pile due to increased pile stiffness. However, loading direction had little or no effect on lateral load capacity of either the three- or the four-fined piles.

6.5 Summary and Conclusions

In this chapter the behavior of laterally loaded finned piles was compared to that of a monopile using a numerical analysis software package, Plaxis 3D. The numerical simulation results were used to validate experimental measurements and study various cases of pile configurations that could not be modeled experimentally. The cases included varying the length and width of the fin, position of the fin and loading direction on finned piles. The numerical analysis showed that:

163

i. The Mohr-Coulomb soil model and the selection of soil parameters as suggested by Peng et al., (2010) provided an adequate soil model for the test soil used and to compare the lateral load and lateral displacement of the mono and finned piles. The results obtained from the numerical models were consistent with the experimental results.

ii. With the length of fin kept constant with respect to the pile embedment depth, the lateral resistance of finned piles increased with increasing fin width. The limiting fin width was found to be $W_f/D_p =1$. The results showed that fins with widths larger than $W_f/D_p =1$ had less effect on further improving the lateral capacity of a pile.

iii. With the width of fin kept constant at $W_f/DL_p =1$, the lateral resistance of finned piles increased with increasing fin length. The limiting fin length was found to be $L_f/L_p =0.45$.

iv. Fins when placed directly below the ground surface provided more resistance than those placed at the middle of the pile or near the pile tip.

v. The change in direction of loading had no significant effect on the lateral resistance of three- and four-finned piles.

6.6 References

1. API (1993): Recommended practice for planning, designing, and constructing fixed offshore platform: Working stress design, RP2A-WSD. 20th edition.

164

2. Ashour M., Norris, G. and Pilling, P. (2002): Strain wedge model capability of analyzing behavior of lateral loaded isolated piles, drilled shafts, and pile groups. *Journal of Bridge Engineering*, ASCE, 7:45–54.

3. Babu, K.V. and Viswanadham, B.V.S (2018): Numerical Investigations on Lateral Load Response of Fin Piles. Numerical Analysis of Nonlinear Coupled Problems, Sustainable Civil Infrastructures: 317-329.

4. Bentlley Inc. (2018). PLAXIS 3D foundation user manual.

5. GAI Consultant Inc., 1982, "Laterally Loaded Drilled Pier Research, Vol. 2, Research Documentation," *GAI Report EL-2197, Research project 1280–1, EPRI*, Monrocville, PA.

6. Duhrkop, J. and Grabe, J. (2007): Laterally loaded piles with bulge. *In Proceedings of the 26th International Conference on Offshore Mechanics and Arctic Engineering.*

7. Nasr, A. M. A. (2013): Experimental and theoretical studies of laterally loaded finned piles in sand. *Canadian Geotechnical Journal*, 51: 381-393

8. Otani, J., Dang, P.K. and Sano, J. (2006): Investigation of failure patterns in sand due to laterally loaded pile using X-ray CT. *Soils and Foundations*, 46 (10): 529-535.

9. Peng, J., Rouainia, M. and Clarke, B. (2010): Finite element analysis of laterally loaded fin piles. Computer and Structures, 88: 21–22.

10. Peng, J. (2005): Behavior of finned piles in sand under lateral loading: PhD Thesis, University of New Castle Upon Tyne

11. Stewart, D.P. 1999. Reduction of undrained lateral pile capacity in clay due to an adjacent slope. Australian Geomechanics Journal, December: 17–23.

12. Wood, D.M. and Crewe, A. (2002): *Shaking table testing of geotechnical models. International Journal of Physical Model in Geotechics*: 1-13.

166

CHAPTER 7

7 SUMMARY AND CONCLUSIONS

7.1 Summary and Conclusion

In this thesis, experimental and numerical investigations were carried out to evaluate the capacity and performance of an innovative foundation system for offshore wind turbine. The hybrid system is composed of a steel pile with fins welded on its side. The performance of the foundation system was gauged against that of monopile, commonly used in offshore foundation structures. The study involved conduction static and cyclic lateral tests on scaled model piles and numerical simulation of the static tests. The results from the study are presented in four major research chapters: Chapter 3, 4, 5 and 6. Summary of the findings, the new knowledge and paradigms explored, and the conclusion derived are outlines below.

In the first part of the study, the main purpose of conducting a comparative static load simulations on monopiles and finned piles in laboratory scale was: to determine the effect of added fins on (i) improving the lateral load capacity of the piles, (ii) reducing the required length of a pile for a required capacity, (iii) the effect of the directional loading (i.e., wind, waves) with respect to fin orientation on the lateral pile response, (iv) the areal extend of the shear zone in front of pile during lateral loading. The experimental simulations revealed that, the lateral load efficiency of the finned piles varied greatly from 15%-98% depending on the number of fins and their

167

orientations to the direction of loading. In addition, it was found that fins could reduce the deflection of piles by over 65% in comparison to monopile and reduce the required length of piles up to 40% which implies cost benefits and the potentially minimized refusal during pile driving. Lastly, the strain wedge (i.e. shear zone) extended ranging up to a distance of $8.0D_p$ -$8.5D_p$ measured from center of pile.

In the next phase, soil pile interaction was studied from model tests of monopiles and finned piles instrumented with strain gauges and earth pressure gauges. LVDTs attached to the pile near the pile head and just above the soil surface were used to measure displacement lateral displacement or pile head rotation. Bending moments were derived from strain gauge measurements while *p-y* curves were developed from pressure and displacement data during lateral loading. The *p-y* curves derived from a combination pressure data and LVDTs measurement compared well with theoretical *p-y* curves derived from a method proposed by Zhang (2009).

In the third phase of the work, cyclic lateral response of finned piles was studied, for which there is little research and finding available in literature. To objective of conducting 1g cyclic lateral loading on model finned piles was to understand the effect of fins in improving the cycling lateral response of the piles, reducing the accumulated pile head rotation during, and improving soil-pile stiffness. Finally, a modified method was applied to predict long-term response of finned piles (i.e. Number of cycles of loading, $N = 10^7$) predicted from the shorter term cyclic load test ($N=10^3$). The accumulated pile head rotation increased rapidly for the initial 100 cycles of loading after which the rate of increase became smaller for all piles. The finned piles had

boilerplatewww.manaraa.com

marked decrease in the accumulated pile head rotation than the monopile at the same number of cycles of loading and magnitude of loading ratios.

The behavior of laterally loaded finned piles was compared to that of a monopile using the FEM software Plaxis 3D. Numerical model was used to study various cases that could not be modeled experimentally. The cases included varying the dimensions and positioning of the fin, and the loading direction with respect to fin orientation. The lateral resistance of finned piles increased with increase in effective area of the fin, resulting in optimal dimensions of $W_f/D_p = 1$ and $L_f/L_p = 4.5$.

7.2 Areas of future research

The research presented in this dissertation has shed the essential light on understanding the behavior of and modeling the response of single finned pile foundation for offshore wind turbine structures through detailed experimental and numerical simulations. A comprehensive study was conducted and the objectives stated in Chapter 1 have been accomplished.

The following suggestions are provided for future research to further develop the cyclic modelling of finned piles for solid design and standardization recommendations on wind turbine pile foundations systems using finned piles:

(1) This study focuses on the wind turbine foundations constructed in homogeneous soil, the theoretical and experimental work are mainly conducted on uniform sand soil layer. However, the soil properties in the field often show significant vertical inhomogeneity. More research should be further extended to

169

heterogeneous soil body conditions. Although experimental data were verified in here through numerical analysis, other soil types (i.e., soft clays and silts) described by more suitable soil models can improve the applicability of the systematic analysis presented here.

(2) For example, in this study, Mohr-Coulomb model was used to describe the sand behavior based on recommendations from prior research, and because of the ease to obtain the required parameters for the model. Even though analysis showed that Mohr-Coulomb model actually could be used to estimate the pile response with some degree of accuracy, other models such as hardening soil with small strain (HSS) model was should be tried to accurately predict the behavior of laterally loaded piles.

(3) The numerical analysis of the cyclic load behavior cyclic load was beyond the scope of this dissertation study. For future work, it is important to develop model that can be used to estimate the cyclic response of the finned piles up to 10^7 cycles of loading to better assess the long-term capacity and behavior of the finned piles under cyclic loading.

7.3 Limitation of research

1) Both static lateral and cyclic lateral loading were conducted in dry sand. Its anticipated that similar results will be obtained under saturated sand due to dissipation of pore water pressure quickly in sand.

170

2) Under centrifuge test, the stress level will be different that of 1 g test. verification of the test results is necessary to ascertain the efficiency of fin under N g condition in centrifuge.

VITA

Kepha Abongo was born on December 27, 1979 in Tagabi Estate in Kericho County, Rift Valley Province of Kenya. He studied his primary education in Jamji Primary School (Kericho) and Get Primary School (Ranen) and Secondary in Kanga High School (Rongo). He received his Bachelor Degree of Civil Engineering at Jomo Kenyatta University of Agriculture and Technology (Kenya) in 2004 and Master of Engineering from Kyoto University (Japan) in 2008. He has worked as Teaching in Jomo Kenya University and Research Assistant Student in Kyoto University. He has also taught courses in Soil Mechanics in Jomo Kenyatta University. He started research on this doctoral dissertation at Lehigh University in August 2012.

172